Maximizing Cooling Energy Savings in Buildings with Climate Change: The Potential of Phase Change Materials and Ventilation Strategies

Author: Saleh Ali Khawaja (MS)

Submitted in fulfilment of the requirements

for the degree of Master of Science

in Civil & Environmental Engineering

School of Engineering and Digital Sciences

Department of Civil & Environmental Engineering

Nazarbayev University

53 Kabanbay Batyr Avenue,

Astana, Kazakhstan, 010000

Supervisors: Shazim Ali Memon

Signature: 

Declaration

I, Mr. Saleh Ali Khawaja declare that the work included in this document which is entitled as " Maximizing Cooling Energy Saving In Building With Climate Change: The Potential Of Phase Change Materials And Ventilation Strategies" is the result of my own work except for quotations and citations which have been duly acknowledged.

I further certify that, to the best of my knowledge, it has not previously or simultaneously been submitted for any other degree or certificate at Nazarbayev University or any other national or international institution, in whole or in part.

Saleh Ali Khawaja

Date: 17/03/2023

Abstract

Due to climate change, the cooling energy demand in the building sector is projected to increase significantly. According to International Energy Agency, energy-efficient technologies should be implemented for a sustainable future. Phase change materials (PCM) potential for reducing building energy consumption have been widely acknowledged by researchers in the recent past. This research evaluates the implementation of PCM for building cooling energy savings (CES) with climate change and assesses the improvement in CES by coupling PCM with free night ventilation and changeover ventilation. Further, the performance of PCM is examined using novel indicators, energy charging, and discharging coefficients. For this purpose, hybrid downscaled weather data for 2095 were obtained, and 39 cities located in 13 different zones of the future Koppen-Geiger climate map were considered. A range of PCMs (PCM 18-32) were incorporated into the mid-rise apartment, and energy simulations were carried out using Energyplus. The results showed that the optimum PCM ranges from PCM27 to PCM30, and substantial CES (1555 kWh-7240 kWh) were obtained in all zones except Cfb, Dfa, and Dfb. The combination of PCM and free night ventilation significantly improved the CES by up to 35%. The CES was further improved up to 96% by coupling the changeover ventilation with PCM compared to the case with no ventilation and no PCM. Overall, coupling PCM with changeover ventilation appeared to be the best strategy for maximizing the CES in all climate zones.

Key words: Cooling energy saving, Climate change, Phase Change Material, Optimization, Performance Indicator, Natural ventilation

Acknowledgements

I want to convey my profound gratitude to my supervisor, **Dr. Shazim Ali Memon** for his guidance, support, and encouragement during the course of my thesis. I appreciate his time and effort in reviewing my work, providing feedback, and suggesting ideas for improvement. His expertise, insights, and suggestions have been crucial in shaping the direction and quality of my research.

I am deeply appreciative of my co-supervisor **Dr. Ferhat Karaca** for his invaluable guidance, support, and mentorship throughout my thesis journey. I am particularly grateful for his unwavering encouragement and patience, which helped me to stay motivated and focused during the entire process.

I also like to extend my heartfelt gratitude to all my lab members and staff, especially **Assemgul** and **Abrar**, for their invaluable support and assistance throughout my thesis work. Their encouragement, positive attitude, and team spirit made the research experience not only productive but also enjoyable.

In the end, I would like to extend my heartfelt thanks to my **parents** and **friends** for their unwavering support and encouragement throughout my journey. Without their love and support, I would not have been able to complete my thesis.

Once again, I am thankful to all who, supported, and encouragement throughout my thesis journey.

Contents

List of Abbreviations & Symbols

PCM	Phase change material
CED	Cooling energy demand
CES	Cooling Energy Savings
NV	Night ventilation
CV	Changeover ventilation
ODT	Outdoor dry bulb temperature
HVAC	Heating, ventilation and air Conditioning
AFN	Airflow Network
EC	Energy charged
ED	Energy Discharged
CF	Charging Fraction
DF	Discharging Fraction
CTF	Charging Time Fraction
DTF	Discharging Time Fraction
ECC	Energy Charging Coefficient
EDC	Energy Discharging Coefficient
TES	Thermal energy storage systems
STES	Sensible Thermal Energy Storage
LTES	Latent Thermal Energy Storage
TCS	Thermo-Chemical Energy Storage
RCM	Regional Climate Model
GCM	Global climate models
PTHP	Packaged terminal heat pump
ConFD	Conduction finite difference

Chapter 1- Introduction

1.1 Background

The building sector is one of the major consumers of global energy production. According to the International Energy Agency (IEA) building sector has around 37% share of the total energy consumption [1], while the value is reported as over 40% in United Nations Environment Programme (UNEP) report for sustainable buildings [2]. A massive portion of the total energy demand of the building sector is allocated for heating and cooling purposes [3]. González-Torres et al. (2022) classified the end energy use in the building sector into heating, cooling, domestic hot water, lighting, and cooking energy demand. The analysis reveals that heating-ventilation-air-conditioning (HVAC) is the most consumer service in both the residential and commercial sectors and holds 38% of the end energy use of the building sector [4]. In residential buildings, over 32% of the total devoted energy is used for space cooling. The fraction is more in US and EU and varies depending upon the climate and economic condition of the regions [4]. At the same time, building energy consumption contributes significantly to greenhouse gases. In 2021, the building operation contributed 27% of the total CO_2 to the total emissions from the energy sector, from which 8% is direct emission from buildings and 19% indirectly from the energy production for building sectors [5].

A small contribution towards the efficiency of CED will substantially impact the total energy demand [6]. Latent energy storage systems (LETS) remain in focus among researchers in combating high energy demand in buildings [7]. In LTES the materials undergo a phase change process during storage and release of thermal energy and are known as phase change materials (PCM) [8]. PCM offers a high capacity of heat storage (5-14 times more than STES) [9] within a small temperature gradient [10,11] and less volume of material [12]. These properties of PCM make them pertinent to be used in buildings for energy efficiency [9]. The benefits of PCM usage in the building have been acknowledged by many researchers [13]. However, the response of PCM integrated into buildings is highly complex and depends upon external and internal environmental conditions [12].

In recent decades, researchers have focused on investigating the energy efficiency, thermal performance, economic efficiency, sustainability, and compatibility of PCM in buildings [14]. For instance, Kenzhekhanov et al. (2020) recommended the best PCM range, layer thickness, and

location for facilities in sub-tropical regions by evaluating the monthly and annual energy savings. For this assessment, optimization of PCM has been undertaken in a four-story residential building conforming to ASHRAE standards (2013). The study disclosed that PCM 23 and PCM 24 showed better performance in the region by reducing the annual energy consumption by up to 10%. Moreover, the incremental increase in the PCM layer thickness up to 50mm revealed that increasing layer thickness positively affects energy saving. The study also recommends the application of PCM to the inner side of the wall [15]. Recent work by Soleiman Dehkordi & Afrand, (2022) proposes an effective PCM for reducing energy demand in the building sector in Iran's cold and hot climate zones. The authors applied the numerical modeling technique using energy and momentum equations with appropriate boundary conditions. The annual energy efficiency analysis was performed for the PCM ranging from PCM 20 to PCM 24. The results demonstrate that PCM 22 performs best in cold climatic zones by reducing the annual heat transfer by up to 32% leading to energy savings of up to 55 kWh/m^2. While for the hot climate zones of Iran, up to 16% reduction in annual heat transfer with an energy saving of 30 kWh/m^2 by PCM 24 was regarded as the best option [16]. Likewise,[17–20] also discussed the energy efficiency of PCM-integrated buildings. One can refer to the study by Akeiber et al. (2016) for extensive literature regarding passive cooling in the building sector using PCM [21].

1.2 Motivation

A massive amount of global energy production is embarked for use in the civil sector [22], and it is foreseeable that the demand will highly increase in the coming decades [23]. A significant part of this energy demand in the building sector is used for heating and cooling [3]. Cao et al. (2016) thoroughly explain the breakdown of building energy end-uses and the energy sources for building energy loads in the U.S., U.K., and China for both the residential and service sectors. In both sectors, the end energy use for heating and cooling was dominant [24]. Ürge-Vorsatz et al. (2015) identified that 60% of residential building energy demand is utilized for space heating and cooling. The author also analyzed the heating and cooling energy demand projection from 2010 to 2050 in the building sector, considering different derives based on Kaya Identity. Based on the analysis, the authors anticipated about a 79% increase in cooling energy demand for residential buildings by mid of century [3]. Dirks et al. (2015) projected a net growth of 42% and 143% for 2052 and 2089, respectively, in cooling energy demand over the portion of the Eastern Interconnection

located in the U.S. [25]. Another study [26] used the STELLA platform to develop a systematic dynamic model for evaluating urban energy consumption and CO_2 emission from 2005 to 2030 in Beijing, China. The results evidence a steady increase in energy consumption with a 2.9% per annum rate from 55.99 million tonnes of coal equivalent (Mtce) to 114.30 Mtce from 2005 to 2030, respectively. Similarly, 118.41 Mt CO2- emission was recorded in 2005, and the anticipated increase is 169.67 Mt CO2-eq in 2030 with a rate of 1.45% per annum. Currently, the overall contribution of building energy consumption to global CO_2 emissions is estimated at 40%, including both the direct and indirect contributions [26].

In the aforementioned literature, researchers predicted a huge increase in building energy demand in the future in response to climate change. At the same time, the world will also face the consequences of high CO_2 emissions associated with building energy consumption [23,27]. This alarming situation threatens the environment, health, and economy [28]. To combat the challenge, countries around the world are establishing goals. For instance, recent political EU Guidelines (2019–2024) aim to reduce greenhouse gas emissions by up to 55% by 2030 [29]. Owing to the increase in energy demand and associated consequences, Sustainable Development Goal (SDG7) "Affordable and Clean Energy" established by the UN targets to double the improvement in energy efficiency by 2030. Accordingly, "Energy efficiency and Eco-design" is one of the main objectives of the European Green Deal strategy, a road-map to have a net zero carbon emission by 2050 [30]. In addition, International Energy Agency (IEA) identifies the implementation of advance and sustainable energy efficiency technologies as a key aspect for sustainable future [5].

Therefore, in the interest of energy-efficient buildings with changing climates, it is essential to observe PCM behavior in future climate scenarios. To the best of the author's knowledge, only the following studies considered PCM-integrated buildings in the future climatic scenario: Sajjadian et al. (2015) assessed the potential of PCM for the cooling loads' reduction in buildings for the U.K.'s current and future climate scenarios. For this purpose, a two-story detached house was designed and modeled using Design Builder software, complying with German Passivhaus standards. The future weather files of the U.K. were obtained from U.K. Climate Impact Programme (UKCIP). After the optimization, PCM wall boards with a thickness of 48 mm and a melting point of 25◦C were applied to the building. The results showed the best performance of PCM in August, with a maximum (128.1 kWh) cooling load reduction in August 2080 [31]. Gassar

& Yun (2017) considered different climatic zones (Seoul, Tokyo, and Hong Kong) to evaluate the reduction in cooling and heating loads with the application of PCM in buildings. Dynamic simulations with the help of Energy Plus were performed on a medium office building model for the years 2020, 2050, and 2080. The current and future weather files source was Energy Efficiency & Renewable Energy (EERE). All the utilized PCMs (BioPCM29, DuPonEnergainPCM 21.6, RUBITHERMPCM25) effectively reduced cooling and heating load under climatic change conditions. Overall, electric load reduction of up to 9.69% and gas savings of up to 93.33% were reported in this research. The research work of Nurlybekova et al. (2021) evaluates the thermal and energy performance of PCM-integrated buildings in subtropical climate zone. The authors used a two-story office building, while the future weather files were generated using the hybrid downscaling method. The results obtained through simulation showed that for the subtropical climate zone, the duration of cooling degree days (CDD) will increase while Heating degree days (HDD) will decrease in 2095. Moreover, the study identified the best-performing PCM for different cities located in the region [32].

1.3 Problem Statement

Although there are few studies on the effective utilization of PCM for building energy efficiency with climate change, however, none of the existing literature examined:

- The PCM exact latent heat exploitation during the energy charging and discharging cycle. Hence, It is essential to know PCM's exact latent heat exploitation during the charging and discharging cycle because not all temperatures within the phase transition range of PCM have the same effect on PCM latent heat exploitation.
- The combination of PCM and passive ventilation strategies for improvement in cooling energy savings with climate change. Therefore, there is a need to evaluate the improvement in energy savings by combining PCM with different ventilation operations to maximize the CES in the future.

In addition, the scope of the available literature on the effective utilization of PCM with climate change is narrow and has the following shortcomings:

- The literature uses office buildings or single rooms except [31]. However, the occupants are more exposed to indoor boundary conditions in the case of residential buildings and have higher control over natural ventilation [33]. Moreover, climate change has projected a significant increase in cooling energy demand in the residential sector [23,27,34,35]. This demands further research on the energy efficiency of residential buildings with climate change.
- Except [32], all the existing literature uses a statistical downscaling technique for future weather files employing stochastic or deterministic methods. Whereas the literature identifies limitations of these methods: the deterministic method has an issue with the prediction of extreme temperature accurately [32]. The drawback associated with the stochastic method is that it considers a few weather variables generating artificial meteorological data [36]. Therefore, hybrid downscaled future weather files are recommended for the energy simulation with climate change.

1.4 Research Hypothesis

Considering the mentioned deficiency in the existing literature, this study will test two hypotheses for the implementation of PCM with climate change:

Hypothesis I: The high energy demand in a residential building with climate change can be reduced by incorporating PCM.

Hypothesis II: Coupling passive ventilation techniques with PCM in a building will result in higher energy efficiency.

A considerable variation in outdoor boundary conditions and more reliable future weather files are required to test the hypothesis. Thus, to have a variation in outdoor environmental boundary conditions, 39 cities located in 13 zones of the future Koppen climate map were considered. In addition, for all the cities, hybrid downscaled future weather files for 2095, generated based on the IPCC Representative Concentration Pathways (RCP8.5) scenario, are used for Energy simulation.

1.5 Objectives

To test these hypotheses This research aims to:

1) Quantify achievable energy savings using PCM
2) Evaluate the passive ventilation combined with PCM for improving cooling energy savings.
3) Assess the performance of PCM.

1.6 Novelty

To evaluate the performance of PCM, it is important to know the exact status of PCM latent heat capacity exploitation, as not all temperatures within the phase transition range of PCM have the same effect on PCM latent heat exploitation [37]. Hence there is a need for an indicator that can identify the performance of PCM based on its latent heat exploitation. For this purpose, Evola et al. (2013) introduced an indicator frequency of activation (FA) and PCM storage efficiency(ϩ) [37]. However, Evola et al. (2013) indicator provides no clarity about the charging and discharging of PCM as the efficiency depends upon the complete daily cycle [38]. Another researcher, Ramakrishnan et al. (2016), used a different approach and used the node temperature to get the exact temperature of PCM during the phase transition process [39]. Based on the node temperature, the fraction of latent capacity charged and discharged (Lc and Dc) were found. Ramakrishnan et al. (2016) considered the ideal situation and assumed PCM charging and discharging follow the 12-hour duration. This is unlikely to be realistic as the PCM energy storage is a function of temperature.

Therefore, to assess the performance of PCM under different indoor boundary conditions, a novel performance indicator, energy-charge and discharge coefficient (ECC and EDC), were introduced in this research. The ECC and EDC use PCM's actual temperature to find the energy charged and discharged by PCM during each cycle. Moreover, ECC and EDC account for the actual time duration for charging and discharging of PCM. Based on the duration, energy charge, and discharge, the values of ECC and EDC were obtained, and the performance of PCM was gauged on a scale (illustrated in Fig. 15). Further details about the novel indicator are presented in chapter 3, section 3.7.

1.7 Thesis Structure

This thesis is organized into five chapters, and apart from the introduction, the following chapters will be discussed:

Chapter 2: Literature review

In Chapter 2, a comprehensive literature review of the existing literature on climate change, building energy, and PCM will be presented. The content of this chapter will enhance the reader's knowledge on the subject: what is climate change? How climate change influences building energy consumption? What is PCM? How effective is PCM in reducing building energy consumption?

Chapter 3: Methodology

This chapter presents a systematic methodology to meet this research's objectives, including the disruption of boundary conditions, building type, and future weather files. In addition, the working principle of simulation software and the validation are also described.

Chapter 4: Result and discussion

Chapter 4 discusses all the results comprehensively, and the optimum PCM is presented for different climate zones under different indoor boundary conditions. The behavior of PCM is evaluated using the novel indicator presented in this research.

Chapter 5: Conclusion

Finally, Chapter 5 summarizes the conclusion drawn for this research. In addition to this, further research into the subject matter is proposed.

Chapter 2- Literature Review

Overview

An extensive literature review covering different aspects of this research is presented in this chapter. The first section introduces the energy demand in the building sector. Afterward, the causes and consequences of climate change are discussed in section 2.2, followed by section 2.3, where a detail about the influence of climate change on building energy demand is included. In section 2.4 PCM and its types are elaborated, and section 2.5 discusses the usage of PCM in the building sector for energy efficiency.

2.1 Energy demand in the building sector

The building sector is one of the major energy consumers and holds a share of about 40% of the total energy production. Fig.1 shows the distribution of energy shares among the major sectors, where the energy demand in the residential sector is 22% of the total, and in the commercial sector, it is 19% [40]. Overall, the energy demand in the building sector is greater than in the industrial and transportation sector. The consumption in the building sector is categorized for different appliances like cooking, hot water, lighting, heating, and cooling [41] and according to the findings of González-torres et al. (2022) among all appliances the energy demand for air conditioning systems (HVAC) is the highest which is almost 38% of total energy in both the residential and commercial sectors [4].

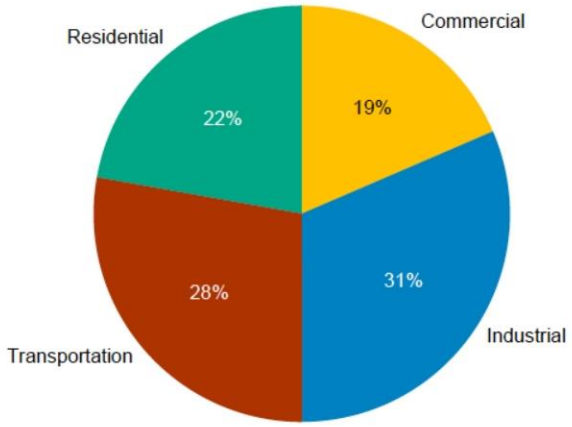

Fig.1 Worldwide energy consumption share of different sectors [40].

The major sources of energy production include coal, oil, and natural gas. In Fig. 2 the proportion of CO_2 emission from these sources is presented [42]. It is estimated that energy production contributes almost 40% to global CO_2 emission, and among the sources of energy production, coal is the highest contributor to global CO_2 emission (72%) followed by natural gas and oil [42]. The IEA reported over 36.8 Gt CO_2 emissions from the energy sector in 2022, the highest ever recorded. IEA identified the increase in cooling and heating energy demand as a key factor contributing to the increase in CO_2 emissions [43].

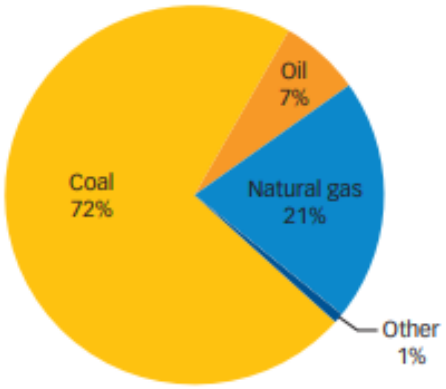

Fig. 2 CO_2 emission from these sources [40].

2.2 Climate change

The expeditious change in climate is one of the widely acknowledged concerns around the globe, which raises the average global temperature and is prone to many other environmental threats [36]. In particular, anthropogenic activities such as burning fossil fuels contribute a huge amount of CO_2 to the environment, accounting for over half of the greenhouse gases (GHG) [44]. Fig. 3 shows the model-simulated global temperature anomalies [45] where the change in the surface temperature of the earth from the past to the present and from the present to the future can be noticed. According to Fig. 1, if the representative concentration pathway (RCP8) is considered, the world temperature will increase by more than 3 °C in 2071 compared to the current surface temperature of the earth.

The Intergovernmental Panel on Global Climate Change (IPCC) reported a 1.6% increase in CO_2 emissions annually. Further, the report indicates a rise of 1.9% in the annual consumption of fossil fuels, and fossil fuel consumption accounted for releasing tremendous amounts of CO_2 into the environment [46]. The high amount of greenhouse gasses in the atmosphere increases the temperature [47]. Besides, urbanization also aggravates the cities' thermal environment, causing the Urban heat Island (UHI) effect. Several factors, such as thermal mass released from concrete and asphalt roads, the poor airflow capacity of urban canyons formed by skyscrapers, and the effect of heat released from vehicles on streets and air conditioners, contribute to UHI [48]. The combined impact of climate change and UHI exacerbates thermal comfort by raising the air temperature, producing heat waves, and exposing the inhabitants to extreme heat stress [48]. Over the last century, the global surface temperature has increased by 0.74 ± 0.18 °C [49]. The IPCC (2014) report associates this mainly with the developmental activities initiated by humankind after the mid-20th century. According to the fifth IPCC report, the anticipated increase in the earth's surface temperature is about 4.8 °C by the end of this century. The increase in ambient temperature will intensify the risk of heat wave events [46] and increase the energy demand.

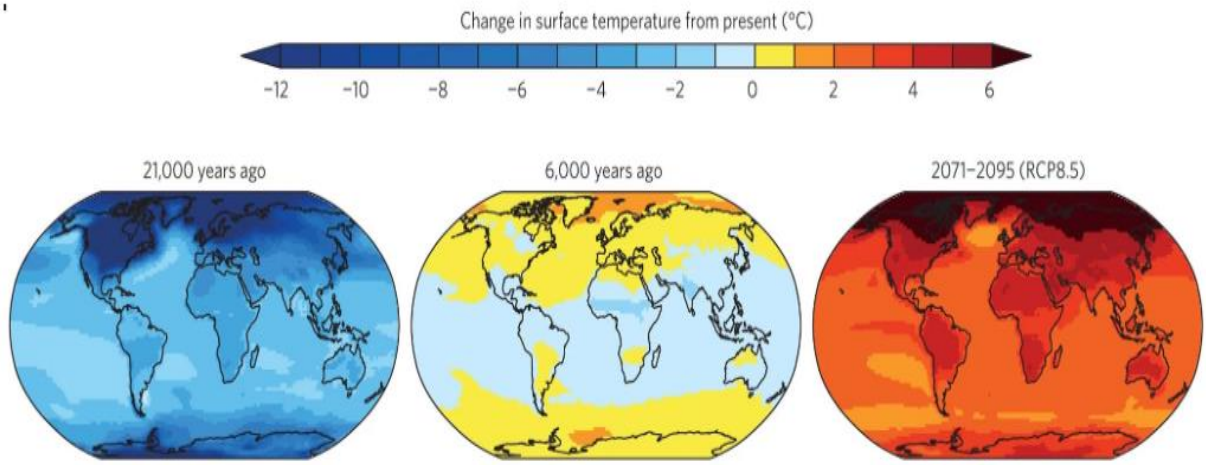

Fig.3 Model-simulated global temperature anomalies [45]

2.3 Climate Change and Building Energy Demand

The high level of CO_2 in the atmosphere disturbs the homeostasis state in the atmosphere [50] and disbalances the earth-atmosphere energy balance resulting in climate change. Climate change is an emerging challenge associated with greenhouse gases in the atmosphere, potentially threatening the ecology and natural environment [51]. In addition to the changing climate, extreme and prolonged weather events, including heatwaves, hot days, and intense precipitation, will alter outdoor environmental conditions [52]. The outdoor environmental conditions highly influence energy demand in the building sector [53]. Fig.2 presents the anticipated increase in air conditioning energy by mid and end of this century. It can be seen from Fig. 4 that the cooling energy demand will increase substantially in the future. This is because, with climate change, the ambient temperature tends to rise, [54,55] and the ambient temperature has a direct correlation with the building cooling energy demand (CED) [53],

Researchers have focused on anticipating the possible increase in CED and consequent CO_2 emissions with climate change. Isaac and van Vuuren (2009) analyzed the energy demand for heating and cooling purposes in residential buildings with climate change. The investigation showed an over 72% increase in CED by the end of the century (2100) in reference to 2000. Further, the analysis projected an increase in CO_2 emissions associated with world energy demand for heating and cooling from 0.8 $GtCO_2eq$ in 2000 to 2.2 GtCO2eq in 2100 [27]. In a study to estimate projected changes in heating and cooling energy demand with climate change in Canada, Berardi, and Jafarpur (2020) simulated 16 building prototypes using statistically downscaled future weather files. The results anticipated an increase in CED from 15% to 126%, with a decrease in heating energy from 15% to 33% by 2070, depending upon the baseline climatic file and building typology [34]. Considering the goal of zero energy building, D'Agostino et al. (2022) assessed the change in cooling and heating energy demand by 2060 in eight cities representing different climate zones in Europe (EU). For this purpose, a two-story residential building as a representative of the European national building was selected, and morphed weather files were used for the simulation. The results revealed that in 2060, heating energy would decrease by 38% to 57%, while cooling energy would increase by 99% to 380%, depending on location [35]. A more comprehensive overview of energy consumption and CO_2 emission in the residential sector is presented in Ref. [23].

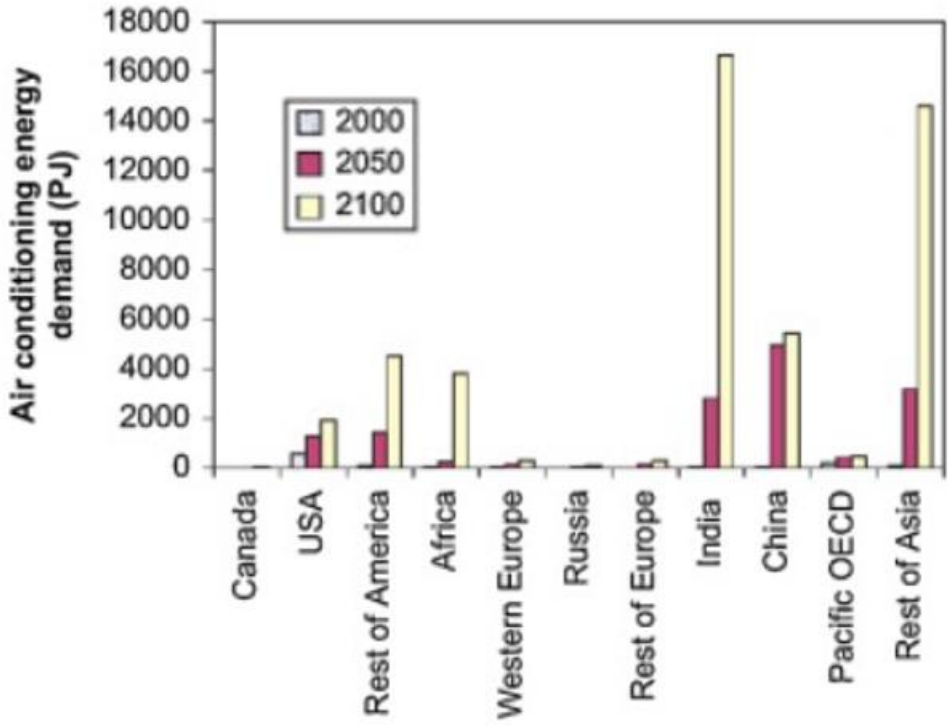

Fig.4. Residential building cooling energy demand in the present and future [24].

2.4 PCM and Building Energy Efficiency

In response to the challenges evolved in the building sector in terms of high energy demand, increasing CO_2 emission, and considering the economy, researchers are focusing on mitigation technologies by using Thermal Energy Storage (TES) technology[56]. The TES is classified into three categories [14]:

- Sensible Thermal Energy Storage (STES): The storage material only undergoes temperature fluctuation during the energy storage process.
- Latent Thermal Energy Storage (LTES): This system involves the phase-changing process of material during the storage and discharge of thermal energy.
- Thermo-Chemical Energy Storage (TCS): A chemical reaction is used to store thermal energy in this method.

A sensible thermal storage system (STES) is convenient for TES. However, Latent Thermal Energy Storage (LTES) has superiority over STES in storing the same thermal energy with less volume of energy storage material [12]. Compared to STES, LTES uses phase-change materials (PCM), which provide large energy density within a small temperature gradient [10,11]. Depending upon the enthalpy, PCM can store and release the thermal energy during the process phase transition [11]. Broadly, there are two types of PCM: 1) organic PCM (made up of hydrocarbons) and 2) inorganic PCM (salt hydrates). The first type offers non-subcooling, non-corrosiveness, and chemical and thermal stability. However, their drawbacks include low phase-change enthalpy, low thermal conductivity, and flammability. Examples of organic PCM are paraffin, fatty acids, and polyethylene glycol. The second type has a greater enthalpy change. However, the usage of inorganic PCM is limited by the potential subcooling, corrosion, phase separation, phase segregation, and lack of thermal stability [11]. Memon, (2014) extensively discussed the critical parameters involved in the PCM's selection, classification, chemical compatibility, thermal conductivity, and their application in buildings [57]. The higher heat capacity of PCM in order of magnitude than traditional building materials and isothermal behavior between melting and freezing cycles makes them suitable for building applications [19].

The melting and solidification of PCM are a function of temperature, and when PCM is integrated into the building the efficiency of the PCM is dependent on the outdoor and indoor temperature. Fig.5 shows the working principle when PCM is integrated into the building wall. Form Fig. 3 It can be observed that during the daytime, when the wall temperature increases, the PCM starts melting and reduces heat travel to the inner side. Eventually, the rise in indoor temperature is prevented by PCM during the day. In the nighttime, when the outdoor temperature drops, the PCM solidifies and releases the stored energy to the inner side resulting in less indoor temperature fluctuation. Thus, the relative less indoor temperature fluctuation with the incorporation of PCM results in less energy demand for indoor thermal comfort.

The overall goal of the research work on PCM integrated buildings is to maximize the following benefits specified by [14]:

a) Economic efficiency: Less capital and operational cost.
b) Energy efficiency: Reducing energy consumption.
c) Environmentally friendly: Reduction in greenhouse gas emissions.
d) Compatibility and reliability: Combine effect with other materials and long-lasting.

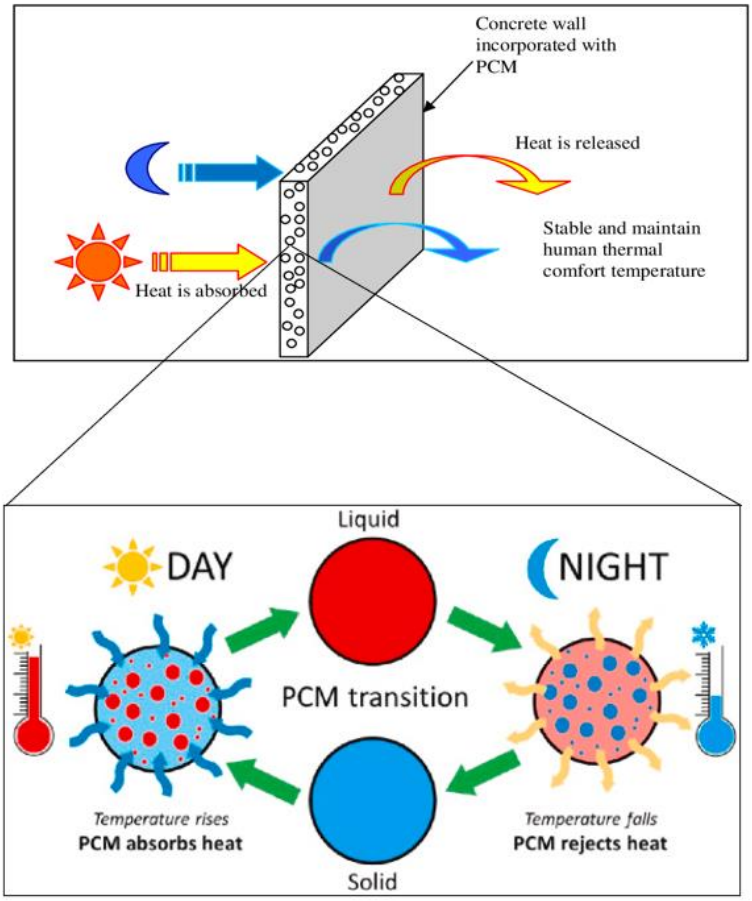

Fig.5 Working principles of PCM [58,59].

Several research works have been carried out on PCM integration in buildings to address intrinsic issues such as PCM melting temperature, convective heat transfer, location of PCM, latent heat of fusion, and indoor and outdoor climatic compatibility [60]. Currently, researchers are relying more on the numerical simulation method for investigating the behavior of PCM in building as it is cost-effective and offers reliable results [32,60]. Saffari et al. (2017) [11] optimized PCM for the energy efficiency of a residential apartment from the ASHRAE Standard 90.1-2013 prototype. Paraffinic PCM with melting points ranging from 20°C to 26°C was incorporated via micro-encapsulation techniques in the building prototype and simulated using Energyplus software. Moreover, a generic optimization program (GenOpt v3.1.1) was coupled with Energyplus to optimize PCM. The study reveals that PCM with lower melting points (PCM20) in heating dominant regions is more suitable, whereas PCM with higher melting points (PCM26) is more favorable in cooling dominant regions. In concluding remarks, the authors confirm that with the proper selection of PCM, a considerable amount of energy can be saved both in heating and cooling dominant regions [11]. Wijesuriya et al. (2018) performed a parametric analysis to shift cooling energy demand from peak hours by integrating PCM in a house in Phoenix, Arizona, USA. In this regard, PCM location, PCM properties, and precooling strategy, in combination with natural and forced convection models, were analyzed by coupling the features of Building Energy Optimization (BEopt) and Energyplus. It is noticed that the application of force convection helps maintain the indoor comfort level during the peak hours and precooling stage. Thus, shifting the energy demand from the peak hours was observed. Combining optimum PCM and precooling strategy maximizes the energy cost reduction (29%) by resulting in a 99% shift in cooling energy for a design day [61]. In another study, Hlanze et al. (2022) used PCM panels in air supply ducts to test the hypothesis that during off-peak hours, the cool air through the duct system would help in the PCM solidification (charging) while in peak hours, the high air temperature will enable the PCM discharging resulting in peak load shift. The simulation results showed that the proposed system of PCM panels in air supply ducts successfully shifts the cooling loads from peak to off-peak hours, resulting in a 31.5% reduction in HVAC energy demand [62]. Using a similar approach, Lizana et al. (2019) assessed free and mechanical ventilation to implement PCM for low cooling energy in buildings effectively. For this purpose, a PCM layer was integrated as an innermost layer. Simulations performed on TRNSYS showed that mechanical ventilation during

the night, in combination with optimum PCM, maintained the inside comfort conditions more frequently in comparison to only night ventilation (NV). Still, the higher electricity consumption penalty makes only NV more favorable [63]. A step forward, Gracia et al. (2019) implemented the control ventilation to enhance the PCM performance using an airflow network algorithm in Energyplus, aiming to increase CES in an office building. The simulation results show that control ventilation enhances PCM performance, and as a result, the CES increased from 8% to 15% [64]. Moreover, Arumugam et al. (2022) summarized the efficient PCM and passive ventilation approaches to improve the thermal performance of buildings in different climates [65].

2.5 Summary of the chapter

This chapter presents a detailed literature review on building energy demand, climate change and its influence on building energy demand. Moreover, the potential of PCM for energy conservation in the building is also discussed comprehensively. The summary of each section is the following:

- Currently, the building sector consumes about one-third of the global energy production, and a major portion of the building energy demand is utilized for space heating and cooling. Besides, the building sector also contributes almost 40% of greenhouse gas emissions.
- The greenhouse gases alter outdoor temperatures and lead to climate change.
- The outdoor temperature directly influences building energy demand, and as a result of the changing outdoor temperature, the cooling energy demand of the building is anticipated to increase.
- PCM can store and release thermal energy during the process phase transition, and when integrated into the building envelope during the daytime, PCM melts, and at night it solidifies. The phenomenon of PCM melting and solidification in the wall prevents indoor temperature fluctuation, resulting in less energy demand for indoor thermal comfort.

Chapter 3- Methodology

Overview

A detailed methodology is presented in this chapter which includes seven sections. The overall idea of the methodology can be obtained from Fig. 6, which shows the three major steps included in this research. In the first step, the boundary conditions are defined by selecting future climate zones, representative cities, PCM, and building models presented in sections 3.1 to 3.5. Afterward, sections 3.6 and 3.7 discuss details about numerical simulation and performance evaluators.

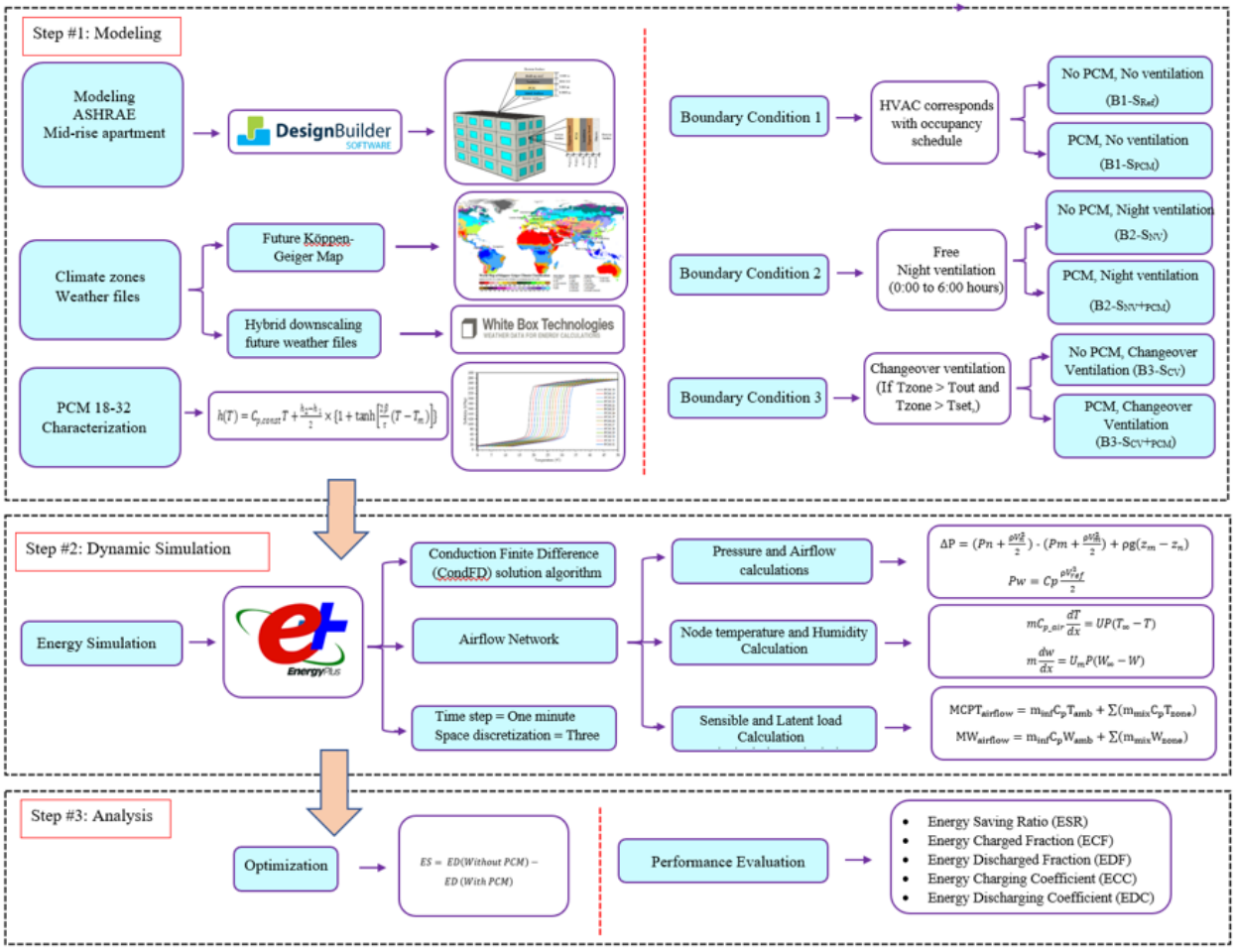

Fig. 6 shows the workflow of the methodology.

3.1 Boundary conditions

The analysis is performed under there different indoor boundary conditions. In each boundary condition further, two different scenarios are considered. The boundary conditions are:

Boundary Condition 1:

In this condition, the cooling operation of the mechanical cooling system (HVAC) corresponds with the occupancy schedule, and indoor temperature is controlled at comfort level all the time (controlled condition). Two different scenarios are considered under this condition:

Scenario (a): The standard building will be simulated without integrating PCM. The CED from this scenario will be a reference for Scenario (b) and evaluation of maximum CES.

Scenario (b): In this case, the PCM layer will be applied as an inner layer in the wall and roof of the building, and the cooling energy savings (CES) will be assessed under boundary condition 1 (b1).

Boundary Condition 2:

To evaluate the impact of free night ventilation (NV), air infiltration will be allowed through openings from 0:00 to 6:00 hours, independent of indoor or outdoor conditions. During free NV, the HVAC will not be functional. Under free NV conditions, two different scenarios will be assessed for CES:

Scenario (c): The standard building will be simulated with free NV without integrating PCM. This scenario will evaluate the solo impact of NV on CED and act as a reference for scenario (d).

Scenario (d): Under this scenario, the PCM will be coupled with NV, and further enhancement in CES will be evaluated.

Boundary Condition 3:

In this condition, changeover ventilation (CV) will be implemented. Changeover ventilation prevents the simultaneous functioning of natural ventilation and HVAC and allows ventilation depending on outdoor conditions. If Tinside > Tout and Tindside > Tset, natural ventilation will be allowed; else, HVAC will be functional. Two different scenarios will be considered to evaluate the impact of CV on CES.

Scenario (e): In this scenario, the CES under CV will be assessed without the integration of PCM into the building. Further, the results of CES from this scenario will act as a benchmark for scenario (f).

Scenario (f): CV's impact on PCM efficiency will be assessed in this scenario.

Table 1. illustrates the condition under different scenarios and the nomenclature of all the scenarios, which will be further used in the article.

Table 1. Different Scenarios of PCM Implementation and Associated Nomenclature

Boundary Condition	Scenario	Building Condition	Nomenclature
1	a	No PCM, No ventilation	B1-S_{Ref}
	b	With PCM, No ventilation,	B1-S_{PCM}
2	c	No PCM, With Night Ventilation	B2-S_{NV}
	d	PCM, With Night ventilation	B2-S_{NV+PCM}
3	e	No PCM, With Changeover ventilation	B3-S_{CV}
	f	With PCM, With Changeover ventilation,	B3-S_{CV+PCM}

3.2 Climate Zones

This research uses future climate zones established in the updated Köppen-Geiger climate classification map for projected climate change. Fig. 7 shows the updated Köppen-Geiger climate classification map for the future climate. The map illustrates the future climate zones (between 2071-2100) by combining climate change forecasts from 32 Coupled Model Intercomparison Project phase 5 (CMIP5) models. For future climate classification, monthly historical and future air temperature and precipitation data were obtained from 32 CMIP5 models. Further, for each CMIP model, climate change offsets were calculated (for temperature and precipitation) between 1980–2016 and 2071–2100. Finally, from the offsets of temperature and precipitation high-resolution future climate map is produced [66].

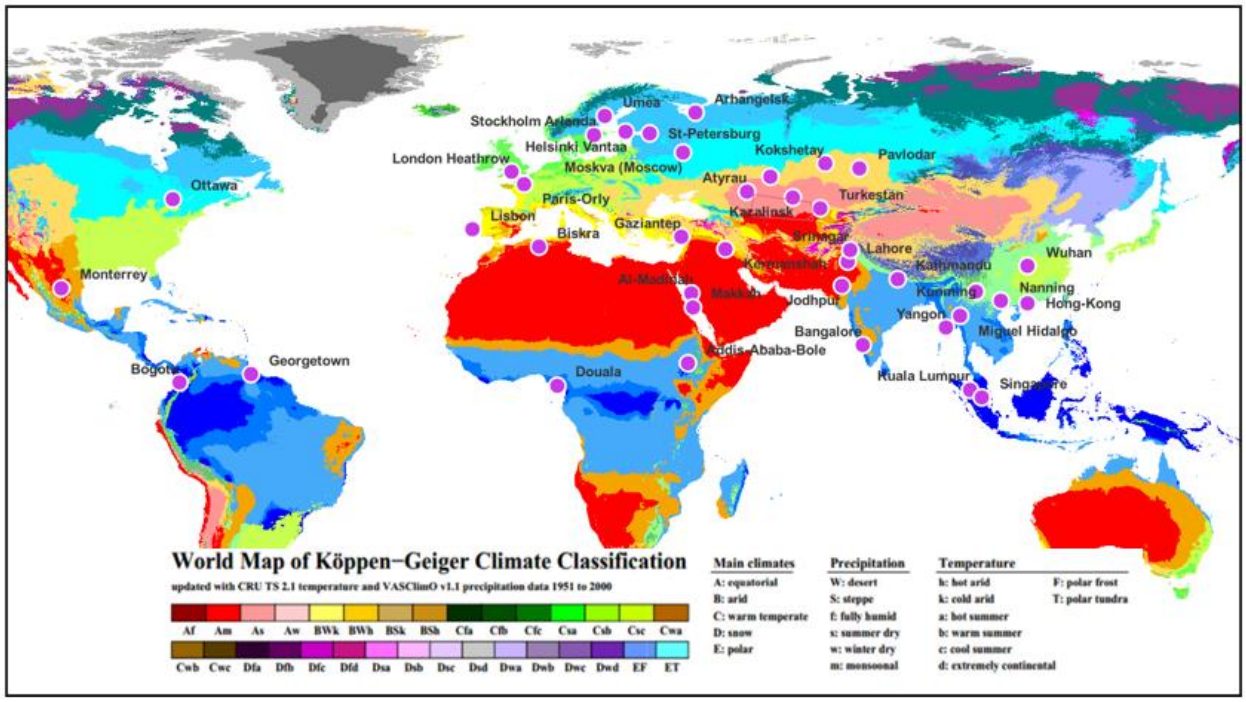

Fig. 7 Koppen Geiger Map [66].

3.3 Selection of cities and Weather files

Table.2 shows the selected cities in the different climatic regions. In total, thirteen different climate zones from the future Koppen map and three representative cities from each zone were considered for this research. The basic criteria for the selection of the cities were set based on their demographic and economic importance. Also, the minimum population limit of a city to be selected is set as 0.1 million.

The future weather files provide typical weather data of a region for a single year, generated based on the historical observation of weather conditions over a time frame [67]. Global climate models (GCMs) are the main source providing credible information about future weather conditions. However, GCMs present the data on a larger scale consisting of monthly and annual average data of large spatial regions (100–300 km^2) [67]. On the other hand, research on building performance considering the impact of climate change needs information on a small scale (hourly and sub-hourly basis) and demands downscaling GCMs data [67,68]. The downscaling of GCMs data can be carried out by three typical methods: statistical, dynamic, and hybrid.

Statistical downscaling relies on statistical rules and correlation for the generation of future weather data. This method is simpler and assumes a constant statistical relationship between the

meteorological parameters [69]. To reproduce weather data for the future, deterministic or stochastic approaches are used. In the deterministic approach, transformation algorithms are applied to change the hourly values of historically recorded weather variables [67]. However deterministic approach does not predict extreme future weather conditions and provides insufficient information on changes in diurnal weather patterns. In addition, the method possesses a lack of physical consistency between weather variables, and there is a high probability of under- or overestimation of the climate change impact [67]. The stochastic approach is based on a statistical analysis of the historic weather data and requires data of a few independent climate variables to generate other weather variables. However stochastic approaches of downscaling assume that future weather patterns will be the same as those observed historically [67].

Dynamical downscaling uses Regional Climate Model (RCM) to generate local or regional future climate information. RCMs use regional or local climate models from GCMs as boundary conditions and create fine-resolution data (2.5 km^2) by accounting for hydrology, topography, and vegetation of the region [67,70]. The dynamically downscaled weather files are more accurate and provide physically consistent data sets for different weather variables. However, it needs large data sets, powerful computational resources, high storage capacity, and expertise [67].

This research uses weather files that are downscaled using the hybrid downscaling method. The method combines dynamic and statistical downscaling techniques, decreasing computational resources and high storage demand. It allows to simulate broad scope of different weather conditions in the future [71]. The hybrid downscaled future weather files for 2095 generated based on the IPCC Representative Concentration Pathways (RCP8.5) scenario were obtained from Whitebox technology [72] due to their extensive experience in processing future weather data for building energy simulations.

Table.2 Selected representative cities in the different climatic regions.

Climate Zone	City	Country	Latitude /Y	Longitude /X	Elevation, m
Am	Yangon	Myanmar	16.8	96.15	23
	Douala	Cameroon	4.0511	9.7679	13
	Hong-Kong	Hong-Kong	22.3080	113.9185	8
Aw	Bangalore	India	12.9716	77.5946	920
	Addis-Ababa	Ethiopia	8.9838	38.7963	2,324
	Miguel Hidalgo	Mexico	19.4307	99.2084	2284
Af	Kuala Lumpur	Malaysia	3.139	101.6869	66
	Singapore	Singapore	1.35	103.82	15
	Georgetown	Guyana	38.9076	77.0723	2,600
BSk	Kokshetay	Kazakhstan	53.29	69.4	234
	Pavlodar	Kazakhstan	52.2873	76.9674	123
	Aktobe	Kazakhstan	50.2839	57.1670	219
BSh	Lahore	Pakistan	31.5204	74.3587	217
	Monterrey	Mexico	25.6866	-100.316	540
	Jodhpur	India	26.2389	73.0243	231
Bwh	Medina	Saudi Arabia	24.5247	39.5692	622
	Makkah	Saudi Arabia	21.3891	39.8579	277
	Biskra	Algeria	34.8449	5.7249	87
BWk	Atyrau	Kazakhstan	47.0945	51.9238	20
	Turkestan	Kazakhstan	43.3051	68.2347	214
	Kazalinsk	Kazakhstan	45.7641	62.0999	68
Cfa	Wuhan	China	30.5928	114.3052	37
	Paris	France	48.7262	2.3652	89
	Srinagar	India	34.0837	74.7973	1,585
Cfb	Stockholm	Sweden	59.65	17.9238	42
	London	UK	51.47	-0.4543	11
	Bogota	Colombia	4.711	-74.0721	935
Csa	Gaziantep	Turkey	37.066	37.3781	850
	Kermanshah	Iran	34.3277	47.0778	1,350
	Lisboa-Portela	Portugal	38.7756	9.1354	114
Cwa	Kathmandu	Nepal	27.7172	85.324	1400
	Kunming	China	24.8797	102.8332	1,892
	Nanning	China	22.8167	108.3669	500
Dfa	Moscow	Russia	55.7558	37.6173	786
	Ottawa	Canada	45.42472	-75.695	70
	St-Petersburg	Russia	59.9343	30.3351	13
Dfb	Helsinki Vantaa	Finland	60.3183	24.9497	19
	Arkhangelsk	Russia	64.5459	40.5506	3
	Umea	Sweden	63.8258	20.2630	12

3.4 PCM Selection

This research considers PCM with melting points ranging from 18°C to 32°C (PCM18 to PCM32) and a latent heat storage capacity of 219kJ/kg. Each PCM experiences a complete phase transition with a range of 4 degrees. For example, PCM26 has a phase transition temperature range from 24°C to 28°C. Once the PCM temperature reaches 24°C, the enthalpy of PCM starts increasing until it reaches 28°C, where the complete phase transition of PCM occurs. Fig. 8 presents the enthalpy temperature (h-T) curves for the selected PCMs. The detail about PCM's conductivity, specific heat, and density of PCM are presented in Table 3.

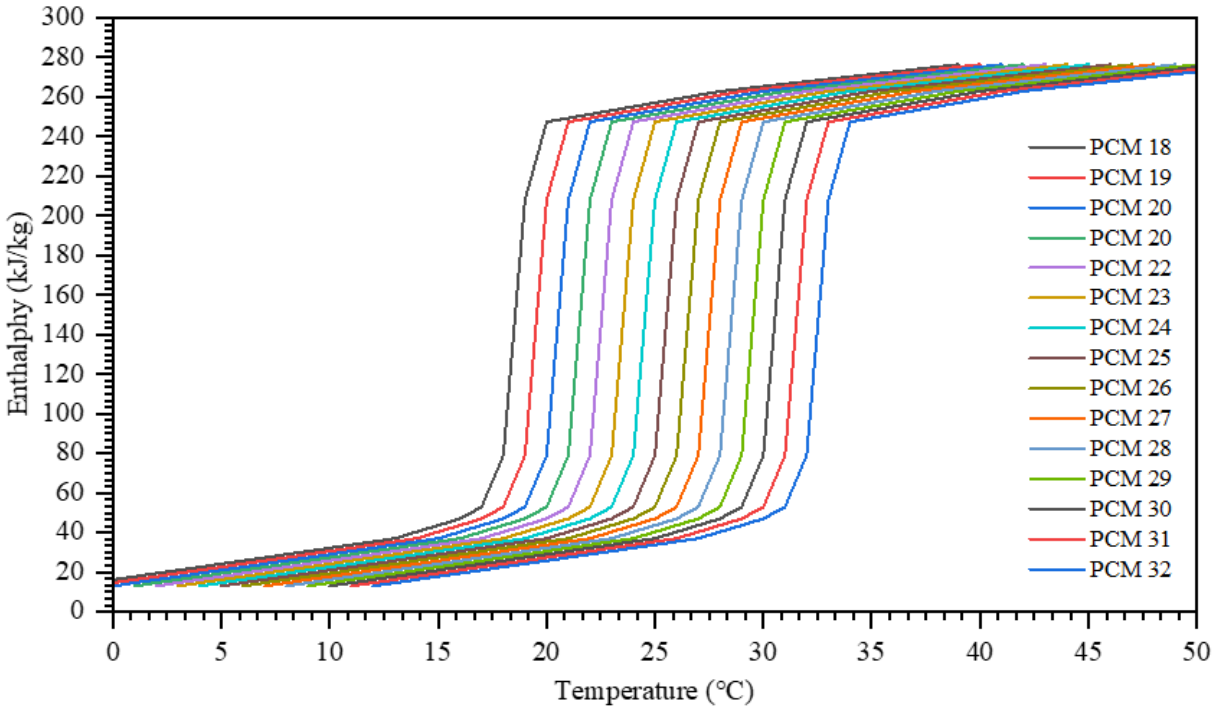

Fig. 8. Enthalpy temperature curve (PCM18-32).

3.5 Building Model

A four-story mid-rise residential apartment building conforming to the ASHRAE Standard 90.1-2013 was selected. Fig. 9 shows the selected building model. The building has a covered area of 8436 ft^2 with window to wall ratio of 20% on each side. Each floor consists of eight apartments except the ground floor, which comprises seven apartments and an office with an equivalent apartment floor area (950ft^2). Table 3 provides the thermal and physical properties of the building materials. Whereas the occupancy fraction of office and residential space are illustrated in Fig.10.

The realistic building attributes and construction of the models satisfy the requirements and are applicable in the research of energy-efficient buildings [20].

The PCM is integrated into the walls and roofs of the buildings as a layer (Cross-sections in Fig.9). The PCM layer's thickness and location significantly affect the specific properties of PCM [74]. Nurlybekova et al. (2021) reported that the greater the thickness, the more it reduces the heat stress risk [32]. However, the thickness of PCM above 30 mm is not feasible in buildings [75]. Therefore, a 20 mm layer of PCM is integrated into the inner side of the roof and the walls.

Accordingly, to maintain thermal comfort in the building, packaged terminal heat pump (PTHP) indicated by ASHRAE Standard 90.1-2013 is installed as an air conditioning (HVAC) system. The PTHP compound is composed of separate components: an outdoor air mixer, supply air fan, direct expansion (DX) cooling, and heating coil. PTHP also comprises a supplementary heating coil (Fig. 11) [76]. The set points and attributes of the HVAC system as per the specification of ASHRAE Standard 90.1-2013 are illustrated in Table 4. Researchers reward the PTHP system for creating a more realistic heating and ventilation system closer to the actual case scenario [17].

Table 3 Details of wall and roof composition.

Layers	Material	d [m]	k [W/m K]	q [kg/m^3]	Cp [J/kg K]	R [W/m^2 K]
Wall						
Layer 1	Stucco	0.0102	0.72	1856	840	-
Layer 2	Gypsum board	0.0159	0.16	800	1090	-
Layer 3	Insulation	-	-	-	-	1.036
Layer 4	PCM	0.020	0.20	860	1970	-
Layer 5	Gypsum board	0.0159	0.16	800	1090	-
Roof						
Layer 1	Built-up roof	0.0095	0.16	1120	1460	-
Layer 2	Insulation	-	-	-	-	4.318
Layer 3	PCM	0.0125	0.20	800	1200	-
Layer 4	Metal surface	0.0008	45.28	7824	500	-

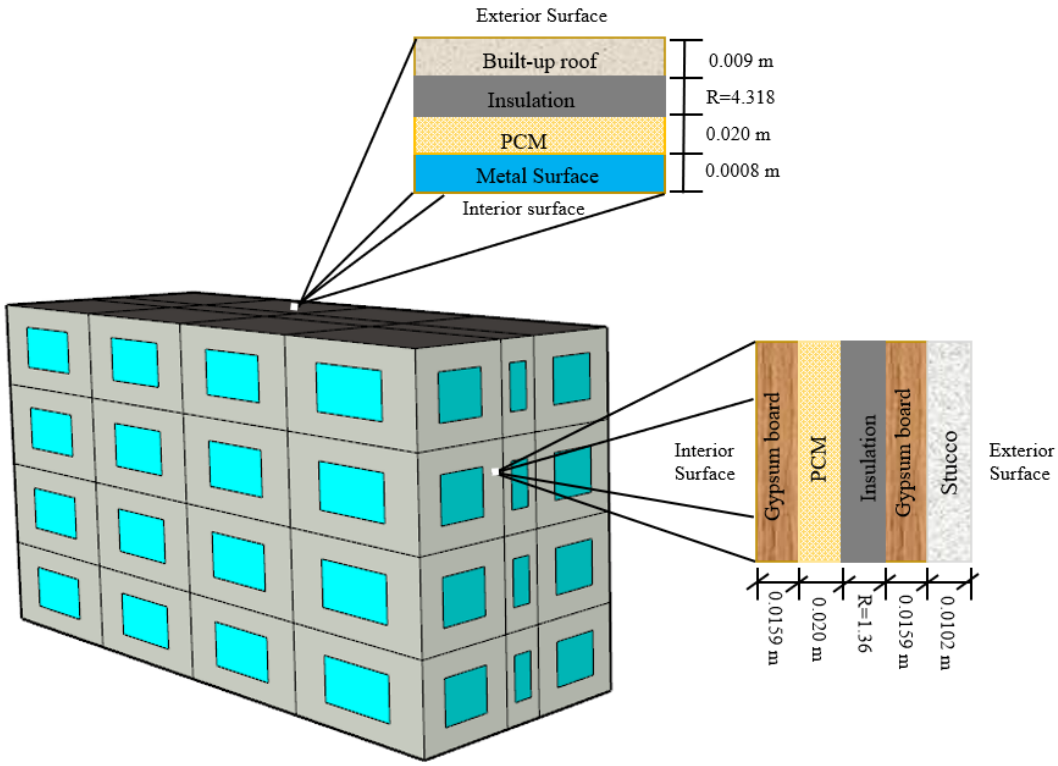

Fig. 9. Mid-rise residential apartment prototype from ASHRAE Standard 90.1-2013.

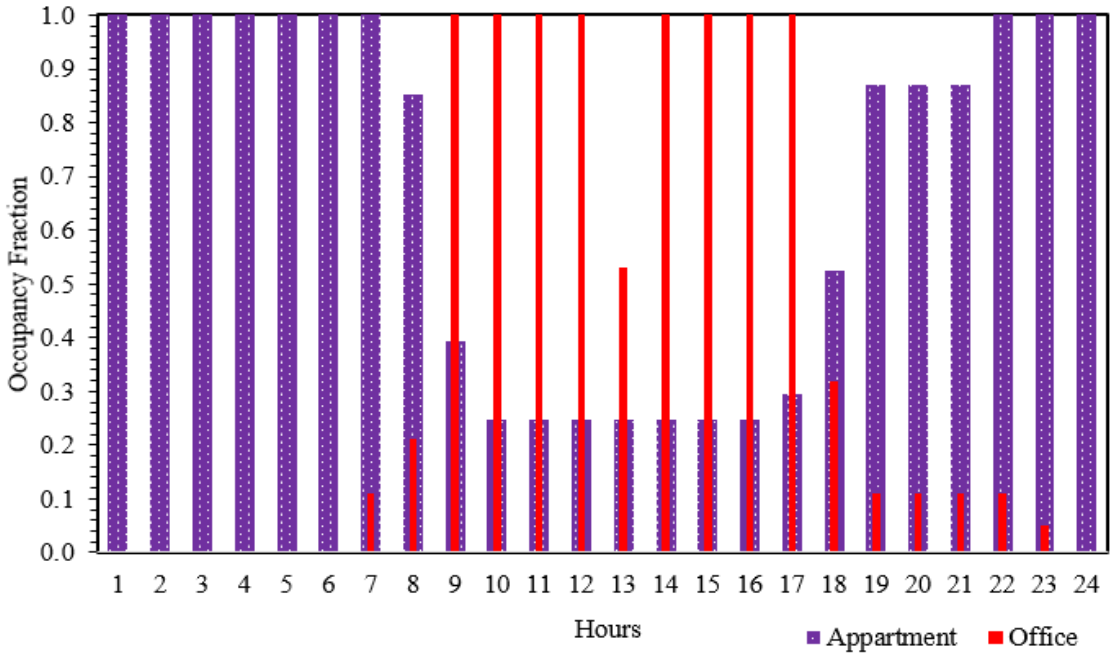

Fig. 10. Occupancy schedules for the office zone (weekdays) and the apartment zones (all days) [77].

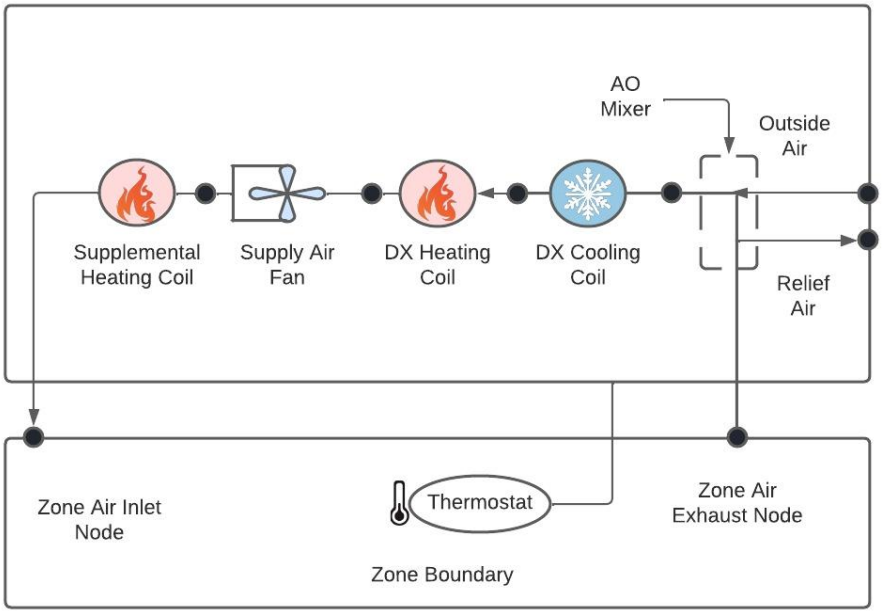

Fig. 11. Packaged Terminal Heat Pump (PTHP) adopted form [78].

Table 4. Set points and HVAC system (PTHP) attributes.

Design Parameters	Values
Supply Fan Total Efficiency	0.7
Motor Efficiency	0.9
Cooling Coil Energy Efficiency Ratio (EER)	2.52 (Wh)
Heating Coil Coefficient of Performance (COP)	2.75
Cooling Set Point	26°C
Cooling Set Back	28°C
Heating Set Point	20°C
Heating Set Back	18°C
Humidification Ratio	25%
Dehumidification Ration	60%

3.6 Numerical Simulation and Optimization

Dynamic energy simulations are performed using EnergyPlus9.2. The Energyplus program works as a modular system and implements the detail of building physics for thermal and energy analysis [79]. Further, Designbuilder, as a graphical interface of Energyplus, allows us to create a virtual environment and build a prototype with controlled and defined parameters. Coupling Designbuilder and EnergyPlus enable us to analyze and evaluate the energy demand for a potential new building envelope system in different environmental conditions [80]. Moreover, Energyplus offers precision and accuracy; owing to this, it has been a valuable tool among researchers for evaluating the thermal and energy performance of several buildings with different mechanical systems and environmental changes [81].

Energyplus uses the conduction finite difference (ConFD) solution algorithm to simulate PCM. The CondFD algorithm applies an implicit finite difference scheme based on Adams-Moulton solution coupled with the enthalpy temperature function to consider the temperature-dependent properties of the material [82]. The implicit formulation for an internal node follows equation 1, and the thermal conductivities (kW and kE) in equation 1 are calculated using equation 2 and equation 3. To implement changes in specific heat capacity at every node during the phase transition of PCM, the value of specific heat (Cp) in equation 1 gets updated in each iteration using equation 4. The variable Cp of phase change material depends upon the changing temperature and enthalpies values at nodes during iteration (equation 4)[82].

$$\rho C_P \Delta x \frac{T_i^{j+1} - T_i^j}{\Delta t} = (k_W \frac{(T_{i+1}^{j+1} - T_i^{j+1})}{\Delta x} + k_E \frac{(T_{i-1}^{j+1} - T_i^{j+1})}{\Delta x}) \quad \ldots\ldots\ldots\ldots\ldots \quad (1)$$

$$k_W = \frac{(k_{i+1}^{j+1} + k_i^{j+1})}{2} \quad \ldots\ldots\ldots\ldots\ldots\ldots\ldots\ldots\ldots\ldots\ldots \quad (2)$$

$$k_E = \frac{(k_{i-1}^{j+1} + k_i^{j+1})}{2} \quad \ldots\ldots\ldots\ldots\ldots\ldots\ldots\ldots\ldots\ldots\ldots \quad (3)$$

$$C_p = \frac{h_{i.new} + h_{i.old})}{T_{i.new} + T_{i.old}} \quad \text{..... (4)}$$

Where:

Cp	Specific heat capacity (kJ/kg-K)
ρ	Density(kg/m^3)
Δx	Layer thickness (m)
Δt	Calculation time step (s)
T	Node temperature (K)
h	Enthalpy (kJ/kg).
$j+1$	Simulation time step
i	Node being modelled
$i+1$	Adjacent nodes towards inner side
$i-1$	Adjacent nodes outer sides
k_W	thermal conductivity for the interface between increase node and $i+1$ node
k_E	is thermal conductivity for the interface between i node and $i-1$ node
j	Previous time step

Accordingly, in CondFD algorithm, elements are discretized using equation 5, creating nodes based on their thermal diffusivity of the material (α), time step (Δt), and space discretization constant (c) selected [82]. For the current research, space discretization constant (c) was set to 3, as recommendation by [83], and a time step of 2 min was selected.

$$\Delta x = \sqrt{c \,.\, \alpha \,.\, \Delta t}\sqrt{\frac{\alpha \,.\Delta t}{F_o}} \quad \text{..... (5)}$$

3.6.1 Validation

To validate the implementation finite-difference algorithm (ConFD) in Energyplus, our research group used the experimental data from [84] and compared the numerical simulation results. Cui et al. examined the impact of PCM23 on the inside temperature of a cubical experimental model having dimensions of 0.5 m, x 0.5 m x 0.5 m, and a thickness of 0.02 m. An identical model was designed in Design-Builder software and simulated using Energyplus for 48 hours with the same weather file used during the experiment. Fig.12 shows the experimental and numerical simulation models. The inside air temperature from the experimental and simulation are shown in Fig.13. The difference between the simulation results and experimental data is less than 4.5%, which falls within the acceptable limit [85]. In addition to this, our research group also analytically verified Stefan's problem performed by Tabares-Velasco et al. [83]. The outcome analytical and numerical solution was in good agreement demonstrating the PCM implementation correctness. More details about the analytical and experimental validation can be found in [85].

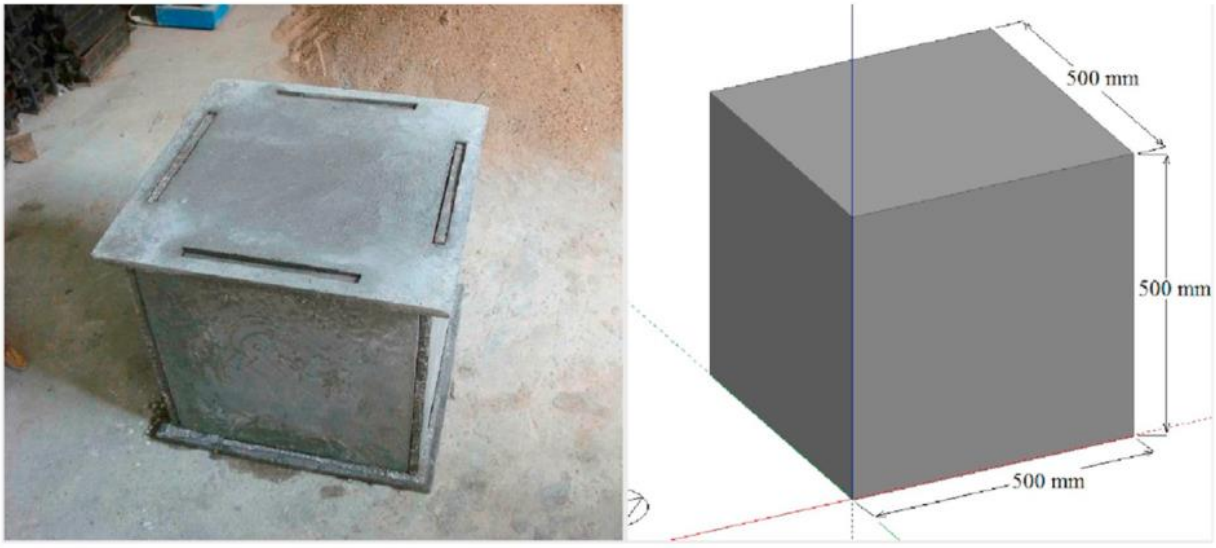

Fig. 12. Experimental and numerical simulation models [85].

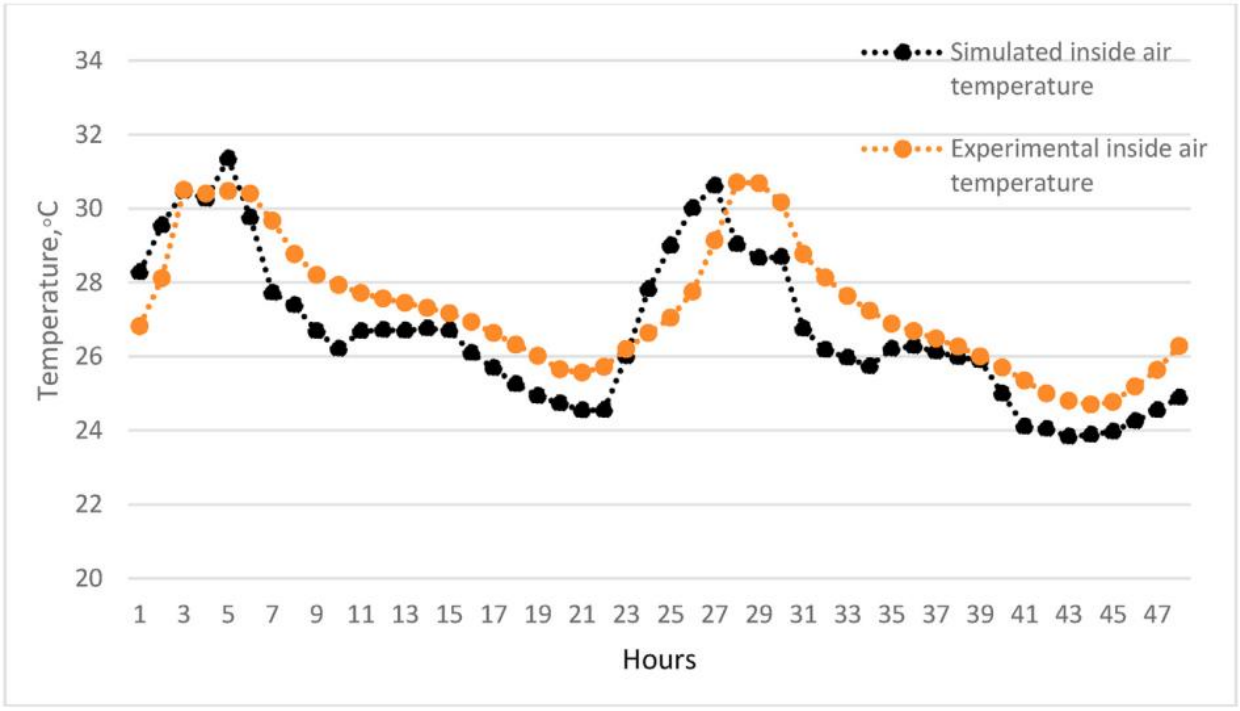

Fig. 13. Simulated and experimental inside air temperature values [85].

3.6.2 Optimization

The change in cooling energy demand (ΔCED) with the incorporation of PCM in the building is the effect of PCM-specific property. Mathematically, the ΔCED is represented by Equation 6. If the results of the ΔCED are positive, the value is regarded as cooling energy saving (CES), which is the potential of PCM in cooling energy conservation. In contrast, the negative results show a further increase in CED, showing the negative impact of PCM incorporation. The current research selected the optimum PCM based on the maximum CES.

$$\Delta\mathrm{CED} = \mathrm{EC(Without\ PCM)} - \mathrm{EC\ (With\ PCM)} \quad \ldots\ldots\ldots\ldots\ldots\ldots\ldots\ldots\ldots\ldots\ldots\ldots\ldots\ldots \quad (6)$$

Where:

ΔCED = Change in cooling energy demand (kWh)

EC (Without PCM) = Energy Consumption without the incorporation of PCM (kWh)

EC (With PCM) = Energy Consumption with the incorporation of PCM (kWh)

3.6.3 Natural Ventilation

In the present research, two different ventilation strategies, free night ventilation, and changeover ventilation, are used: For the free night ventilation, the building windows are kept open from 0:00 to 6:00 hours irrespective of the outdoor and indoor conditions (Boundary Condition 2). In case of changeover ventilation, windows and doors are open if the inside temperature is greater than outside (Tinside > Tout) and the inside temperature is higher than the set temperature for ventilation (Tinside > Tset) (Boundary Condition 3). To avoid over-cooling, the ventilation set temperature is adjusted to 22°C. In both the ventilation strategies, the maximum window opening fraction is fixed at 50%, and natural ventilation is implemented using an Airflow Network (AFN).

Compared to airflow calculation by the design rate, AFN modeling offers more advanced calculations by providing the ability to simulate wind-driven multizone airflows and forced air circulation with HVAC system. In addition, AFN model takes into account the infiltration and leakages during the performance evaluation of the distribution system. The airflow into the zone during Natural ventilation is governed by pressure differences caused by buoyancy and wind. [20]. The ANF models work in three sequential steps:

i. Pressure and airflow calculations:

The ANF model comprises two nodes, an inlet and an outlet, linked by airflow components. The variable at the node is pressure, and at the linkage, it is airflow. Bernoulli's equation governs the pressure difference between the inlet and outlet: Equation 7. The wind pressure calculated from Bernoulli's equation with the assumption of no height change or pressure losses can be written as Equation 8. By adding wind pressure impacts and with the rearrangement of terms, Bernoulli's equation (Equation 7) can be written as Equation 9.

$$\Delta P = (Pn + \frac{\rho V_n^2}{2}) - (Pm + \frac{\rho V_m^2}{2}) + \rho g(z_m - z_n) \quad \ldots\ldots\ldots\ldots\ldots\ldots\ldots (7)$$

$$Pw = Cp\,\frac{\rho V_{ref}^2}{2} \quad \ldots\ldots\ldots\ldots\ldots\ldots\ldots\ldots\ldots\ldots (8)$$

$$\Delta P = Pn - Pm + P_s + P_w \quad \ldots\ldots\ldots\ldots\ldots\ldots\ldots\ldots\ldots\ldots (9)$$

Where:

ΔP	Pressure difference between the nodes (Pa)	Vn	Airflow velocity at nodes n (m/s)
Pn	Total pressures at nodes n (Pa)	Vm	Airflow velocity at nodes m (m/s)
Pm	Total pressures at nodes m (Pa)	ρ	Air density (kg/m³)
P_s	Pressure difference due to density and height (Pa)	g	Gravitational acceleration (m/s²)
P_w	Pressure difference due to wind (Pa)	z_n	Elevation at nodes n (m)
V_{ref}	Reference wind speed at local height (m/s)	z_m	Elevation at nodes m (m)
		Cp	Wind surface pressure coefficient

ii. Node temperature and humidity calculation

First, equation 10 is used for node temperature to find temperature distribution across the duct. After that, the air temperature at the outlet is calculated using Equation 11. Similarly, the humidity ratio distribution and the humidity ratio at the outlet can be found using Equations 12 and 13, respectively.

$$mC_{p\_air}\frac{dT}{dx} = UP(T_\infty - T) \ldots\ldots\ldots\ldots\ldots\ldots\ldots\ldots\ldots\ldots (10)$$

$$T_0 = T_\infty + (T_i - T_\infty).\exp\left(-\frac{UA}{mC_p}\right) \ldots\ldots\ldots\ldots\ldots\ldots\ldots\ldots\ldots\ldots (11)$$

$$m\frac{dw}{dx} = U_m P(W_\infty - W) \ldots\ldots\ldots\ldots\ldots\ldots\ldots\ldots\ldots\ldots (12)$$

$$W_o = W_\infty + (W_i - W_\infty).\exp\left(-\frac{U_m A}{m}\right) \quad \text{..... (13)}$$

Where:

C_p Specific heat of airflow (J/kg-K)

m Airflow rate (kg/s)

T Temperature (°C)

$\frac{dT}{dx}$ Rate of change in temperature

T_∞ Surrounding temperature (°C)

U Overall heat transfer coefficient (W/m2-K)

T_i Inlet air temperature

T_0 Outlet air temperature

P Perimeter (m)

W Humidity ratio (kg/kg)

$\frac{dw}{dx}$ Rate of change in humidity

W_∞ Humidity ratio of surrounding air (kg/kg)

U_m Moisture transfer coefficient (kg/m^2-s)

A Surface area (m^2)

W_i Inlet air humidity ratio(kg/kg)

W_o Outlet air humidity ratio(kg/kg)

iii. Sensible and latent load calculations

The Airflow Network (AFN) model calculates the sensible and latent loads for multizone, duct conduction, and leakage. Besides, AFN also considers the impact of infiltration and mixings in the load calculations. The multizone load calculation includes the airflow from the outside (Infiltration) or adjacent zone (Mixing) into the zone and is distinguished into two categories: constant and variable. Under the constant categories, the mass flow rate is summed and multiplied by specific heat for both infiltration and mixing (Equation 14) to calculate sensible loads. In addition, Equation 15 is used under variable categories where the impact of indoor (zone) and outdoor air temperature is considered in calculating the sensible load for multizone. Similarly, the latent load for multizone can be calculated using Equation 16 and Equation 17. The air distribution system (ADS) loads due to duct conduction and leakage are computed using Equation s 18 and 19. For a more comprehensive overview, one can refer to [86].

$$MCP_{airflow} = m_{inf}C_p + \sum(m_{mix}C_p) \quad \text{..... (14)}$$

$$MCPT_{airflow} = m_{inf}C_pT_{amb} + \sum(m_{mix}C_pT_{zone}) \quad \text{..... (15)}$$

Where:

$MCP_{airflow}$ Sum of air mass flow rate multiplied by specific heat for infiltration heat for infiltration and mixing (W/K)

$MCPT_{airflow}$ Sum of air mass flow rate multiplied by specific heat and temperature for infiltration and mixing (W)

m_{inf} Incoming air mass flow rate from outdoors (kg/s)

T_{amb} Outdoor air dry-bulb temperature (°C)

T_{zone} Adjacent zone air temperature (°C)

$$M_{airflow} = m_{inf}C_p + \sum m_{mix} \quad (16)$$

$$MW_{airflow} = m_{inf}C_pW_{amb} + \sum(m_{mix}W_{zone}) \quad (17)$$

Where:

$M_{airflow}$ Sum of air mass flow rates for infiltration and mixing (kg/s)

$MW_{airflow}$ Sum of air mass flow rate multiplied by humidity ratio for infiltration and mixing (kg/s)

m_{inf} Incoming air mass flow rate from outdoors (kg/s)

W_{amb} Outdoor air humidity ratio (kg/kg)

W_{zone} Adjacent zone air humidity ratio (kg/kg).

$$Q_{ADS,i} = \sum_j Q_{cond(i,j)} + Q_{leak(i,j)} \quad (18)$$

$$Q_{ADS,m,i} = \sum_j Q_{cond\ m(i,j)} + Q_{leak\ m(i,j)} \quad (19)$$

Where:

$Q_{ADS,i}$ Total sensible load in the i-th zone due to ADS losses (W)

$Q_{cond(i,j)}$ Duct wall conduction loss at the j-th duct located in the i-th zone (W)

$Q_{leak(i,j)}$ Sensible supply leak loss at the j-th linkage located in the i-th zone (W)

$Q_{ADS,m,i}$ Total latent load in the i-th zone due to ADS losses (kg/s)

$Q_{cond\,m\,(i,j)}$ Duct wall vapor diffusion loss at the j-th duct located in the i-th zone (kg/s)

$Q_{leak\,m\,(i,j)}$ is latent supply leak loss at the j-th linkage located in the i-th zone (kg/s).

3.7 Performance Indicator

To evaluate the performance of PCM, it is important to know the exact status of PCM latent heat capacity exploitation [37]. To this aim, researchers come up with different efficiency indicators. Evola et al. (2013) introduced frequency of activation (FA) and PCM storage efficiency(ἡ) [37]. The author considered the inside surface temperature of the wall, claiming that when the surface temperature is in the range of the PCM melting point, the PCM is active. At the same time, this is only valid for the condition where the PCM layer is located on the innermost side. For the PCM storage efficiency(ἡ), Evola et al. (2013) consider a ratio of positive heat flux entering the wall over 24 hours to the latent capacity of PCM (Equation 20) [37]. However, there is no clarity about the charging and discharging of PCM as the efficiency depends upon the complete daily cycle [38]. Castell and Farid (2014) [38] experimentally examined the indicator presented by Evola et al. (2013) [37] and concluded that the proposed indicator considers complete solidification of PCM during the night, which is unlikely and unrealistic. Moreover, it seems to fail to present the benefits of PCM when buildings have high thermal inertia, heavy insulation, and no solar gains [37].

$$ἡ_{PCM} = \frac{E_{st}}{LC} = \frac{\int_p (q_L^+ + q_R^+) \times d_t}{LC} \quad (20)$$

Ramakrishnan et al. (2016) used a different approach and used the node temperature from the Energyplus output to get the exact temperature of PCM during the phase transition process [39]. Based on the node temperature, the fraction of latent capacity charged and discharged (Lc and Dc) were found. In addition, the time fractions of charging and discharging (Tc and TDC) were also observed by limiting each cycle to 12 hours. Combining the fraction of latent capacity and time fraction, Ramakrishnan et al. (2016) [39] introduced the cooling efficiency coefficient (CE) and

heating efficiency coefficient (HE) to observe the efficiency of PCM. The Equation s for CE and HE presented by Ramakrishnan et al. (2016) are shown in Equation s 21 and 22, respectively.

$$CE = \sqrt{L_c \times T_c} \quad \text{..... (21)}$$

$$HE = \sqrt{L_{Dc} \times T_{Dc}} \text{..... (22)}$$

Where:

$$L_c = \frac{diurnal\ latent\ charge}{Latent\ heat\ capcity} \qquad D_c = \frac{diurnal\ latent\ discharge}{Latent\ heat\ capcity}$$

$$T_c = \frac{charging\ duration\ minutes}{Daytime = 720\ minutes} \qquad T_{Dc} = \frac{charging\ duration\ minutes}{Night\ time = 720\ minutes}$$

However, the author limits the charging and discharging cycle to day and night by assuming that the PCM follows 12 hours duration in each cycle. This ideal situation may not be realistic as the PCM charging and discharging are temperature dependent and may not follow the 12-hour duration for charging and discharging. Furthermore, efficiency coefficients are presented using the linear relation with the latent capacity and time fraction (Equation s 21 and 22), which is only applicable in an ideal situation. The values may lead to misinterpretation of the performance of PCM in a real case.

To have a realistic perspective of PCM performance, new performance indicators, energy-charged coefficient (ECC), and energy discharged coefficient (EDC) are presented in this research. The ECC and EDC consider the actual energy stored or released by PCM calculated on hourly basis from the exact temperature of PCM inside the wall. Further, to account the deviation from ideal behavior, the new indicators consider the actual duration of charging or discharging. In this context, firstly, the actual temperature of PCM was recorded using the actual node temperature of PCM from Energyplus output. Using the actual temperature of PCM, energy charged (EC) and discharged (ED) during a cycle would be found according to the process demonstrated by [39]. The calculation of EC and DC is further explained using the enthalpy curve of PCM26 presented in Fig. 14. The phase transition temperature of PCM26 ranges from 24°C to 28 °C and the total latent energy storage (TLES) capacity is 219 kJ/kg. Assuming that for a particular duration, the PCM26 temperature increased from 24°C to 27°C. At the point when the PCM26 temperature

reaches 27°C, the latent energy stored by PCM corresponds to point (a) (Fig.14). The energy charge (EC) by the PCM26 can be obtained using Equation 23, which is the difference of latent energy at 24°C (Base value) and 27°C. At this point, it is assumed that the PCM26 start discharging and release stored energy to the surrounding until the temperature of PCM26 drops to 26°C (point (b)). Now, Energy discharge (ED) can be calculated using Equation 24. The actual charging fraction (CF) and discharging fraction (DF) can be calculated using Equations 25 and 26, respectively. The information CF and DF identify to what extent the PCM is active during each cycle. One can also observe the inactive state of PCM as the observed node temperature above the peak transition temperature (The peak value in Fig. 9) shows the liquid state of PCM. Similarly, the temperature below the solidification point (Base value in Fig. 9), PCM will be in a solid state. Accordingly, the actual time taken for EC and ED would be calculated and further used to find the deviation of PCM from ideal behavior. In an ideal condition, the PCM is expected to charge and discharge following 12 hours duration. Hence, the time fraction of charging (CTF) and discharging (DTF) would be calculated against 12 hours using Equations 27 and 28. Also, the time duration for which PCM remains inactive can be found.

$$\mathrm{EC}_{PCM} = \text{Enthalpy value at point(a)} - \text{Base value} \quad \ldots\ldots\ldots\ldots\ldots\ldots\ldots\ldots (23)$$

$$\mathrm{ED}_{PCM} = EC_{pcm} - \text{Enthalpy value at point(b)} \quad \ldots\ldots\ldots\ldots\ldots\ldots\ldots\ldots (24)$$

$$\mathrm{CF} = \left(\frac{\mathrm{EC_{PCM}}}{LC}\right) \ldots\ldots\ldots\ldots\ldots\ldots\ldots\ldots\ldots\ldots\ldots\ldots\ldots\ldots\ldots\ldots (25)$$

$$\mathrm{DF} = \left(\frac{\mathrm{ED_{PCM}}}{LC}\right) \ldots\ldots\ldots\ldots\ldots\ldots\ldots\ldots\ldots\ldots\ldots\ldots\ldots\ldots\ldots\ldots (26)$$

$$\mathrm{CTF} = \left(\frac{\text{Actual time of Charging}}{\text{12 hours}}\right) \ldots\ldots\ldots\ldots\ldots\ldots\ldots\ldots\ldots\ldots\ldots\ldots\ldots\ldots\ldots (27)$$

$$\mathrm{DTF} = \left(\frac{\text{Actual time of discharging}}{\text{12 hours}}\right) \ldots\ldots\ldots\ldots\ldots\ldots\ldots\ldots\ldots\ldots\ldots\ldots\ldots\ldots\ldots (28)$$

Here, when actual energy is charged and discharged, and the corresponding time fractions are known, the behavior of PCM during each cycle can be evaluated using the energy charged coefficient (ECC) and energy discharged coefficient (EDC). The values of these novel indicators (ECC and EDC) can be found using Equation s 29 and 30. The values can be gauged against the scale presented in Fig.13. For illustration purposes, three different cases are considered:

– Case 1: It is assumed that the PCM is fully charged within 12 hours. Thus, the values of CF and CTF will be equal to one. Putting the values of CF and CFT in Equation 29, the

value of ECC will also be equal to one. The value of one on the scale (Fig.15) will show the expectational behavior of PCM.

- Case 2: For this case, it is assumed that the CF value is one and the CTF value is 0.5, reflecting the short duration of charging (6 hours). The value of ECC on the scale (Fig.15) will be greater than one showing the exponential behavior of PCM during charging. The higher the value from one, the more the behavior of PCM is uncertain. A maximum value of 12 can be observed which will reflect the full charging of PCM in one hour. However, this situation is unlikely and unrealistic.
- Case 3. Similarly in this case, the CF value is assumed to be one, but the value of CTF is 1.5 reflecting the longer duration of charging (18 hours). In such situation, the value of ECC will be lower than one. The closer the value of ECC to zero, the higher the inefficiency of PCM.

The same applies for the energy discharged coefficient (EDC). To sum up, the closer the value of ECC and EDC to one, the better the PCM performance is during an individual cycle.

$$\text{ECC} = \left(\frac{\text{Charging Fraction}}{\text{Charging Time fraction}}\right) \quad (29)$$

$$EDC = \left(\frac{Disharging\ Fraction}{Discharging\ Time\ fraction}\right) \quad (30)$$

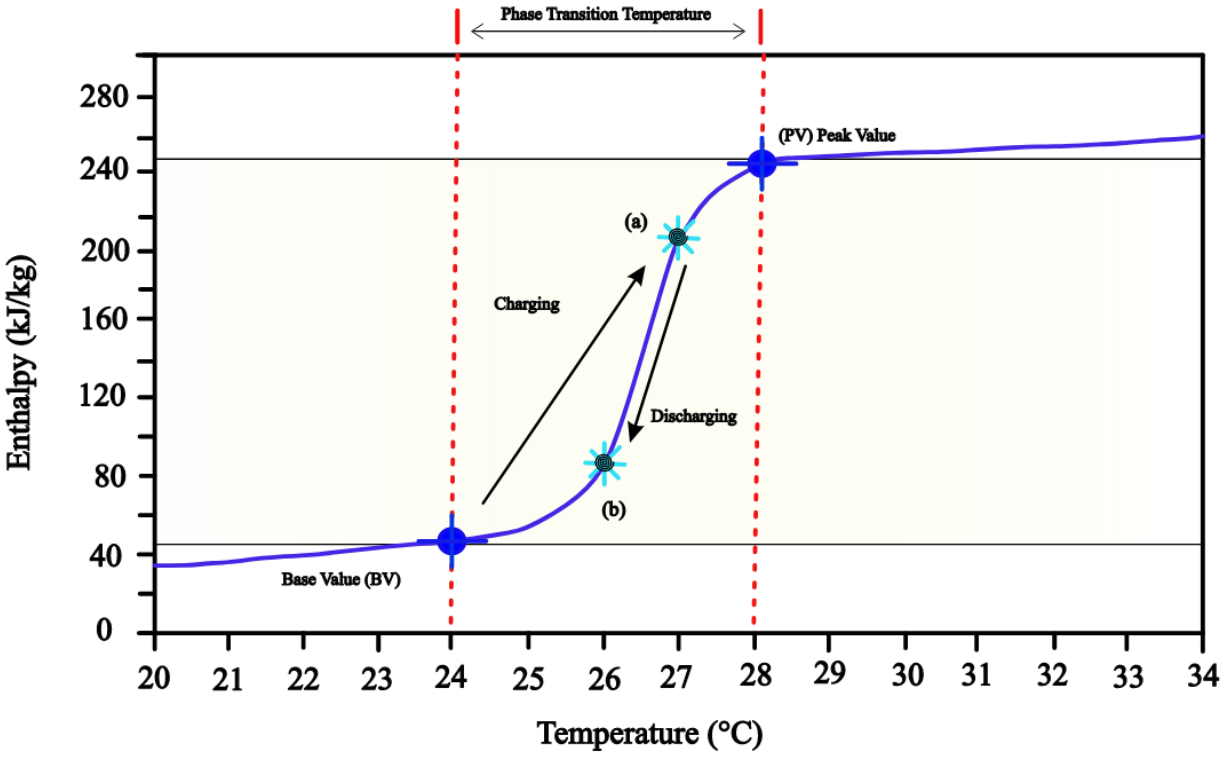

Fig. 14. Enthalpy curve of PCM26 presented for charging and discharging demonstration

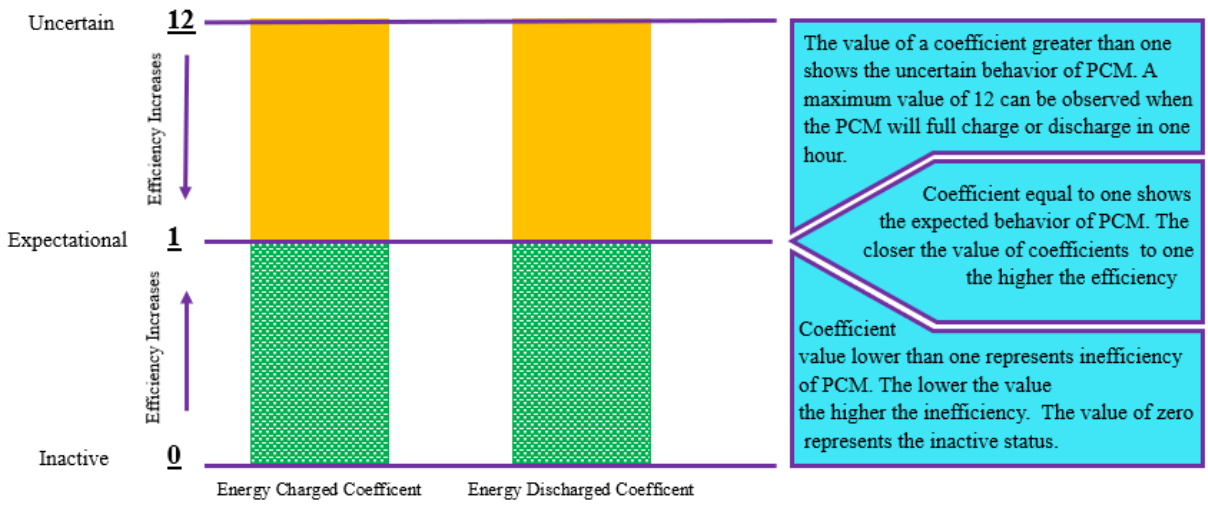

Fig.15 Efficiency scale based on the values of energy charged coefficient (ECC) and energy discharged coefficient (EDC)

In combination with the new proposed indicator, a very popular indicator, energy saving rate (ESR), shows the percentage reduction in CED with the application of PCM can be calculated using Equation 31. The higher value of ESR shows the better performance of PCM in energy conservation. Contrary, if the value of ESR is negative, it shows a further increase in CED, and evidently, PCM use is unfavorable [81]. Although the ESR is a widely used indicator for PCM performance, the value is highly influenced by initial energy demand; lower energy demand sometimes results in a higher ESR value. Thus, using ESR alone is not enough to determine the PCM CES potential [11].

$$\mathrm{ESR_{pcm}} = \left(1 - \frac{\mathrm{CED_{pcm}}}{\mathrm{CED_{ref}}}\right) \times 100 \quad \ldots\ldots\ldots\ldots\ldots\ldots\ldots\ldots\ldots\ldots \quad (31)$$

3.8 Summary

The content discussed in each section of Chapter 3 (methodology) is summarized as follows:

- In the first section, the indoor boundary conditions are defined, including the HVAC schedule, natural ventilation, and changeover ventilation details.
- Thirteen different zones from the Koppen climate classification for the future were considered, and three representative cities from each zone were selected.
- Mid-rise apartment building from ANSI/ASHRAE is used as a building model. The PCM layer is introduced to the inner side of the wall and the roof.
- Energyplus as a simulation engine was introduced, and the results of Energyplus were validated with experimental data. Moreover, the Airflow network is used to implement the ventilation strategies.
- Novel performance indicators ECC and EDC were introduced.

Chapter 4- Result and Discussion

Overview

This chapter is divided into four major sections, which include the results and discussion under different boundary conditions. Section 4.1 presents energy savings with the PCM incorporation under indoor temperature control conditions. In the next section, section 4.2, the savings with the night ventilation are discussed, followed by the discussion on the combination of changeover ventilation and PCM in section 4.3. In the last section, the best energy-saving strategy is presented.

4.1 Energy saving with PCM under control condition

This section presents the cooling energy savings (CES) with the refurbishment of PCM under controlled conditions. In the control condition, the mechanical cooling (HVAC) operation is matched with the occupancy fraction (Fig. 10), and the CES in B1-SPCM were observed against B1-SRef. Table 5 (b1) shows the optimum PCM and the corresponding CES for each city. The optimum PCM in B1-SPCM ranges from PCM27 to PCM30, and the CES corresponding to the optimum PCM in each city varies according to climatic conditions. All the simulation results for PCM integration under controlled conditions are attached in Appendix-A.

In the tropical region (Koppen map A-zone), PCM28 remains an optimum PCM for all the cities except Yangon (Am), where the optimum is PCM27. Despite having a narrow range of optimum PCM, a variation in CES can be observed. The highest CES was obtained in Hong Kong (Am), where PCM28 tends to reduce 3514 kWh (2.7%). Similarly, in Addis Ababa (Aw) with PCM28, the CES was 754 kWh (1.2%), the lowest in the tropical region. Although Hong Kong and Addis Ababa share the same optimum PCM (PCM28), the lower savings show insignificant PCM performance in Addis Ababa. Looking at Fig.16 (a), it is apparent that the energy stored by PCM28 in Addis Ababa is very low and does not exceed 12% of its capacity.

Similarly, the energy charging coefficient (ECC) values are close to zero in Addis Ababa (Fig.16 (b)), which shows the inefficiency of PCM. The insignificant performance of PCM can be associated with the meteorological conditions of Addis Ababa. To get more insight, the outdoor dry-bulb temperature of Addis Ababa is presented in Fig.17. As can be seen from the figure, most of the time the outdoor temperature is in the range of HVAC setpoints and under the indoor boundary conditions where HVAC is operational for 24 hours the temperature gradient between indoor and outdoor environment is insignificant. In conditions with less indoor and outdoor

temperature gradient, the integration of PCM will result in limited energy savings [87]. This can be attributed to the insufficient temperature fluctuation inside the wall, which is not enough to charge and discharge the PCM located on the inner side of the wall.

Likewise, in Bangalore and Miguel Hidalgo, located in the same climate zone (Aw) as Addis Ababa, the CES were modest compared to the CES reported in other zones (Am and Af) of the tropical region. The CES in Bangalore and Miguel Hidalgo were 1876 kWh (2.0%) and 2351 kWh (2.5%), respectively, while the CES in Am and Af zones varied from 2753 kWh to 3505 kWh. The results show that in control conditions, the PCM performs more effectively for CES in the Am and Af zone of the tropical region.

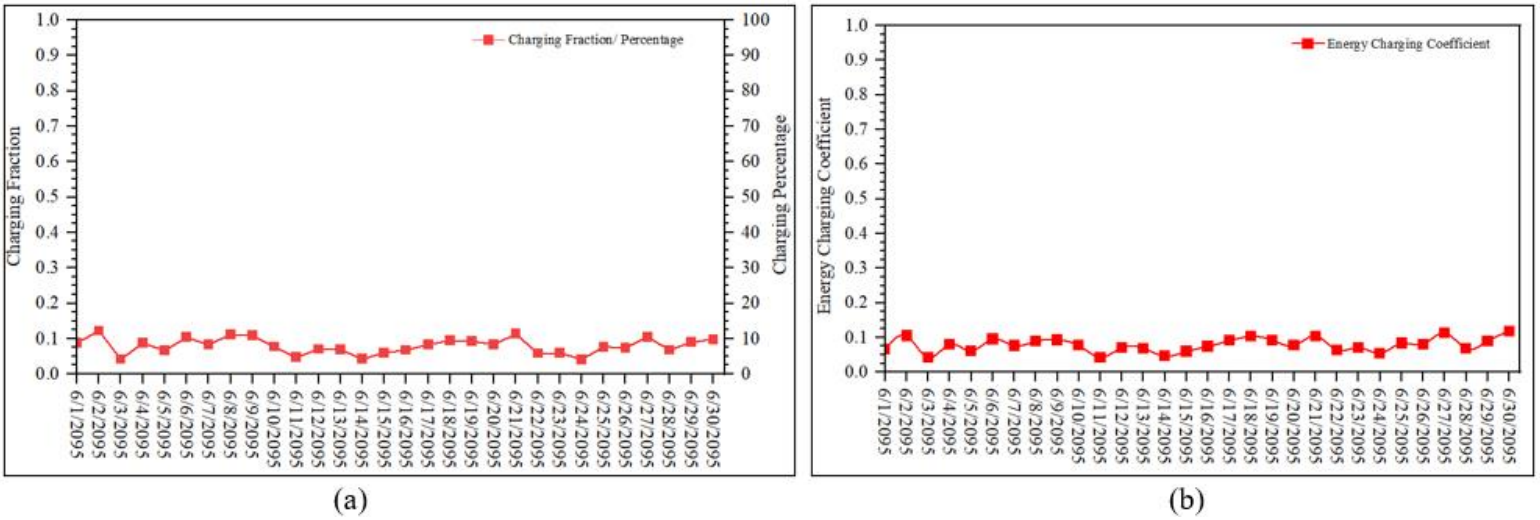

Fig. 16. (a) Charging fraction and (b) Energy charging coefficient of PCM28 for the month of June in Addis-Ababa

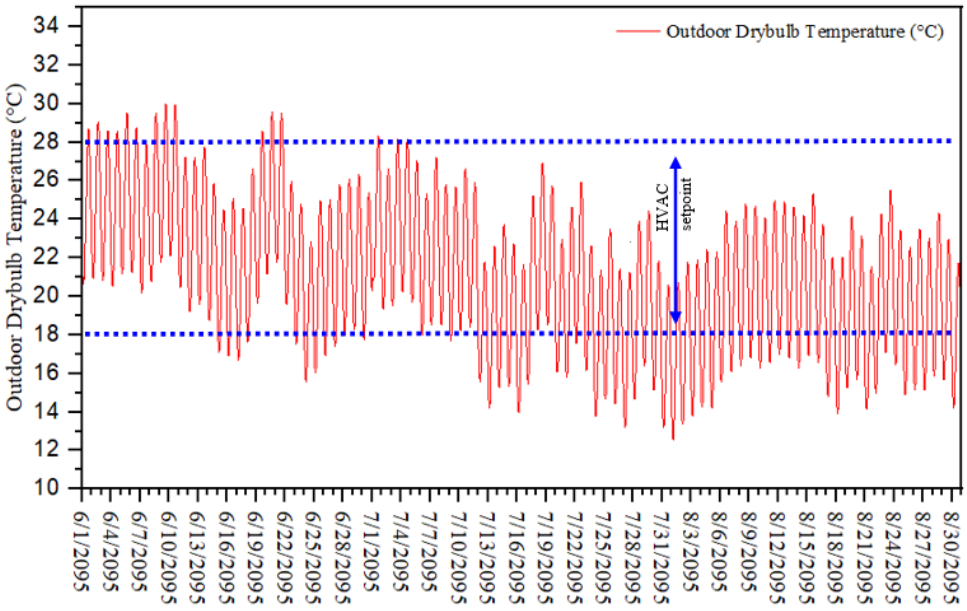

Fig. 17. Outdoor Dry bulb Temperature of Addis Ababa.

Table 5. Cooling Energy Savings and corresponding optimum PCM under different indoor boundary conditions.

		Boundary condition 1 (b1)				Boundary condition 2 (b2)				Boundary Condition 3 (b3)			
		B1-SRef	B1-SPCM			B2-SNV	B2-SNV+PCM			B3-SCV	B3-SCV+PCM		
Zone	City	CED [kWh]	Opt- PCM	CES [kWh]	ESR %	CED [kWh]	Opt- PCM	CES [kWh]	ESR %	CED [kWh]	Opt- PCM	CES [kWh]	ESR%
Am	Yangon	124835	PCM27	3108	2.5	80778	PCM30	773	1.0	83561	PCM27	2006	2.4
	Douala	118151	PCM28	2753	2.3	78016	PCM27	736	0.9	80190	PCM29	851	1.1
	Hong-Kong	128859	PCM28	3514	2.7	87558	PCM28	1236	1.4	86196	PCM28	906	1.1
Aw	Bangalore	94042	PCM28	1876	2.0	62006	PCM27	1292	2.1	68685	PCM23	170	0.2
	Addis-Ababa	60641	PCM28	754	1.2	39709	PCM28	1572	4.0	20681	PCM25	2900	14.0
	Miguel Hidalgo	92531	PCM28	2351	2.5	65399	PCM27	2472	3.8	67900	PCM23	294	0.4
Af	Kuala Lumpur	128240	PCM28	3251	2.5	89462	PCM31	849	0.9	89773	PCM27	1168	1.3
	Singapore	129732	PCM28	3505	2.7	88070	PCM28	962	1.1	88373	PCM26	1083	1.2
	Georgetown	117828	PCM28	3031	2.6	79778	PCM28	1222	1.5	83494	PCM29	1076	1.3
BSk	Kokshetay	84234	PCM27	1999	2.4	65266	PCM28	1864	2.9	60539	PCM26	2077	3.4
	Pavlodar	95225	PCM27	2243	2.4	75552	PCM29	1683	2.2	71852	PCM26	1647	2.3
	Aktobe	77920	PCM27	1473	1.9	59999	PCM28	1598	2.7	52602	PCM26	1583	3.0
BSh	Lahore	173554	PCM28	6814	3.9	138651	PCM30	2135	1.5	123413	PCM28	2257	1.8
	Monterrey	130859	PCM28	4076	3.1	97558	PCM31	1295	1.3	98537	PCM28	1886	1.9
	Jodhpur	153416	PCM28	5300	3.5	115011	PCM31	1265	1.1	109596	PCM28	2166	2.0
Bwh	Medina	146810	PCM28	5542	3.8	131384	PCM30	1638	1.2	119518	PCM29	3107	2.6
	Makkah	169722	PCM28	6321	3.7	139022	PCM30	2440	1.8	126084	PCM29	2772	2.2
	Biskra	147729	PCM28	5458	3.7	130287	PCM30	1244	1.0	118805	PCM30	2482	2.1
BWk	Atyrau	91984	PCM27	2328	2.5	71177	PCM27	1699	2.4	71817	PCM27	1532	2.1
	Turkestan	121376	PCM28	3973	3.3	104447	PCM29	1498	1.4	103109	PCM30	1845	1.8
	Kazalinsk	79768	PCM27	1701	2.1	62985	PCM28	1647	2.6	58298	PCM26	1402	2.4
Cfa	Wuhan	161723	PCM28	7240	4.5	124014	PCM29	2291	1.8	108919	PCM29	1844	1.7
	Paris	59939	PCM27	729	1.2	41436	PCM26	1872	4.5	23496	PCM26	2036	8.7
	Srinagar	59998	PCM27	907	1.5	43015	PCM26	2061	4.8	30078	PCM25	2530	8.4
Cfb	Stockholm	48485	PCM28	161	0.3	32594	PCM25	1795	5.5	4640	PCM25	2150	46.3
	London	53866	PCM28	435	0.8	35340	PCM25	2125	6.0	6514	PCM25	2408	37.0
	Bogota	54820	PCM28	521	0.9	35128	PCM26	1942	5.5	1556	PCM25	1202	77.2
Csa	Gaziantep	115691	PCM28	3933	3.4	95226	PCM29	2490	2.6	96126	PCM28	1755	1.8
	Kermanshah	113869	PCM28	4018	3.5	97238	PCM29	2229	2.3	98815	PCM30	2159	2.2
	Lisboa	87581	PCM27	2117	2.4	63367	PCM27	1910	3.0	62507	PCM25	1010	1.6
Cwa	Kathmandu	69133	PCM27	1214	1.8	45656	PCM26	1771	3.9	41251	PCM26	506	1.2
	Kunming	78094	PCM27	1555	2.0	50136	PCM27	2018	4.0	43440	PCM25	1805	4.2
	Nanning	165711	PCM28	6520	3.9	123433	PCM29	2239	1.8	109168	PCM29	1633	1.5
Dfa	Moscow	54913	PCM30	372	0.7	41844	PCM28	1060	2.5	26349	PCM25	1200	4.6
	Ottawa	87681	PCM28	1857	2.1	63717	PCM28	1636	2.6	57726	PCM26	1288	2.2
	St-Petersburg	44755	PCM30	21	0.0	31642	PCM28	1172	3.7	6020	PCM25	2269	37.7
Dfb	Helsinki	52153	PCM28	257	0.5	35456	PCM25	1745	4.9	7574	PCM26	1107	14.6
	Arhangelsk	35829	PCM30	-178	-0.5	24924	PCM24	1973	7.9	6000	PCM24	900	15.0
	Umea	45089	PCM30	-3	0.0	33229	PCM26	1433	4.3	3313	PCM25	737	18.2

Note: Boundary Condition 1: HVAC operation correspond with occupancy schedule
Boundary Condition 2: Free night ventilation (0:00 to 6:00 hours)
Boundary Condition 2: Changeover ventilation

In the arid region (Koppen map B-zone), PCM 28 remains optimum for the cities in BSh and BWh, while BWk and BSk report PCM27 as optimum. Further, the CES against the optimum PCM in BSh and BWh zones is higher compared to BWk and BSk. Lahore, located in the BSh zone, has the highest saving in the arid region, where the PCM28 reduces 6814 kWh (3.9%). In addition, Makkah and Biskra observed a substantial reduction in CED, where the PCM28 reduced 6321 kWh and 5458 kWh, respectively. In both cities, the ESR value remains at 3.7%. The PCM integration yields lower savings in the BSk zone. The CES in Pavlodar, Kokshetay, and Aktobe are 2243 kWh (2.4%), 1999 kWh (2.4%), and 1473 kWh (1.9%), respectively. Besides, the CES in Aktobe (1473 kWh) is the lowest in the arid region. The lower performance of PCM in the BSk zone is associated with the climatic condition of the BSk zone, where the summer is moderate and has a low indoor-outdoor temperature gradient [88]. This phenomenon is explained earlier for Addis Ababa.

In the temperate climate (Koppen map C-zone), most cities report PCM28 as optimum. In addition, higher saving values are observed in cities having PCM28 as an optimum. The city of Wuhan (Cfa) with PCM28 as an optimum shows the maximum saving in a temperate region with CES values of 7240 kWh (4.5%). Other cities, Nanning (Cwa), Kermanshah, and Gaziantep (Csa), also report PCM28 as an optimum with an ESR value greater than 3% and CES 6520, 4018, and 3933 kWh, respectively. On the other hand, despite sharing the same zone (Cfa) with Wuhan, the CES in Srinagar and Paris were reportedly very low, having a value of 907 kWh and 729 kWh in corresponding cities. To better understand the disparity of CES, direct normal solar radiation, wind speed, and humidity level are observed in Wuhan and Paris [87]. The direct normal radiation and wind speed directly relate to PCM performance, and the humidity level influences the CED [11]. From Fig.18, it can be observed that during the summer, most of the time, the direct normal radiations are higher in Wuhan, enhancing PCM charging capacity. The figure also shows that the wind speed is usually higher in Wuhan. The higher wind speed enhances the discharging capacity of PCM by increasing the convective heat transfer coefficient [11]. In addition, the humidity level in Paris (Fig.18) is higher than in Wuhan, and the dehumidification level (60%). Thus, to maintain the determined humidity level, HVAC will

demand additional energy in Paris, and the additional energy demand will reduce the potential energy savings with the refurbishment of PCM [11].

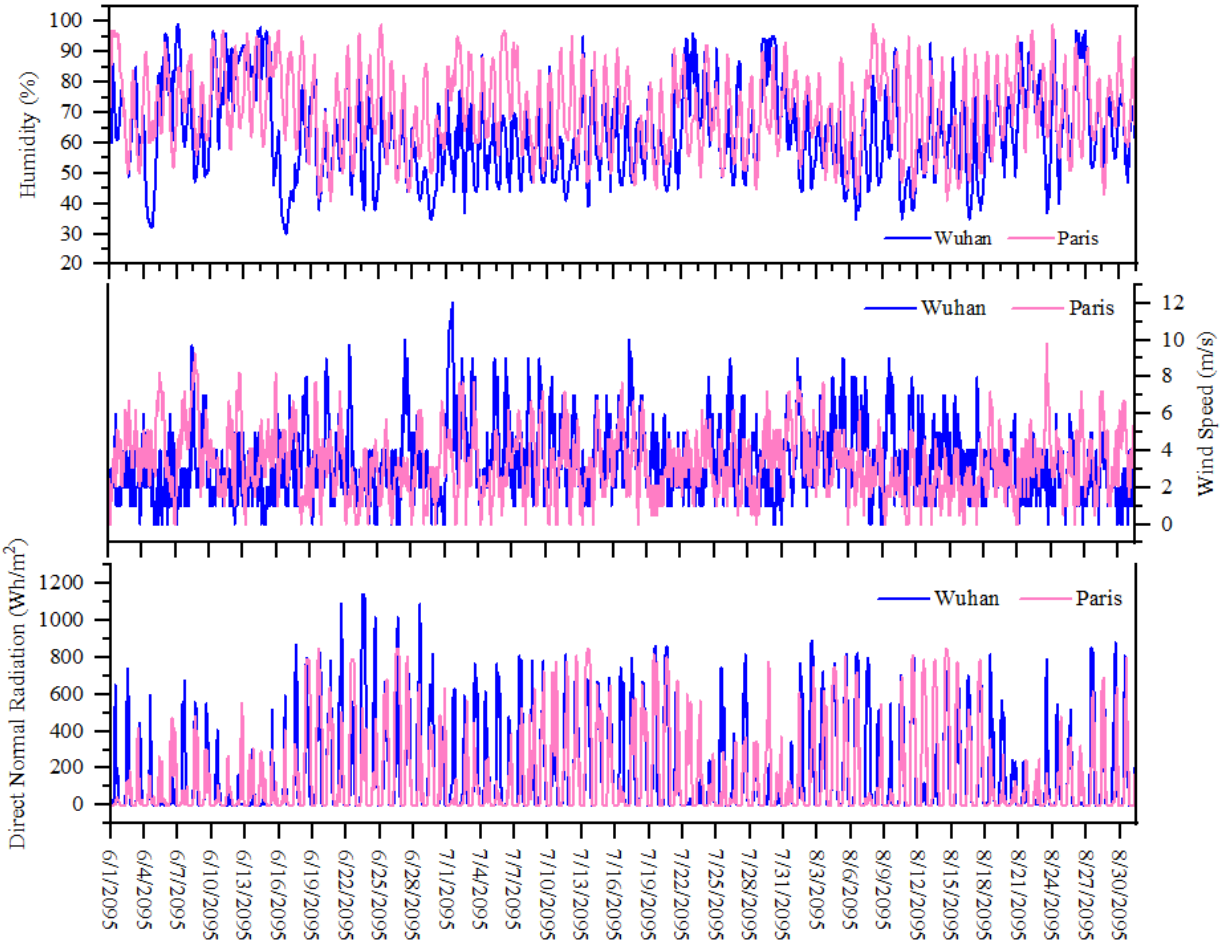

Fig. 18. Direct normal radiation, Wind speed, and humidity in Wuhan and Paris during the summer.

The refurbishing PCM in the Cfb zone results in very limited CES. The CES in Bogota (Cfb), London (Cfb), and Stockholm (Cfb) are 521 kWh (0.9%), 435 kWh (0.8%), and 161 kWh (0.3%), respectively. Further observation of the climate condition of the Cfb zone shows that the summer is moderate [88]. In such conditions, the outdoor temperature is comparable with the maintained indoor temperature by HVAC, and the PCM integration will be ineffective for CES. For clear understanding, the charging fraction (CF) of PCM and the heat flux through the wall in Stockholm, where the CES is lowest (161 kWh), are presented in Fig.19 and Fig.20, respectively. Fig. 19 shows that during June, the fraction of active PCM remains below 10% for the maximum time and does not exceed 20% of its capacity. As a greater portion of PCM remains inactive, this increases the thermal inertia of the wall and reduces the heat flux. The increase in thermal inertia of the wall is clear from Fig.20, where the heat flux through the wall with PCM is less compared

to the wall without PCM. Tunçbilek et al. (2020) also mentioned in their research that above or below the phase transition temperature, PCM only contributes to the thermal inertial of the wall [89].

The reported results of CES in humid continental climates (D region) corroborate the argument that inactive PCM in the wall only contributes to its thermal mass. Due to the increment in thermal inertia by inactive PCM, the CES values are negligible in humid continental climates (D region). Even in Arkhangelsk and Umea, the CED tends to increase by 178 kWh and 3 kWh, respectively, with the incorporation of PCM. To elucidate further, the PCM charging fraction (CF) and energy charging coefficient for the city of Arkhangelsk are presented in Fig .21. It can be seen from the Fig .21 that most of the time CF and ECC values are equal to zero showing that PCM is inactive. As specified earlier, the inactive PCM in the wall increases thermal inertia and creates a heat trap by reducing the heat flow. The trapped heat creates an overheating condition and increases the indoor temperature. Consequently, the CED by the HVAC increases and eventually lead to the adverse effect of PCM integration. Based on the results, it can be said that under controlled conditions (b1), where the building is mechanically cooled for 24 hours, the PCM use is unfavorable in humid continental climates for CES.

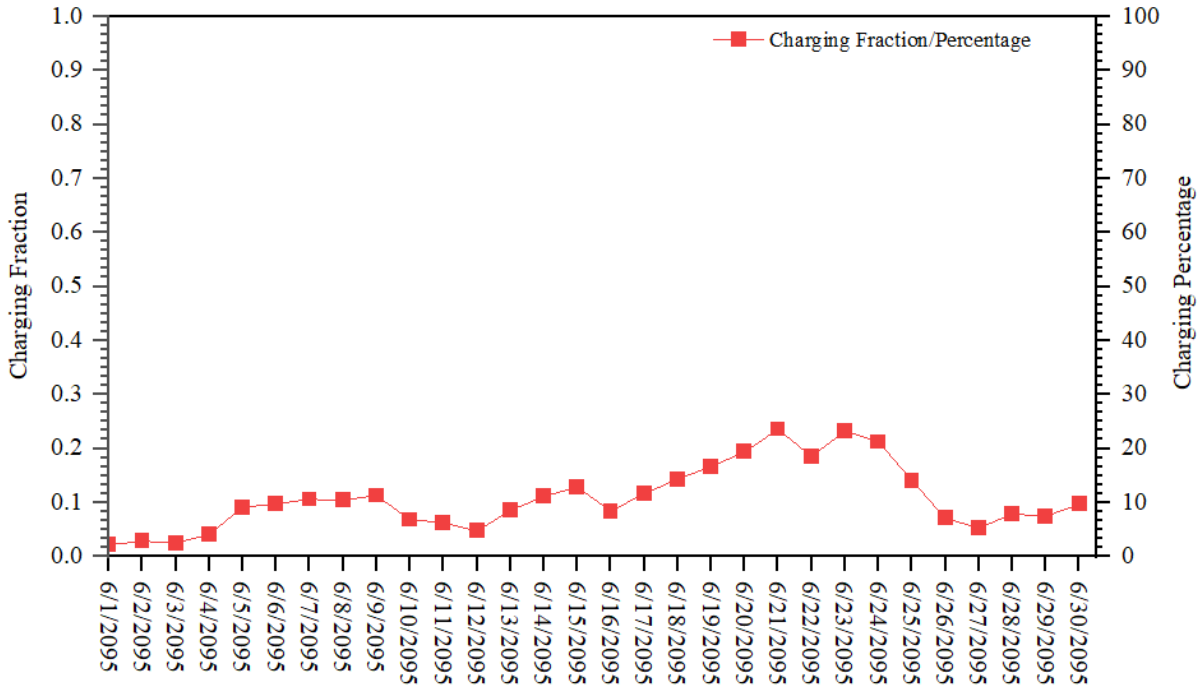

Fig. 19. Percentage/ Fraction of PCM charging in Stockholm for the month of June

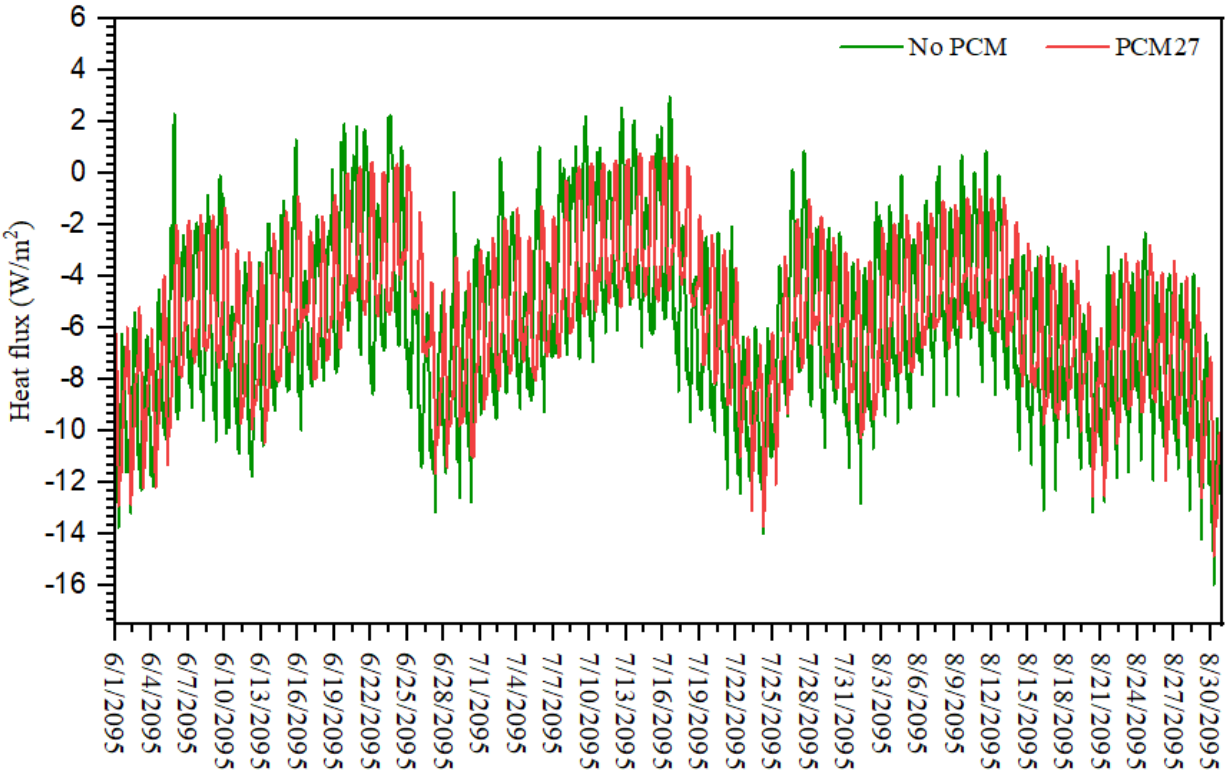

Fig. 20. Heat flux through the south face wall Stockholm during the summer.

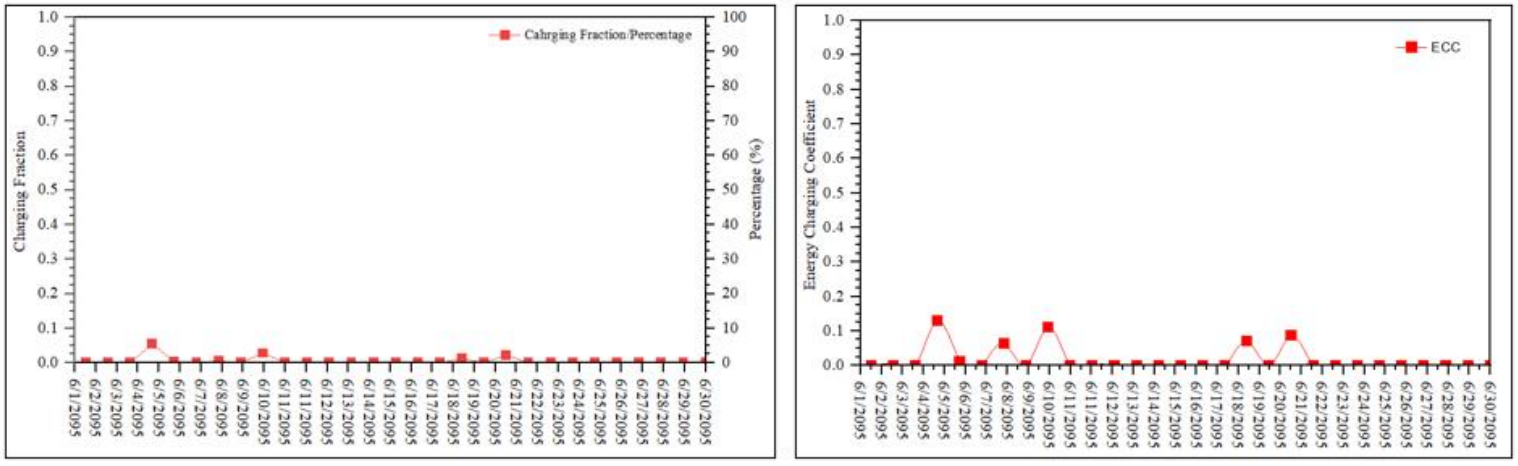

(a) (b)

Fig. 21. (a) Charging fraction and (b) Energy charging coefficient of PCM30 for the month of June in Arkhangelsk

4.2 Energy saving with night ventilation.

This section evaluates the influence of nocturnal natural convective cooling on building energy demand by free night ventilation (NV). To ensure free air circulation during nighttime, the windows were kept open from 0:00 to 6:00 hours regardless of the indoor thermal comfort conditions (i.e., HVAC is off). Further, in the second part of this section, the impact of free NV on PCM performance in the reduction of CED will be assessed.

4.2.1 Impact of night ventilation on cooling energy savings.

Compared to the control condition (B1-SRef), the CED reduction in free NV (B2-SNV) was remarkable, showing CES from 10% to 35%. The results of all the simulations results where B2-S_{NV} is compared with B1-S_{Ref} are shown in Appendix B. However, the CES, when free NV (B2-S_{NV}) is compared with the control condition (B1-S_{Ref}), can be attributed to the reduction in HVAC operation to 18 hours (as 0:00 to 6:00 hours HVAC is switched off) and the natural convective cooling due to NV. Whereas this is not a fair comparison as in free NV (B2-S_{NV}), the energy demand of the building is reduced to 18 hours resulting in savings of 6 hours of CED. Therefore, a new benchmark is introduced to have a fair comparison of CES due to free NV, where ventilation is completely prevented, and HVAC operation is 18 hours (same as in free NV). This new benchmark is named BM, and CES values, due to free NV, assessed against this new benchmark (BM) are presented in Fig. 22.

From Fig.22, it is apparent that B2-S_{NV} yields considerable savings in all the cities compared to BM. The highest savings are observed in Yangon, where the CES is 35136 kWh (30%), and the lowest CES is 7792 kWh, reported in Medina. The reason for this energy conservation is the drop in indoor temperature during free NV due to convective heat transfer, and as the temperature drops due to free NV, the HVAC system will require less cooling load to bring the indoor temperature back in the comfort range. To further explain, Fig.23 illustrates the phenomenon for two consecutive days in Yangon, where the cooling loads and the indoor temperatures for the following day are presented for both cases (BM and B2-S_{NV}). It can be observed that during B2-S_{NV}, the indoor air temperature drops and becomes closer to the HVAC setpoint in comparison to BM. Thus, the following day, HVAC needs less energy to bring the zone to the comfort range. The influencing factors in the application of NV for CES are inside temperature drop and temperature deviation from the setpoint identified by [90]. The relationship of inside temperature drop and temperature deviation from setpoint with CES was further analyzed using multi-regression analysis. Regression analysis is a powerful tool to predict the response of dependent variables toward independent variables [91]. Fig.24 shows the variation in

CES with the changing inside temperature drop, which follows the Equation $S=3.9044\Delta T+2.8186$ showing direct linear relation. Whereas the relation between CES and temperature deviation from the set points shows inverse relation following the Equation $y=-2.2116x+21.301$ (Fig.25). The relationships of both the inside temperature drop and temperature deviation from the setpoint with CES are statistically significant, indicating the R^2 values 0.8103 and 0.8424 respectively.

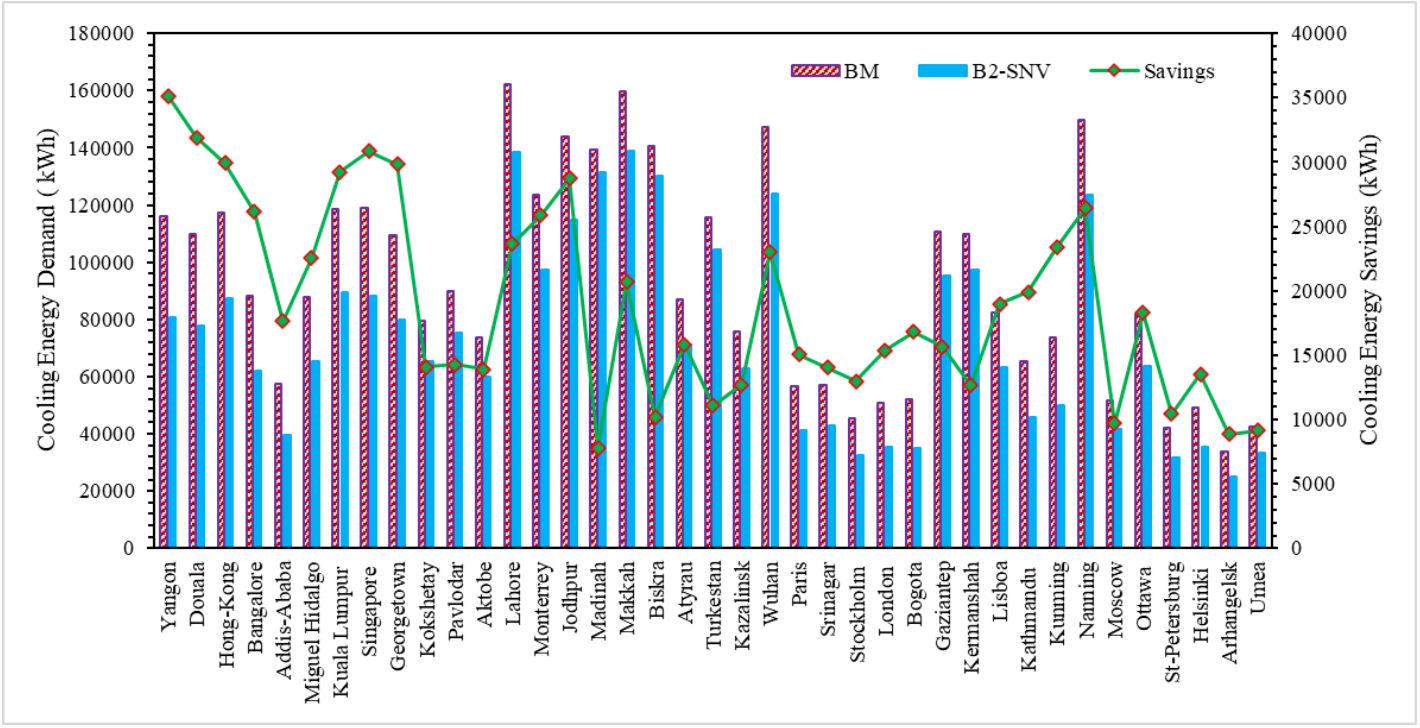

Fig. 22. Cooling energy demand and the corresponding savings under BMF_{-NV} and $B2\text{-}S_{NV}$

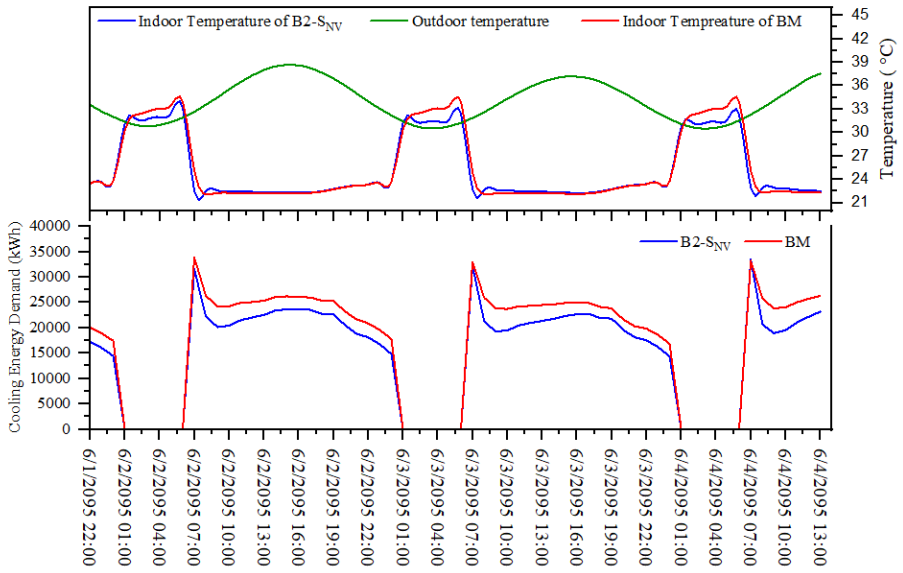

Fig. 23. Cooling energy demand and temperature profiles of one floor with NV in Yangon (two consecutive days).

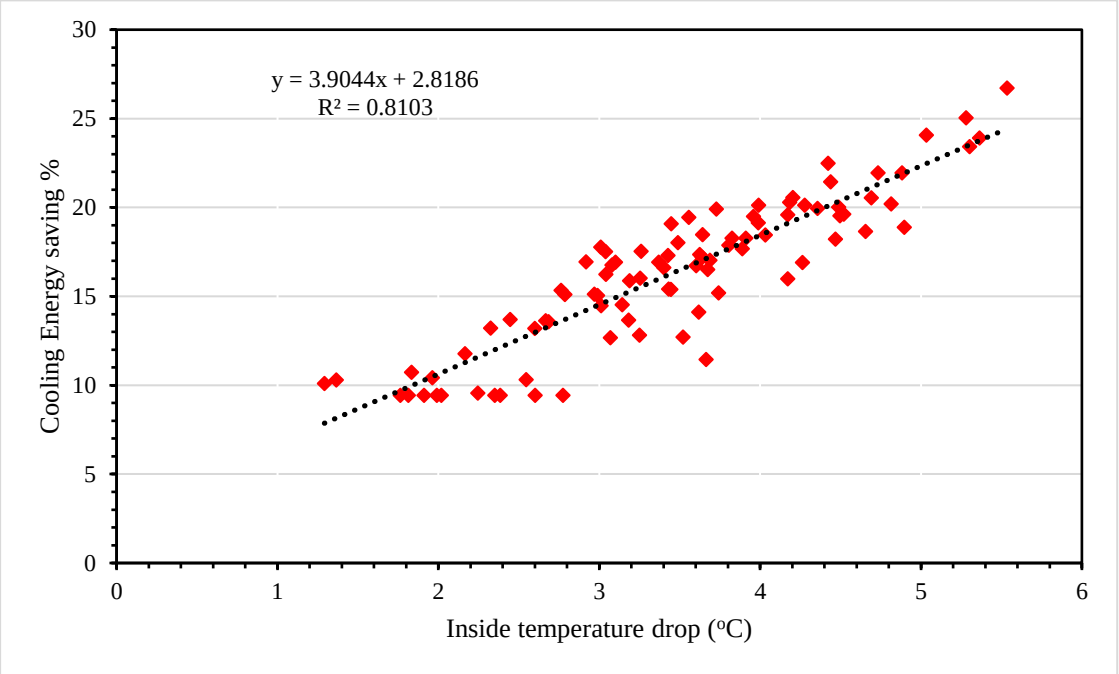

Fig. 24. Relationship between indoor temperature drop during NV and CES

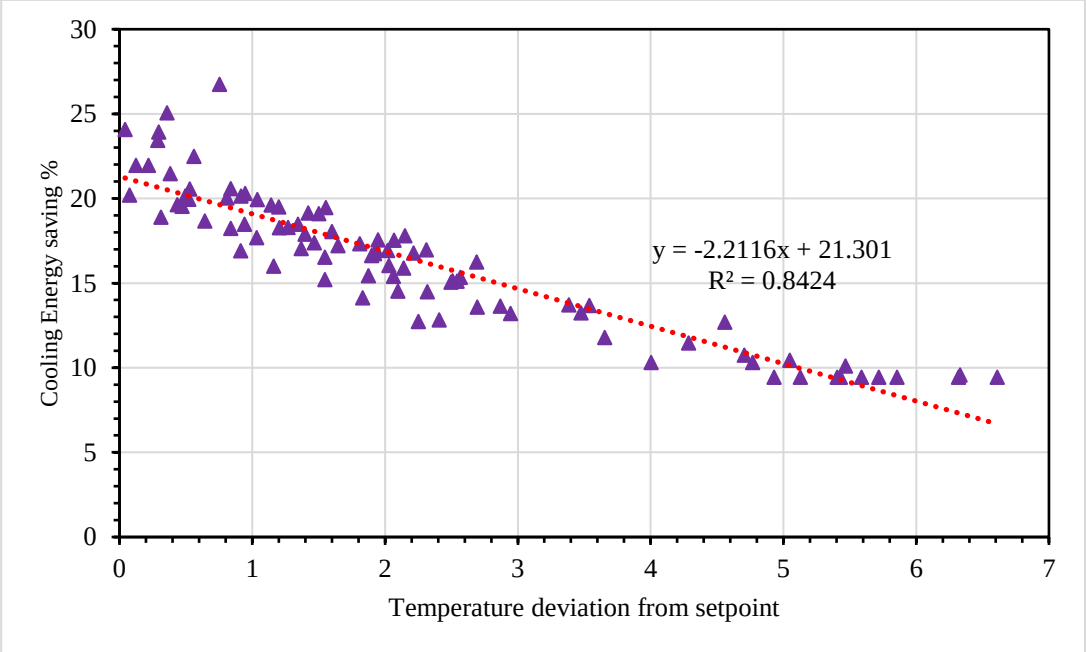

Fig. 25. Relationship between temperature deviation form set point during NV and CE

4.2.2 Energy efficiency with PCM and night ventilation

This section presents further enhancement in CES by coupling PCM and free NV (B2-S_{NV+PCM}). The potential CES of PCM with free NV can be obtained as a difference of CED values from B2-S_{NV} and B2-S_{NV+PCM} scenarios, and all the simulation results are attached in Appendix C. Further, the shift in optimum PCM in the case of free NV is observed by comparing the optimum PCM in B1-S_{PCM} (Controlled condition) and B2-S_{NV+PCM}.

Table 5 (b2) shows that coupling PCM with NV (B2-S_{NV+PCM}) in all the zones has a positive impact, resulting in additional CES compared to B2-S_{NV}. The magnitude of CES differs from region to region depending upon the metrological conditions. In addition, some cities experience a shift in optimum PCM. In tropical regions, all the cities in the Aw zone show significant CES in the case of B2-S_{NV+PCM}. For instance, in Miguel Hidalgo (Aw), the optimum PCM27 reduces the CED by 2472 kWh (3.8%), which is quantitatively the highest saving in the tropical region. In addition, Miguel Hidalgo also observed a shift in optimum PCM with free NV from PCM28 (In B1-S_{PCM}) to PCM27. In Addis-Ababa (Aw), the optimum PCM 28 tends to reduce 1521 kWh in the case of B2-S_{NV+PCM}. Compared to B1-$S_{PCM,}$ the CES in Addis-Ababa increased almost double in the case of B2-S_{NV+PCM} (754 kWh to 1572 kWh). However, the optimum PCM was PCM28 in both cases (B1-S_{PCM} and B2-S_{NV+PCM}). The CES increase in free NV (B2-S_{NV+PCM}) with the same optimum PCM28 as in B1-S_{PCM} shows the performance enhancement of PCM28 with NV in Addis-Ababa. To have clear evidence of PCM28 performance improvement in Addis-Ababa, energy-charge and discharge by PCM28 in both the cases (B1-S_{PCM} and B2-S_{NV+PCM}) are presented in Fig. 26. Additionally, for both cases, the charging and discharging coefficients are shown in Fig. 27. From Fig. 26 it can be observed that in B2-S_{NV+PCM}, the overall energy stored and released by PCM 28 is higher than B1-S_{PCM}. In addition, the high peak shows the better charging of PCM in B2-S_{NV+PCM} where the air circulation, due to the stack effect, tends to reduce the inside wall temperature by increasing the convective heat transfer coefficient. The convective heat transfer has a linear impact on heat transmission [11]; the lower value will prevent the significant utilization of PCM[92] by reducing the recharging potential of PCM. The performance improvement can also be depicted in Fig.27, where PCM charging and discharge coefficients are presented for both cases. It is apparent from the figure that in B2-S_{NV+PCM} the values of the charging and discharging coefficient are higher, revealing the better performance of PCM.

The cities in the Af zone and Am zone showed insignificant CES with the integration of PCM under free NV conditions. The highest CES in Am zone was obtained in Hongkong, where

PCM28 reduced 1236 kWh (1.4%), while in the Af zone, the highest CES was 1222 kWh (1.5%) in Georgetown with optimum PCM28. On the other hand, the lowest CES was 736 kWh and 849 kWh in the Douala Af zone and Kuala Lumpur Am zone. In fact, the low CES with PCM integration under free NV makes it unfavorable for Am and Af zone. This can be associated with almost stable diurnal temperature with less temperature drop during the night in Af and Am regions. To observe this, the hours during which the outdoor temperature drops in Douala is below the optimum PCM peak melting point (29 °C) during the free NV night (0:00 to 6:00 hours) are presented in Fig.28. It can be seen that the drop in ambient temperature below the peak melting point of PMC27 during the free NV is 23%, 47%, and 53% for June, July, and August. This shows that in Douala, most of the time, during free NV, the ambient temperature is above the peak melting point of PCM and results in limited CES (736 kWh (0.9%)). The application of free NV in conditions where the ambient temperature is above the peak melting point of PCM during nighttime had an adverse effect and prevented the PCM solidification. Panchabikesan et al. (2020) also specified that in tropical regions with high ambient temperatures, the complete solidification of PCM through the free cooling concept is challenging [93].

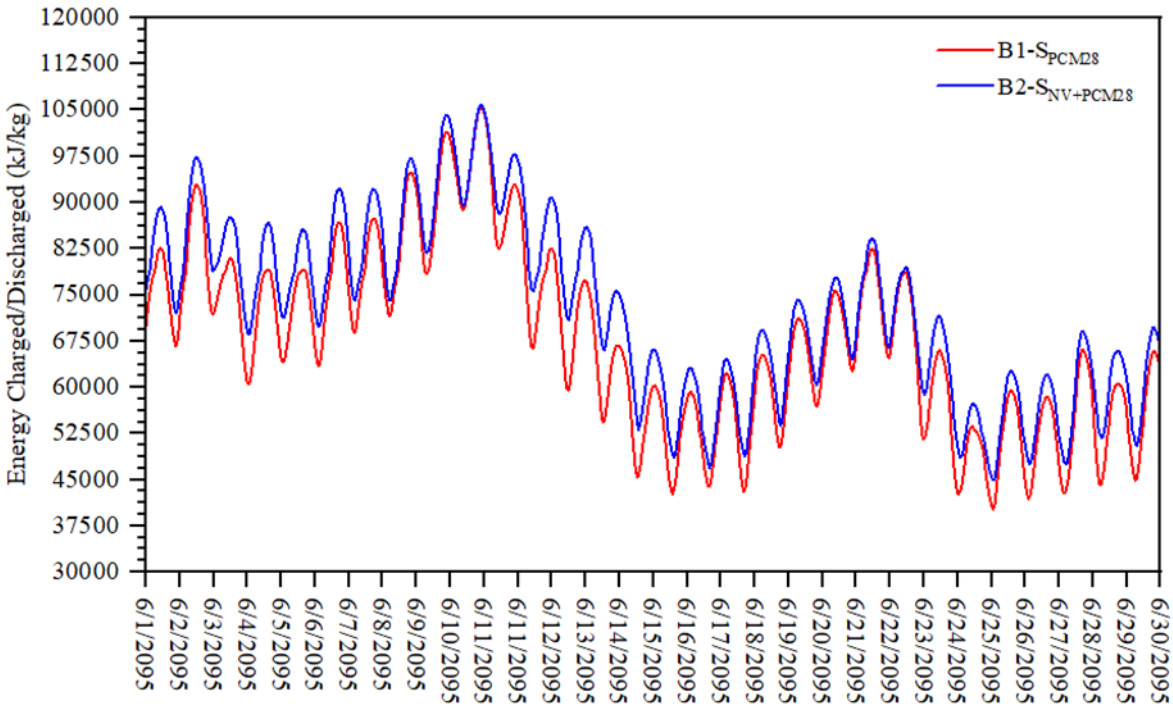

Fig. 26. Energy charged and discharged by PCM 28 layer located in south facing wall in Addis-Ababa

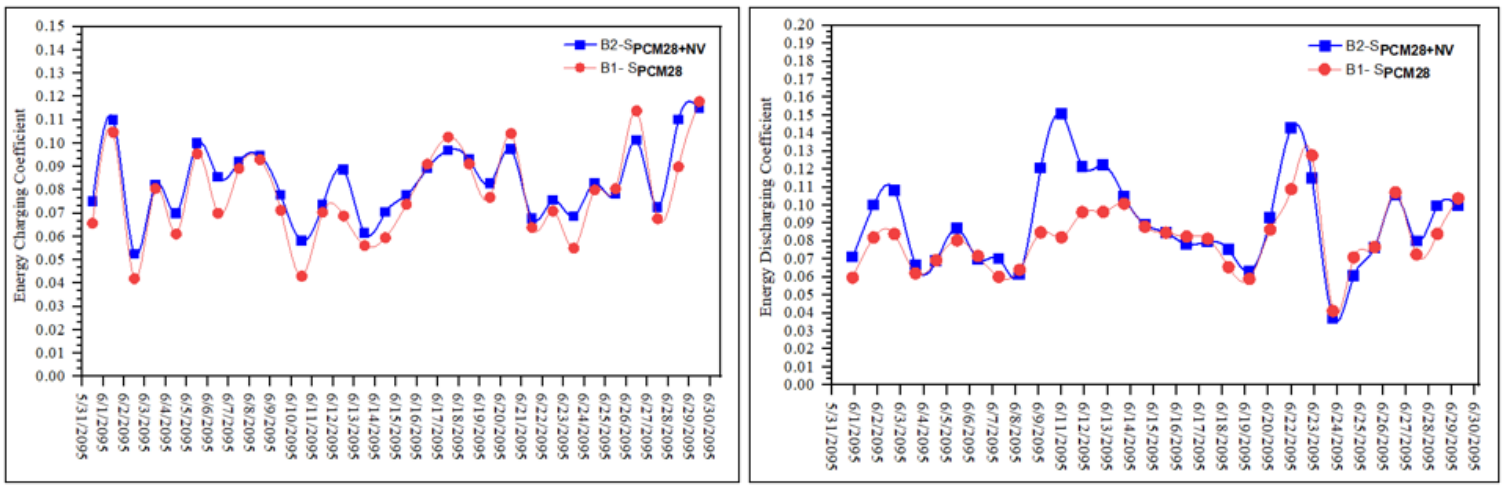

(a) (b)

Fig. 27. (a) Charging coefficient and (b) Discharging coefficient of PCM28 for June in Addis-Ababa

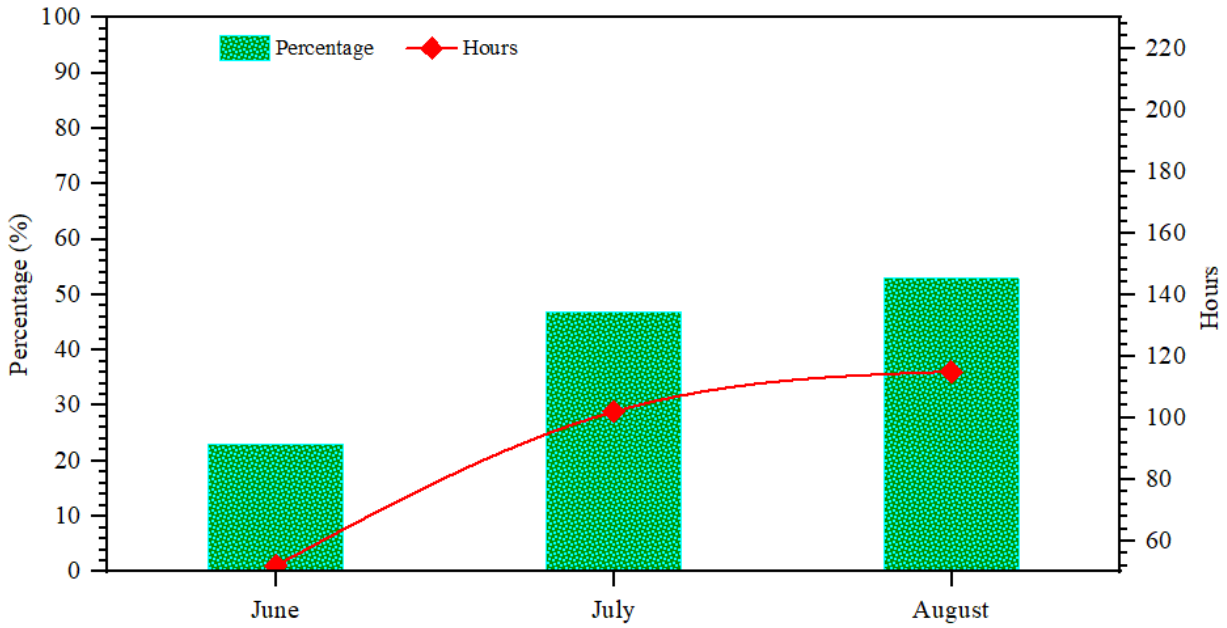

Fig. 28. Temperature drops hours/ percentage below 29 °C at night (0:00 to 6:00) in Douala

In an arid region, PCM integration with free NV (B2-S_{NV+PCM}) further reduces the CED in all the cities (Table 5 (b2)). Considerable CES were observed in Makkah (BWh), Lahore (BSh), and Kokshetay (BSk), where the reduction in CED were 2440 kWh, 2135 kWh, and 1864 kWh compared to B2-S_{NV}. The ESR values for Makkah and Lahore are 1.8% and 1.5%, respectively. Conversely, Aktobe (BSk) and Kazalinsk (BWk) show CES of 1598 kWh and 1647 kWh with ESR of 2.7% and 2.6%, respectively. The CES in Aktobe and Kazalinsk are quantitatively lower than Makkah and Lahore, but the ESR values are higher. Here it can be argued that evaluating the behavior of PCM with respect to the ESR may not appropriately signify the performance, as ESR depends on the initial CED. Therefore, [11] recommended considering both ESR and energy savings values in kilowatt-hours to observe the fundamental behavior of PCM. Regarding the performance improvement of PCM with free NV in the arid region, all the cities have low ESR and CES values compared to B1-S_{PCM} except in Aktobe. In Aktobe, the CES were 1473 kWh with optimum PCM28 and ESR of 1.9% in the case of B1-$S_{PCM,}$ which increased to 1598 kWh and ESR of 2.7% with a shift to PCM27 as optimum in case of B2-S_{NV+PCM}.

In temperate regions, most cities experience a shift in optimum PCM with significant improvement in CES. For instance, in Stockholm, London, and Bogota (Cfb zone), the CES were very low (ESR below 1%) in the case of B1-S_{PCM}, with free NV (B2-S_{NV+PCM}), the CES values increased by 1634 kWh, 1690 kWh, and 1035 kWh showing a remarkable enhancement in PCM performance. To have a clear perspective of PCM enhancement in B2-S_{NV+PCM}, the charging fraction (CF) and a discharging fraction (DF) of optimum PCM are compared with B1-S_{PCM} for Stockholm and presented in Fig. 29. From the figure it is clear that with free NV, the PCM 25 performs better during charging and discharging. The better performance of PCM25 can be associated with cool air infiltration during the free NV, which enhances the PCM charging capacity. In addition, Paris, Srinagar in the Cfa zone and Kathmandu, Kunming in the Cwa zone showed considerable enhancement in PCM performance in B2-S_{NV+PCM}. The CES, in Paris, Srinagar, were 729 kWh and 907 kWh in B2-$S_{PCM,}$ which increased to 1872 kWh and 2071 kWh, respectively, with free NV (B2-S_{NV+PCM}). Also, In Kathmandu, Kunming, the CES were 1214 kWh, and 1555 kWh in the case of B2-S_{PCM}, with the free NV increased to 1771 kWh, 2018 kWh. On the other hand, in Wuhan and Nanning, the application of NV has a detrimental effect on PCM performance as the CES were less compared to case B1-S_{PCM}.

Similarly, in the humid continental region, the application of PCM with free NV (B2-S_{NV+PCM}) tends to have a positive impact and shows pronounced CES in all the cities. Even in the cities of Arkhangelsk and Umea, where the PCM was performing negatively in B1-S_{PCM},

coupling PCM with free NV (B2-S_{NV+PCM}) results in substantial CES. The CES were 1973 kWh and 1433 kWh in Arkhangelsk and Umea, respectively in B2-S_{NV+PCM}. In addition, the shift in optimum PCM can be observed in the humid continental region. For instance, in the case of B1-S_{PCM} the optimum PCM was PCM30 for Arkhangelsk and Umea. The free NV (B2-S_{NV+PCM}) shifts the optimum PCM to PCM24 in Arkhangelsk and PCM26 in Umea. The shift in optimum PCM with free NV in the humid continental region can be associated with the climate condition of the region. The humid continental region possesses a moderate summer with considerable diurnal temperature fluctuation [94]. Thus in such conditions, the free NV favors PCM with lower melting points by enhancing the PCM recharging capacity for the next cycle [95,96].

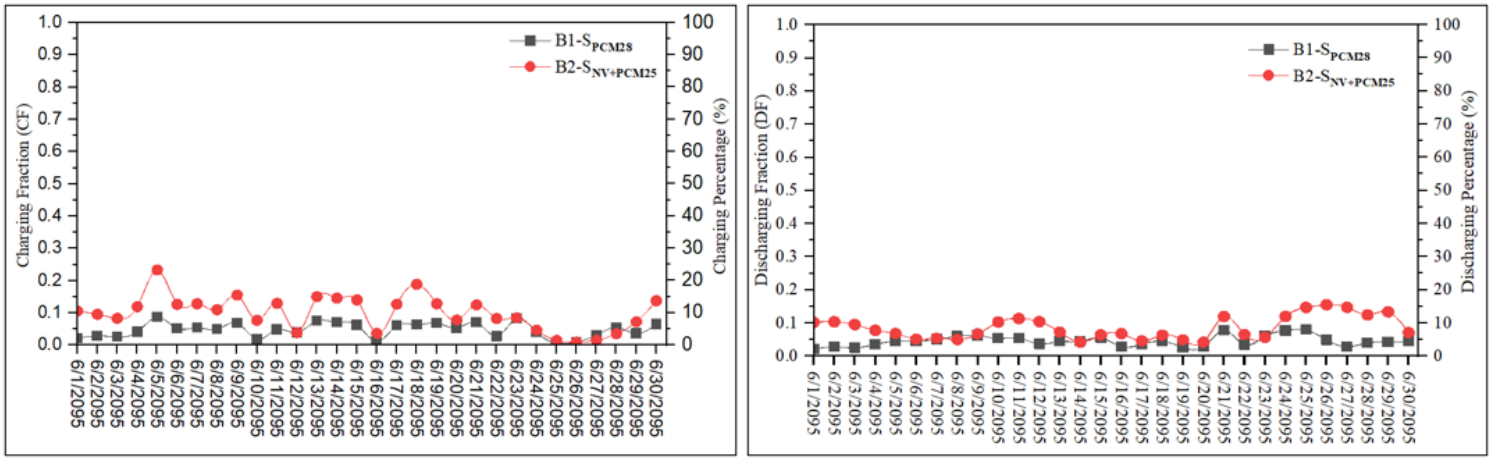

Fig. 29. Energy charging and discharging fraction of optimum PCM in case of B1-S_{PCM} and B2 S_{NV+PCM} in Stockholm

4.3 Energy saving with Changeover ventilation

This section evaluates the influence of changeover ventilation (CV) on CED. All the simulation results for changeover ventilation combined with PCM are presented in Appendix D. In changeover ventilation, the natural ventilation and HVAC operate singly depending upon the set conditions. The ventilation is allowed when Tinside > T outside and Tinside > Tset; else, HVAC will operate. Afterward, in the second part of this section, further reduction in CED by coupling PCM and CV is discussed.

4.3.1 Impact of Changeover ventilation on cooling energy savings.

The changeover ventilation (CV) not only infiltrates the fresh air but also improves thermal comfort without imposing additional loads on the HVAC system [97]. Fig. 30 shows the reduction in CED with the application of CV (B3-S_{CV}) compared to B1-S_{ref}. Overall, CV tends to reduce a

tremendous cooling load in all the climate zones. As in the CV, depending upon the favorable outdoor conditions, the HVAC and natural ventilation work in a seriatim manner. This results in less energy demand for cooling by HVAC [97]. The reduction in CED is more pronounced in the cities of the Cfb and Dfb zones. In Cfb and Dfb, the summer is moderate [94] and creates favorable conditions for CV. For instance, in Bogota (Cfb), the highest CES was observed, where the CV eventually reduced 53264 kWh (96%) of CED. The CES observed in Turkestan, and Kermanshah were 18267 kWh (15%) and 15053 kWh (13%), respectively. The relatively lower values of CES in Turkestan and Kermanshah can be associated with fewer ventilation hours in these cities. The total hours during which, indoor comfort is maintained with natural ventilation in Bogota, Turkestan, and Kermanshah are presented in Fig. 31. All clear from the figure, the ventilation hours in Bogota are 2163, which is 96% time of the total summer. Contrary to this, the ventilation hours in Turkestan and Kermanshah were 2.7% and 1.2% of total summer. Although the CES in Turkestan and Kermanshah were less than other cities, but the benefits in kWh were high enough to consider CV for energy conservation in these cities.

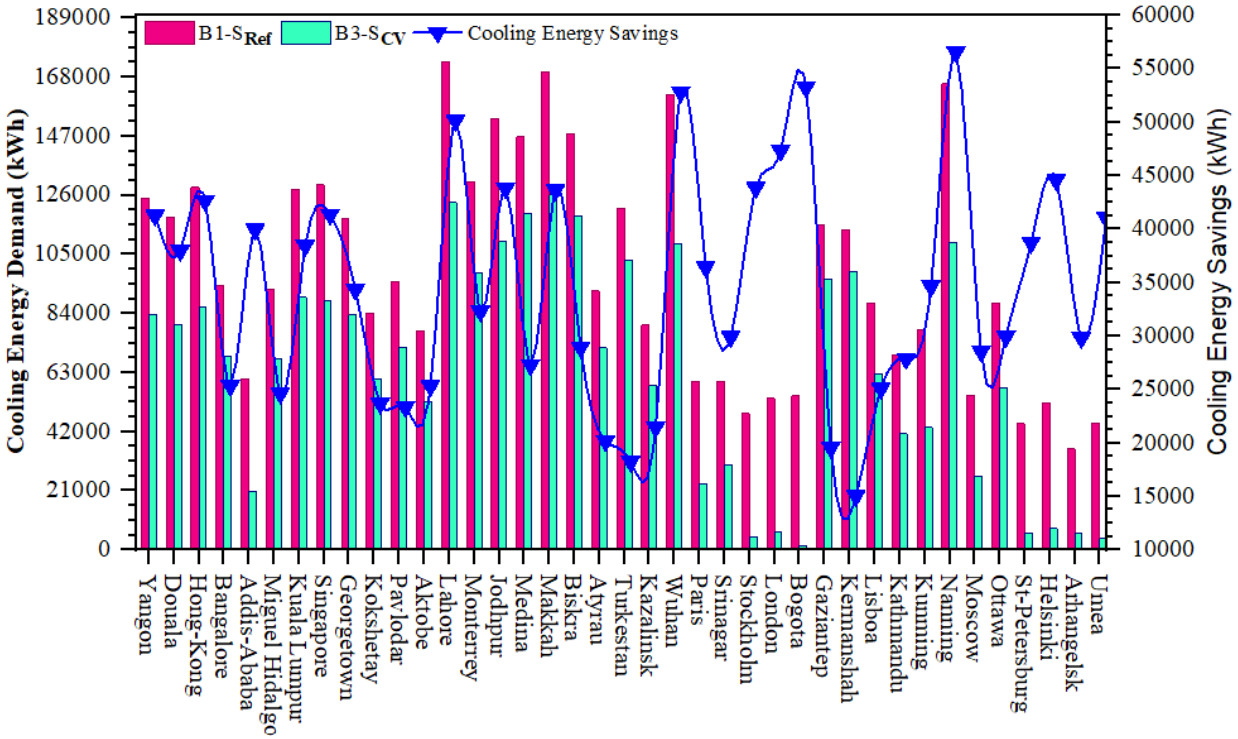

Fig. 30. Cooling energy savings with the application of CV in comparison to B1-S$_{Ref}$

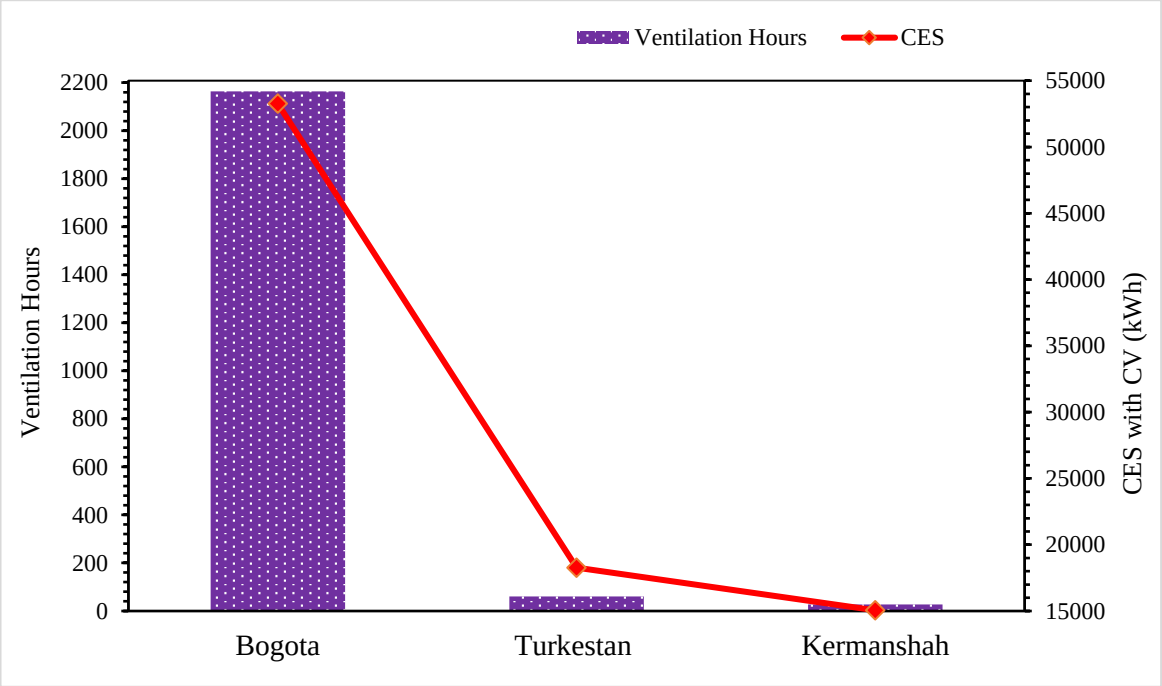

Fig.31. Ventilation hours in Bogota, Turkestan and Kermanshah in Case of CV and corresponding Cooling energy savings

4.3.2 Energy efficiency with PCM and Control ventilation

The implementation of CV appeared to be very beneficial for CES (Fig.30). In this section, further improvement in CES by integration of PCM under CV is discussed. The potential CES with the integration of PCM was evaluated by estimating the reduction in CED with the integration of PCM (B3-S_{PCM+CV}) compared to only CV (B3-S_{CV}).

Table 5 (b3) displays the CES under B3-S_{PCM+CV}. From the table, it can be noticed that integration of PCM has a positive impact and results in considerable CES in all the cities. Even in some cities like Bogota, Stockholm, and St-Petersburg, the ESR value recorded over 77% (1202 kWh),46% (2150 kWh), and 36% (2269 kWh), respectively. However, a higher ECR does not always signifies a higher CES quantitatively. In terms of kWh, the city of Addis-Ababa in the tropical zone, Medina in the arid zone, London in the temperate zone, and St-Petersburg in the humid continental zone shows higher CES in their corresponding zones with CES of 2900, 3107, 2408, and 2269 kWh respectively. In addition, most cities observed a shift in optimum PCM to the lower melting point in B3-S_{PCM+CV} compared to case B1-S_{PCM}. The lowest optimum PCM was recorded in Bangalore and Miguel Hidalgo, with a melting point of 23°C. Interestingly, despite being located in the same zone as Addis-Ababa, where the CES was high (2900 kWh),

the integration of PCM with CV in Miguel Hidalgo and Bangalore was ineffective, with the CES of 294 kWh and 170 kWh in the corresponding cities. For the possible explanation, the window opening fraction, indoor and outdoor temperature fluctuation in Bangalore is presented in Fig.32. The figure shows that for the whole summer, the indoor temperature fluctuates between 22°C to 25°C and from window opening fraction and outdoor temperature fluctuations it is clear that the CV conditions (Tinside > Toutside and Tinside> Tset) are mostly meet in July and August. All said, in such condition, where the outdoor temperature is mostly below the indoor temperature and favorable for CV, and the zone temperature do not provide enough temperature fluctuation, the optimum PCM23 does not operate efficiently.

Regarding the performance of PCM under B3-S_{CV+PCM}, in most cities, the CES values were lower compared to B1-S_{PCM} and B2-S_{NV+PCM} (Table 5). However, PCM performance tends to increase in Cfb and Dfa zone cities under B3-S_{CV+PCM} and shows more CES compared to B1-S_{PCM}. At the same time, Stockholm and London of Cfb show higher CES in B3-$S_{CV+PCM\ than}$ B1-S_{PCM} and B2-S_{NV+PCM}. In addition, the CES in Addis-Ababa in the Aw zone and Kokshetay in the BSk zone with CV coupled and PCM (B3-S_{CV+PCM}) are also higher than B1-S_{PCM} and B2-S_{NV+PCM}. To have a look into the performance enhancement ECC and EDC for optimum PCM25 in B2-S_{NV+PCM} and B3-S_{CV+PCM} in Stockholm (Cfb) are presented in Fig.33. From the figure, it can be seen that in B3-S_{CV+PCM} the ECC and EDC values are higher compared to B2-S_{NV+PCM} showing the better performance of PCM25. From the results, it can be derived that coupling PCM and CV is more favorable in moderated climate conditions.

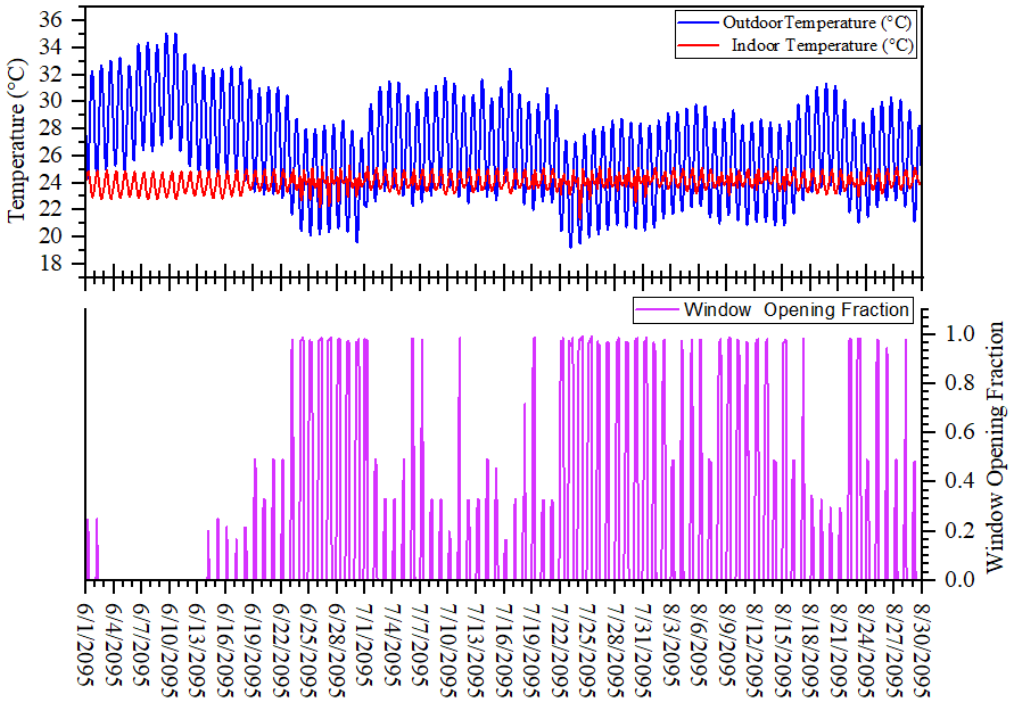

Fig. 32. Window Opening Fraction, Indoor and Outdoor Temperature Fluctuation for Bangalore in Case of CV

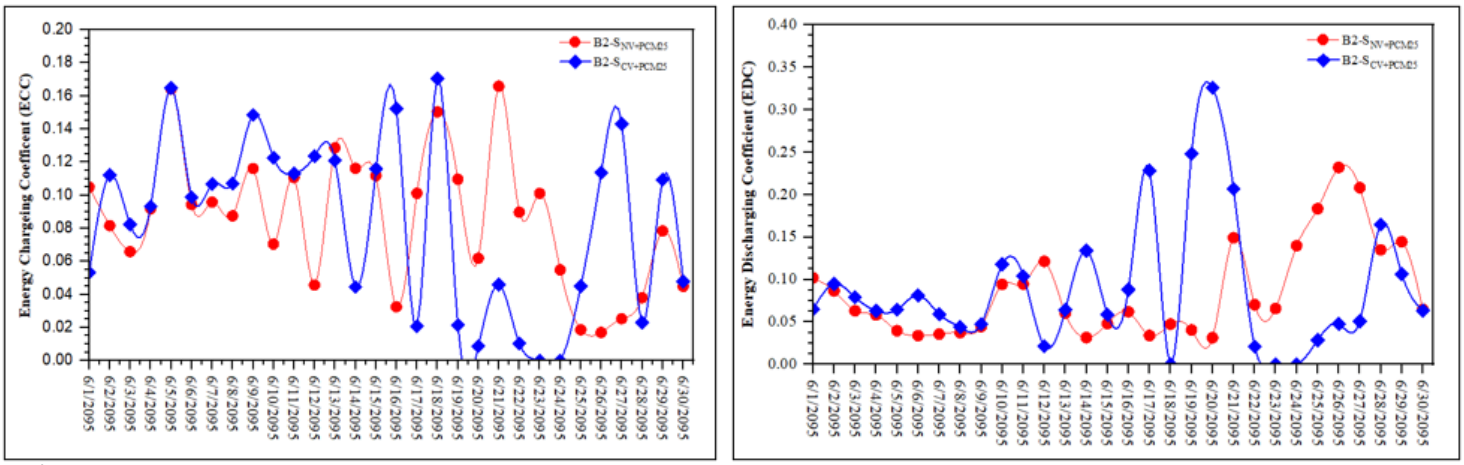

(a) (b)

Fig. 33. Energy charged coefficient and Energy discharged coefficient of PCM25 in case of B2-S_{NV+PCM} and B3-S_{CV+PCM} in Stockholm

4.4 Establishing the Best Energy saving strategy

The research findings indicate that coupling PCM with ventilation strategies is effective for cooling energy savings. However, to establish the best strategy for cooling energy conservation, the CED in B2-S_{NV+PCM} and B3-$_{SCV+PCM}$ are compared with B1-S_{Ref} as shown in Fig.34. The figure highlights that CV in combination with PCM (B3-S_{CV+PCM}) clearly shows superiority with a substantial reduction in CED in most of the cities. In some cities like Douala, Bangalore, and Georgetown, the CED with B3-S_{CV+PCM} is slightly higher than the CED B2-S_{NV+PCM}. Although in these cities, the CED with free NV (B2-S_{NV+PCM}) is less in comparison to B3-$S_{CV+PCM,}$ but in free NV, the indoor comfort is compromised and alone is not sufficient for adequate comfort [65]. This gives superiority to CV, where the optimized window operation ensures indoor thermal comfort. The results of the research show that CV offers optimized window operation, and coupling CV with optimum PCM offers the best energy-saving strategy.

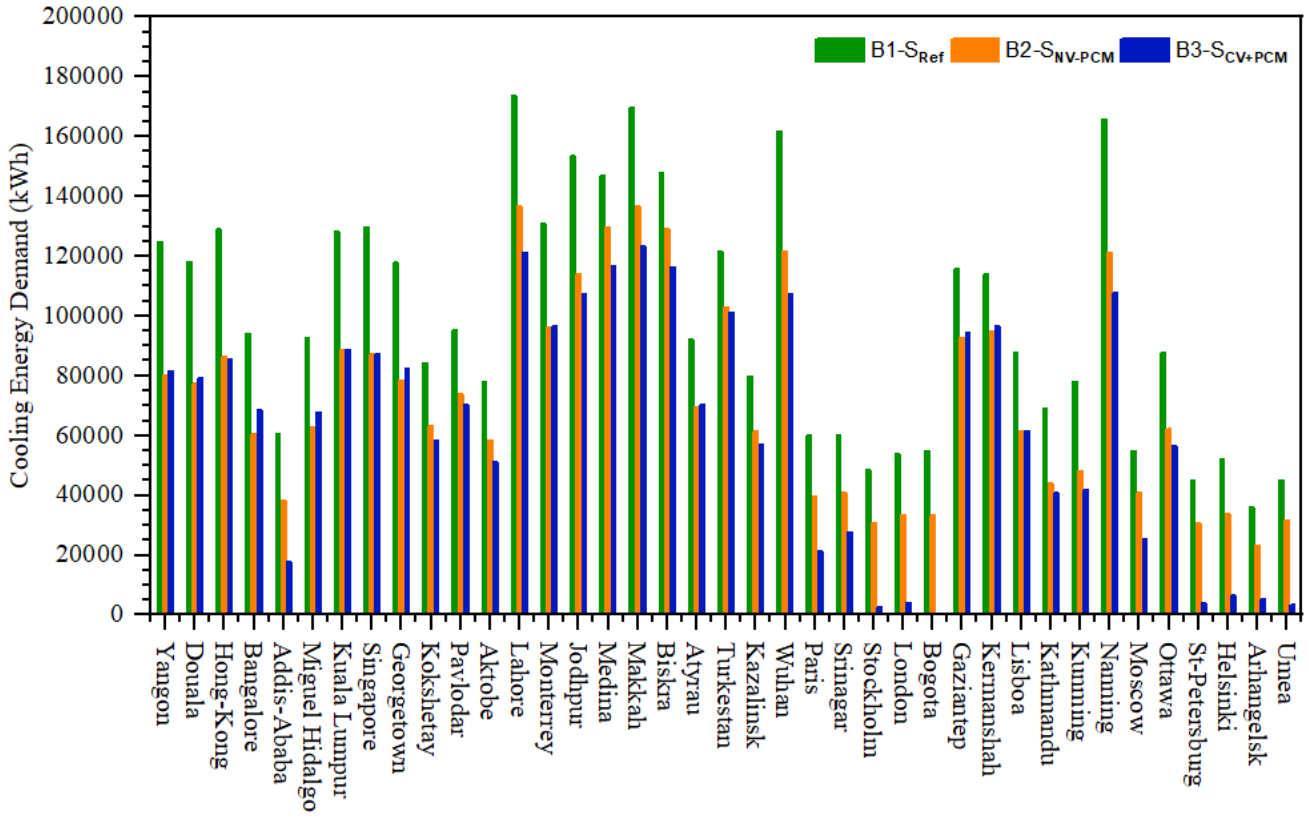

Fig. 34. Comparison of cooling energy demand in B1-S_{Ref}, B2-S_{NV+PCM} and B3-S_{CV+PCM} cases

4.5 Summary

This chapter presents the optimum PCM for each city located in a different climate zone. Moreover, the maximum cooling energy savings (CES) obtained with the application of optimum PCM under different indoor boundary conditions are also illustrated. The results presented in each section of this chapter are summarized as follows:

- Under the indoor control condition where the indoor temperature is maintained within the thermal comfort range for 24 hours, the optimum PCM melting point ranges from 27 °C to 30 °C, slightly above the HVAC cooling set point (26 degrees). Moreover, considerable CES is obtained in all the climate zone except Dfa and Dfb zones, where the PCM performance for energy saving was not satisfactory under control conditions.
- When PCM is integrated into the building and free night ventilation is applied, the PCM performance for CES increases in those cities where the diurnal temperature fluctuation is high. However, in the cities where the outdoor temperature is high during the night, free night ventilation had no significant impact on the PCM performance.
- The combination of changeover ventilation (HVAC and ventilation operate singly) and PCM turned out to be very effective for CES in all the climate zones.

Chapter 5- Conclusions and Recommendations

5.1 Conclusions

In view of the anticipated increase in cooling energy demand in the residential sector with climate change and considering the recommendation of the IEA for the implementation of energy-efficient technologies in the future, this research assessed: The potential of PCM for cooling energy savings in future climate by integration of PCM into a multi-story residential apartment building. In addition, free night ventilation and changeover ventilation were coupled with PCM to enhance cooling energy savings. The performance of PCM is evaluated using a new performance indicator. In this context, hourly energy simulations were carried out using Energyplus for 39 cities in 13 zones of the updated future Koppen climate map. The findings clearly indicate that:

- Under the indoor HVAC controlled condition, the optimum PCM performs effectively in all the zones resulting in cooling energy savings ranging from 1214 kWh to 7240 kWh except in humid continental climates. In a humid continental climate (Dfa and Dfb) where the summer is moderate, PCM integration under a controlled condition increases the thermal inertia of the wall and results in insignificant cooling energy savings. Thus, the PCM integration is unfavorable under the controlled scenario in these climate regions.
- The application of free night ventilation for the improvement of PCM performance is more favorable in the climate zone where the diurnal temperature fluctuation is high (Cwa, Cfb, Dfa, and Dfb zones). The cooling energy savings of PCM and NV combination varied from 773 kWh to 2490 kWh.
- Changeover ventilation implementation offer optimized window operation without disturbing indoor thermal comfort and the combination of PCM with changeover ventilation resulted in substantial cooling energy saving (506 kWh to 2772 kWh) in all climate zones. In comparison to the controlled and free night ventilation cases, PCM with changeover ventilation offers maximum savings (up to 96%).
- The energy charging and discharging fraction shows the utilized capacity of the PCM and the energy charged and discharged coefficients show the performance of the PCM. The maximum capacity of the PCM utilized remains below 0.5 (50%) and the energy changed and discharged coefficients values recorded were below 1 in all the examined zones. Therefore further studies should be considered to utilize the maximum capacity of the PCM by enhancing the charging and discharging of PCM during each cycle.

- Overall, this study strengthens the idea of implementing energy efficiency technology in the future by evaluating the potential of PCM for cooling energy savings with climate change. The findings of this research can be used as a guideline for energy-efficient building design in the future.

  .

5.2 Recommendations

In light of the results and conclusions of this research, it is recommended that further studies should be considered to enhance the performance of PCM in the climate zones where the PCM integration results in limited savings. In addition to this, to implement PCM integration in the construction sector, future research should be done to evaluate the environmental and building parameters. To advance the knowledge about the PCM integration into building envelopes with climate change, research may be carried out on the life cycle analysis of PCM-integrated buildings. In addition, the combination of PCM technology with other renewable energy systems, such as solar panels or solar chimney, should be investigated

References

[1] IEA. Roadmap for Energy-Efficient Buildings and Construction in ASEAN Timelines and actions towards net zero-carbon buildings and Construction 2019:1–171.

[2] Programme UNE. Buildings and Climate Change: Summary for Decision Makers 2009.

[3] Ürge-Vorsatz D, Cabeza LF, Serrano S, Barreneche C, Petrichenko K. Heating and cooling energy trends and drivers in buildings. Renew Sustain Energy Rev 2015;41:85–98. https://doi.org/10.1016/j.rser.2014.08.039.

[4] González-torres M, Pérez-lombard L, Coronel JF, Maestre IR, Yan D. A review on buildings energy information : Trends , end-uses , fuels and drivers. Energy Reports 2022;8:626–37. https://doi.org/10.1016/j.egyr.2021.11.280.

[5] Buildings – Analysis - IEA n.d. https://www.iea.org/reports/buildings (accessed October 30, 2022).

[6] Feng Y, Duan Q, Chen X, Yakkali SS, Wang J. Space cooling energy usage prediction based on utility data for residential buildings using machine learning methods. Appl Energy 2021;291:116814. https://doi.org/10.1016/j.apenergy.2021.116814.

[7] Navarro L, Gracia A De, Niall D, Castell A, Browne M, Mccormack SJ, et al. Thermal energy storage in building integrated thermal systems : A review . Part 2 . Integration as passive system 2016;85:1334–56. https://doi.org/10.1016/j.renene.2015.06.064.

[8] Cárdenas B, León N. High temperature latent heat thermal energy storage : Phase change materials , design considerations and performance enhancement techniques. Renew Sustain Energy Rev 2013;27:724–37. https://doi.org/10.1016/j.rser.2013.07.028.

[9] Hossein A, Shafaghat AH, Mohammed HI, Eisapour M, Talebizadehsardari P, Brambilla A, et al. A new design to enhance the conductive and convective heat transfer of latent heat thermal energy storage units. Appl Therm Eng 2022;215:118955. https://doi.org/10.1016/j.applthermaleng.2022.118955.

[10] Tao YB, He YL. A review of phase change material and performance enhancement method for latent heat storage system. Renew Sustain Energy Rev 2018;93:245–59. https://doi.org/10.1016/j.rser.2018.05.028.

[11] Saffari M, De Gracia A, Fernández C, Cabeza LF. Simulation-based optimization of PCM melting temperature to improve the energy performance in buildings. Appl Energy 2017;202:420–34. https://doi.org/10.1016/j.apenergy.2017.05.107.

[12] Soares N, Costa JJ, Gaspar AR, Santos P. Review of passive PCM latent heat thermal energy storage systems towards buildings' energy efficiency. Energy Build 2013;59:82–103.

[13] Lassandro P, Di Turi S. Energy efficiency and resilience against increasing temperatures in summer: the use of PCM and cool materials in buildings. Int J Heat Technol 2017;35:S307-15.

[14] Cabeza LF, Martorell I, Miró L, Fernández AI, Barreneche C. Introduction to thermal energy storage (TES) systems. Adv. Therm. energy storage Syst., Elsevier; 2015, p. 1–

28.

[15] Kenzhekhanov S, Memon SA, Adilkhanova I. Quantitative evaluation of thermal performance and energy saving potential of the building integrated with PCM in a subarctic climate. Energy 2020;192:116607. https://doi.org/10.1016/j.energy.2019.116607.

[16] Soleiman Dehkordi B, Afrand M. Energy-saving owing to using PCM into buildings: Considering of hot and cold climate region. Sustain Energy Technol Assessments 2022;52:102112. https://doi.org/10.1016/j.seta.2022.102112.

[17] Kabdrakhmanova M, Memon SA, Saurbayeva A. Implementation of the panel data regression analysis in PCM integrated buildings located in a humid subtropical climate. Energy 2021;237:121651. https://doi.org/10.1016/j.energy.2021.121651.

[18] Salihi M, El Fiti M, Harmen Y, Chhiti Y, Chebak A, Alaoui FEM, et al. Evaluation of global energy performance of building walls integrating PCM: Numerical study in semi-arid climate in Morocco. Case Stud Constr Mater 2022;16:e00979. https://doi.org/10.1016/j.cscm.2022.e00979.

[19] Lei J, Yang J, Yang EH. Energy performance of building envelopes integrated with phase change materials for cooling load reduction in tropical Singapore. Appl Energy 2016;162:207–17. https://doi.org/10.1016/j.apenergy.2015.10.031.

[20] Prabhakar M, Saffari M, de Gracia A, Cabeza LF. Improving the energy efficiency of passive PCM system using controlled natural ventilation. Energy Build 2020;228:110483. https://doi.org/10.1016/j.enbuild.2020.110483.

[21] Akeiber H, Nejat P, Majid MZA, Wahid MA, Jomehzadeh F, Zeynali Famileh I, et al. A review on phase change material (PCM) for sustainable passive cooling in building envelopes. Renew Sustain Energy Rev 2016;60:1470–97. https://doi.org/10.1016/j.rser.2016.03.036.

[22] Ciancio V, Salata F, Falasca S, Curci G, Golasi I, de Wilde P. Energy demands of buildings in the framework of climate change: An investigation across Europe. Sustain Cities Soc 2020;60:102213. https://doi.org/10.1016/j.scs.2020.102213.

[23] Nejat P, Jomehzadeh F, Taheri MM, Gohari M, Muhd MZ. A global review of energy consumption, CO2 emissions and policy in the residential sector (with an overview of the top ten CO2 emitting countries). Renew Sustain Energy Rev 2015;43:843–62. https://doi.org/10.1016/j.rser.2014.11.066.

[24] Cao X, Dai X, Liu J. Building energy-consumption status worldwide and the state-of-the-art technologies for zero-energy buildings during the past decade. Energy Build 2016;128:198–213. https://doi.org/10.1016/j.enbuild.2016.06.089.

[25] Dirks JA, Gorrissen WJ, Hathaway JH, Skorski DC, Scott MJ, Pulsipher TC, et al. Impacts of climate change on energy consumption and peak demand in buildings: A detailed regional approach. Energy 2015;79:20–32. https://doi.org/10.1016/j.energy.2014.08.081.

[26] Feng YY, Chen SQ, Zhang LX. System dynamics modeling for urban energy consumption and CO2 emissions: A case study of Beijing, China. Ecol Modell 2013;252:44–52. https://doi.org/10.1016/j.ecolmodel.2012.09.008.

[27] Isaac M, van Vuuren DP. Modeling global residential sector energy demand for heating and air conditioning in the context of climate change. Energy Policy 2009;37:507–21. https://doi.org/10.1016/j.enpol.2008.09.051.

[28] World Economic Forum. Global Risks 2020: An Unsettled World. World Econ Forum 2020:8–17.

[29] Zerbes I. “A Union that strives for more.” Eur Crim Law Rev 2020;10:253–4. https://doi.org/10.5771/2193-5505-2020-3-253.

[30] Commission E. Energy and the Green Deal. Eur Comm 2018. https://ec.europa.eu/info/strategy/priorities-2019-2024/european-green-deal/energy-and-green-deal_en (accessed January 10, 2023).

[31] Sajjadian SM, Lewis J, Sharples S. The potential of phase change materials to reduce domestic cooling energy loads for current and future UK climates. Energy Build 2015;93:83–9. https://doi.org/10.1016/j.enbuild.2015.02.029.

[32] Nurlybekova G, Memon SA, Adilkhanova I. Quantitative evaluation of the thermal and energy performance of the PCM integrated building in the subtropical climate zone for current and future climate scenario International Weather for Energy Calculation. Energy 2021;219:119587. https://doi.org/10.1016/j.energy.2020.119587.

[33] Piselli C, Prabhakar M, Gracia A De, Saffari M, Laura A, Cabeza LF. Optimal control of natural ventilation as passive cooling strategy for improving the energy performance of building envelope with PCM integration. Renew Energy 2020;162:171–81. https://doi.org/10.1016/j.renene.2020.07.043.

[34] Berardi U, Jafarpur P. Assessing the impact of climate change on building heating and cooling energy demand in Canada. Renew Sustain Energy Rev 2020;121:109681. https://doi.org/10.1016/j.rser.2019.109681.

[35] D’Agostino D, Parker D, Epifani I, Crawley D, Lawrie L. How will future climate impact the design and performance of nearly zero energy buildings (NZEBs)? Energy 2022;240:122479. https://doi.org/10.1016/j.energy.2021.122479.

[36] Guan L. Preparation of future weather data to study the impact of climate change on buildings. Build Environ 2009;44:793–800. https://doi.org/10.1016/j.buildenv.2008.05.021.

[37] Evola G, Marletta L, Sicurella F. A methodology for investigating the effectiveness of PCM wallboards for summer thermal comfort in buildings. Build Environ 2013;59:517–27. https://doi.org/10.1016/j.buildenv.2012.09.021.

[38] Castell A, Farid MM. Experimental validation of a methodology to assess PCM effectiveness in cooling building envelopes passively. Energy Build 2014;81:59–71. https://doi.org/10.1016/j.enbuild.2014.06.011.

[39] Ramakrishnan S, Wang X, Alam M, Sanjayan J, Wilson J. Parametric analysis for performance enhancement of phase change materials in naturally ventilated buildings. Energy Build 2016;124:35–45. https://doi.org/10.1016/j.enbuild.2016.04.065.

[40] Energy Use by Buildings - GreenBuildingAdvisor n.d. https://www.greenbuildingadvisor.com/article/energy-use-by-buildings (accessed March 14, 2023).

[41] Palacios-Garcia EJ, Moreno-Munoz A, Santiago I, Flores-Arias JM, Bellido-Outeirino FJ, Moreno-Garcia IM. A stochastic modelling and simulation approach to heating and cooling electricity consumption in the residential sector. Energy 2018;144:1080–91. https://doi.org/10.1016/J.ENERGY.2017.12.082.

[42] Group WB. A KNOWLEDGE NOTE SERIES FOR THE ENERGY PRACTICE. Understanding CO2 emissions from the global energy sector. 2014:1–12.

[43] CO2 Emissions in 2022 – Analysis - IEA n.d. https://www.iea.org/reports/co2-emissions-in-2022 (accessed March 15, 2023).

[44] Chen PY, Chen ST, Hsu CS, Chen CC. Modeling the global relationships among economic growth, energy consumption and CO2 emissions. Renew Sustain Energy Rev 2016;65:420–31. https://doi.org/10.1016/j.rser.2016.06.074.

[45] Clark PU, Shakun JD, Marcott SA, Mix AC, Eby M, Kulp S, et al. Consequences of twenty-first-century policy for multi-millennial climate and sea-level change. Nat Clim Chang 2016;6:360–9. https://doi.org/10.1038/nclimate2923.

[46] IPCC CC. Synthesis Report,[RK Pachauri, et al.(eds.)], 148 pp 2014.

[47] World Meteorological Organization. Greenhouse gases | World Meteorological Organization 2021. https://public.wmo.int/en/our-mandate/focus-areas/environment/greenhouse gases (accessed September 11, 2022).

[48] Kim SW, Brown RD. Urban heat island (UHI) intensity and magnitude estimations: A systematic literature review. Sci Total Environ 2021;779:146389. https://doi.org/10.1016/j.scitotenv.2021.146389.

[49] You Q, Kang S, Pepin N, Flügel W-A, Sanchez-Lorenzo A, Yan Y, et al. Climate warming and associated changes in atmospheric circulation in the eastern and central Tibetan Plateau from a homogenized dataset. Glob Planet Change 2010;72:11–24.

[50] Sinha A, Thakkar H, Rezaei F, Kawajiri Y, Realff MJ. Reduced building energy consumption by combined indoor CO2 and H2O composition control. Appl Energy 2022;322:119526. https://doi.org/10.1016/j.apenergy.2022.119526.

[51] Wang H, Chen Q. Impact of climate change heating and cooling energy use in buildings in the United States. Energy Build 2014;82:428–36. https://doi.org/10.1016/j.enbuild.2014.07.034.

[52] Pachauri RK, Allen MR, Barros VR, Broome J, Cramer W, Christ R, et al. Climate change 2014: synthesis report. Contribution of Working Groups I, II and III to the fifth assessment report of the Intergovernmental Panel on Climate Change. Ipcc; 2014.

[53] Chakraborty D, Alam A, Chaudhuri S, Başağaoğlu H, Sulbaran T, Langar S. Scenario-based prediction of climate change impacts on building cooling energy consumption with explainable artificial intelligence. Appl Energy 2021;291:116807. https://doi.org/10.1016/j.apenergy.2021.116807.

[54] Wilbanks T, Bhatt V, Bilello D, Bull S, Ekmann J, Horak W, et al. Effects of climate change on energy production and use in the United States. US Dep Energy Publ 2008:12.

[55] van Ruijven BJ, De Cian E, Sue Wing I. Amplification of future energy demand growth due to climate change. Nat Commun 2019;10:1–12. https://doi.org/10.1038/s41467-019-10399-3.

[56] Kamal R, Moloney F, Wickramaratne C, Narasimhan A, Goswami DY. Strategic control and cost optimization of thermal energy storage in buildings using EnergyPlus. Appl Energy 2019;246:77–90. https://doi.org/10.1016/j.apenergy.2019.04.017.

[57] Memon SA. Phase change materials integrated in building walls: A state of the art review. Renew Sustain Energy Rev 2014;31:870–906. https://doi.org/10.1016/j.rser.2013.12.042.

[58] Ling TC, Poon CS. Use of phase change materials for thermal energy storage in concrete: An overview. Constr Build Mater 2013;46:55–62.

https://doi.org/10.1016/J.CONBUILDMAT.2013.04.031.

[59] Phase Change Materials (PCMs) for Building Applications - The Constructor n.d. https://theconstructor.org/building/phase-change-materials-pcms-for-building-applications/564050/ (accessed May 3, 2023).

[60] Saffari M, De Gracia A, Ushak S, Cabeza LF. Economic impact of integrating PCM as passive system in buildings using Fanger comfort model. Energy Build 2016;112:159–72. https://doi.org/10.1016/j.enbuild.2015.12.006.

[61] Wijesuriya S, Brandt M, Tabares-Velasco PC. Parametric analysis of a residential building with phase change material (PCM)-enhanced drywall, precooling, and variable electric rates in a hot and dry climate. Appl Energy 2018;222:497–514. https://doi.org/10.1016/j.apenergy.2018.03.119.

[62] Hlanze P, Elhefny A, Jiang Z, Cai J, Shabgard H. In-duct phase change material-based energy storage to enhance building demand flexibility. Appl Energy 2022;310:118520. https://doi.org/10.1016/j.apenergy.2022.118520.

[63] Lizana J, de-Borja-Torrejon M, Barrios-Padura A, Auer T, Chacartegui R. Passive cooling through phase change materials in buildings. A critical study of implementation alternatives. Appl Energy 2019;254:113658. https://doi.org/10.1016/j.apenergy.2019.113658.

[64] Gracia D, Luisa F, Saffari M, Prabhakar M, Gracia A De, Mangina E, et al. Provided by the author (s) and University College Dublin Library in accordance with publisher policies . Please cite the published version when available . Title Controlled Natural Ventilation Coupled with Passive PCM System to Improve the Cooling Energ 2019.

[65] Arumugam P, Ramalingam V, Vellaichamy P. Effective PCM, insulation, natural and/or night ventilation techniques to enhance the thermal performance of buildings located in various climates – A review. Energy Build 2022;258:111840. https://doi.org/10.1016/j.enbuild.2022.111840.

[66] Beck HE, Zimmermann NE, McVicar TR, Vergopolan N, Berg A, Wood EF. Present and future köppen-geiger climate classification maps at 1-km resolution. Sci Data 2018;5:1–12. https://doi.org/10.1038/sdata.2018.214.

[67] Moazami A, Nik VM, Carlucci S, Geving S. Impacts of future weather data typology on building energy performance – Investigating long-term patterns of climate change and extreme weather conditions. Appl Energy 2019;238:696–720. https://doi.org/10.1016/j.apenergy.2019.01.085.

[68] Erlandsen HB, Parding KM, Benestad R, Mezghani A, Pontoppidan M. A hybrid downscaling approach for future temperature and precipitation change. J Appl Meteorol Climatol 2020;59:1793–807. https://doi.org/10.1175/JAMC-D-20-0013.1.

[69] Hosseini M, Bigtashi A, Lee B. Generating future weather files under climate change scenarios to support building energy simulation – A machine learning approach. Energy Build 2021;230:110543. https://doi.org/10.1016/j.enbuild.2020.110543.

[70] Nik VM. Making energy simulation easier for future climate - Synthesizing typical and extreme weather data sets out of regional climate models (RCMs). Appl Energy 2016;177:204–26. https://doi.org/10.1016/j.apenergy.2016.05.107.

[71] Eames M, Kershaw T, Coley D. On the creation of future probabilistic design weather years from UKCP09. Build Serv Eng Res Technol 2011;32:127–42. https://doi.org/10.1177/0143624410379934.

[72] About White Box Technologies Weather Data n.d. http://weather.whiteboxtechnologies.com/aboutus (accessed December 25, 2022).

[73] ASHRAE Standard 90.1-2013. Energy Standard for Buildings Except Low-Rise Residential Buildings. n.d.

[74] Arıcı M, Bilgin F, Nižetić S, Karabay H. PCM integrated to external building walls: An optimization study on maximum activation of latent heat. Appl Therm Eng 2020;165. https://doi.org/10.1016/j.applthermaleng.2019.114560.

[75] Ramakrishnan S, Wang X, Sanjayan J, Wilson J. Thermal performance of buildings integrated with phase change materials to reduce heat stress risks during extreme heatwave events. Appl Energy 2017;194:410–21. https://doi.org/10.1016/j.apenergy.2016.04.084.

[76] EnergyPlus. Input Output Reference. Encycl Ref to EnergyPlus Input Output 2010;c.

[77] ASHRAE Standard 90.1. Prototype Building Models. Pacific Northwest Natl Lab 2018. https://www.energycodes.gov/prototype-building-models.

[78] v9.1.0 E, EnergyPlus. Input Output Reference. Encycl Ref to EnergyPlus Input Output 2010;c:1996–2016.

[79] DOE. EnergyPlus | Department of Energy. EnergyGov 2021. https://www.energy.gov/eere/buildings/downloads/energyplus-0 (accessed September 15, 2022).

[80] Cabeza LF. Advances in thermal energy storage systems: Methods and applications. Adv. Therm. Energy Storage Syst., Elsevier; 2021, p. 37–54.

[81] Ascione F, Bianco N, De Masi RF, de' Rossi F, Vanoli GP. Energy refurbishment of existing buildings through the use of phase change materials: Energy savings and indoor comfort in the cooling season. Appl Energy 2014;113:990–1007. https://doi.org/10.1016/j.apenergy.2013.08.045.

[82] Tabares-Velasco PC, Griffith B. Diagnostic test cases for verifying surface heat transfer algorithms and boundary conditions in building energy simulation programs. J Build Perform Simul 2011;5:329–46. https://doi.org/10.1080/19401493.2011.595501.

[83] Tabares-Velasco PC, Christensen C, Bianchi M. Verification and validation of EnergyPlus phase change material model for opaque wall assemblies. Build Environ 2012;54:186–96. https://doi.org/10.1016/j.buildenv.2012.02.019.

[84] Cui H, Memon SA, Liu R. Development, mechanical properties and numerical simulation of macro encapsulated thermal energy storage concrete. Energy Build 2015;96:162–74. https://doi.org/10.1016/j.enbuild.2015.03.014.

[85] Adilkhanova I, Memon SA, Kim J, Sheriyev A. A novel approach to investigate the thermal comfort of the lightweight relocatable building integrated with PCM in different climates of Kazakhstan during summertime. Energy 2021;217:119390. https://doi.org/10.1016/j.energy.2020.119390.

[86] EnergyPlus. AirflowNetwork Model: Engineering Reference — EnergyPlus 8.3 n.d. https://bigladdersoftware.com/epx/docs/8-3/engineering-reference/airflownetwork-model.html#node-temperature-calculations (accessed December 9, 2022).

[87] Guo J, Zhang G. Investigating the performance of the PCM-integrated building envelope on a seasonal basis. J Taiwan Inst Chem Eng 2021;124:91–7. https://doi.org/10.1016/j.jtice.2021.04.066.

[88] Köppen Climate Classification (KCC) | SKYbrary Aviation Safety n.d. https://www.skybrary.aero/articles/koppen-climate-classification-kcc (accessed December 27, 2022).

[89] Tunçbilek E, Arıcı M, Krajčík M, Nižetić S, Karabay H. Thermal performance based optimization of an office wall containing PCM under intermittent cooling operation. Appl Therm Eng 2020;179. https://doi.org/10.1016/j.applthermaleng.2020.115750.

[90] Yang L, Li Y. Cooling load reduction by using thermal mass and night ventilation. Energy Build 2008;40:2052–8. https://doi.org/10.1016/j.enbuild.2008.05.014.

[91] Catalina T, Iordache V, Caracaleanu B. Multiple regression model for fast prediction of the heating energy demand. Energy Build 2013;57:302–12. https://doi.org/10.1016/j.enbuild.2012.11.010.

[92] Álvarez S, Cabeza LF, Ruiz-Pardo A, Castell A, Tenorio JA. Building integration of PCM for natural cooling of buildings. Appl Energy 2013;109:514–22. https://doi.org/10.1016/j.apenergy.2013.01.080.

[93] Panchabikesan K, Joybari MM, Haghighat F, Ramalingam V, Ding Y. Feasibility study on the year-round operation of PCM based free cooling systems in tropical climatic conditions. Energy 2020;192:116695. https://doi.org/10.1016/j.energy.2019.116695.

[94] Köppen climate classification - World distribution of major climatic types | Britannica n.d. https://www.britannica.com/science/Koppen-climate-classification/World-distribution-of-major-climatic-types (accessed December 21, 2022).

[95] de Gracia A, Navarro L, Castell A, Cabeza LF. Energy performance of a ventilated double skin facade with PCM under different climates. Energy Build 2015;91:37–42. https://doi.org/10.1016/j.enbuild.2015.01.011.

[96] Souayfane F, Fardoun F, Biwole PH. Phase change materials (PCM) for cooling applications in buildings: A review. Energy Build 2016;129:396–431. https://doi.org/10.1016/j.enbuild.2016.04.006.

[97] Wang L, Greenberg S. Window operation and impacts on building energy consumption. Energy Build 2015;92:313–21. https://doi.org/10.1016/j.enbuild.2015.01.060.

Appendix-A: Simulation Results for PCM Integration Under Controlled Conditions.

			B1-Sref	B1-SPCM																	
	Climate zone	City	CED	PCM18	PCM19	PCM28	PCM29	PCM30	PCM31	PCM32	PCM20	PCM21	PCM22	PCM23	PCM24	PCM25	PCM26	PCM27	Opt - PCM	CED Opti-PCM	CES	ECR
1	Am	Yangon	124835	123502.1	123502	121801.17	121988.1	122254	122710.9	123003.4	123502.1	123502.1	123502	123501.3	123498.9	123421.8	122809.1	121727.11	PCM27	121727.1	3108	2.5
2	Am	Douala	118151	116985.6	116986	115397.89	115595.2	115799.4	116179.3	116442.5	116985.6	116985.6	116985.5	116984.9	116981	116907.4	116416	115638.02	PCM28	115397.9	2753	2.3
3	Am	Hong-Kong	128859	127555	127555	125345.79	125948.5	126383.5	126857.2	127134	127555	127555	127554.8	127553.9	127550.2	127478.7	126747.4	125516.26	PCM28	125345.8	3514	2.7
4	Aw	Bangalore	94042	93256.24	93256	92165.9	92277.72	92451.12	92749.75	92934.48	93256.24	93256.24	93256.15	93255.71	93252.69	93180.44	92816.25	92198.84	PCM28	92165.9	1876	2.0
5	Aw	Addis-Ababa	60641	60489.51	60490	59887.6	59967.68	60070.22	60242.25	60309.43	60489.51	60489.51	60489.99	60485.99	60478.42	60478.72	60344.29	60050.07	PCM28	59887.6	754	1.2
6	Aw	Miguel Hidalgo	92531	91626.55	91627	90179.63	90461.62	90645.13	91045.59	91286.77	91626.55	91626.55	91626.45	91625.98	91614.37	91517.9	91094.5	90223.76	PCM28	90179.63	2351	2.5
7	Af	Kuala Lumpur	128240	126877.4	126877	124988.72	125313.9	125530.4	125940.5	126264.6	126877.4	126877.4	126877.3	126876.6	126871.1	126781.6	126217.5	125325.1	PCM28	124988.7	3251	2.5
8	Af	Singapore	129732	128328	128328	126226.3	126648.9	126899.3	127372.3	127693.6	128328	128328	128327.9	128327.2	128323.1	128241.5	127704.2	126667.34	PCM28	126226.3	3505	2.7
9	Af	Georgetown	117828	116653.9	116654	114796.51	115191.6	115430.5	115844.3	116121.8	116653.9	116653.9	116653.8	116653.2	116650.3	116581.9	116087.9	115088.58	PCM28	114796.5	3031	2.6
10	BSk	Kokshetay	84234	83504.14	83504	82432.96	82676.9	82841.56	83017.95	83156.09	83504.14	83504.15	83504.17	83504.76	83423.74	83269.85	82879.26	82431.96	PCM27	82431.96	1802	2.1
11	BSk	Pavlodar	95225	94218.57	94219	93369.33	93404.25	93454.39	93592.11	93775.42	94218.57	94218.57	94218.49	94218.32	94213.51	94162.28	93911.12	93368.33	PCM27	93368.33	1856	1.9
12	BSk	Aktobe	77920	77275.84	77276	76636.03	76696.4	76653.1	76821.48	76953.99	77275.84	77275.84	77276.08	77275.19	77279.92	77234.43	77054.34	76635.03	PCM27	76635.03	1285	1.6
13	Bsh	Lahore	173554	170697.7	170698	166740.11	167585.7	168317	169193.8	169732.6	170697.7	170697.7	170697.4	170673.9	170480	169841	169036.1	167066.64	PCM28	166740.1	6814	3.9
14	Bsh	Monterrey	130859	128959.4	128959	126783.82	127234.4	127505.2	127965.6	128329.1	128959.4	128959.4	128959.3	128944.1	128828.3	128694	128013.4	126949.71	PCM28	126783.8	4076	3.1
15	Bsh	Jodhpur	153416	151083.2	151083	148116.11	148766.2	149196.3	149779.4	150257.5	151083.2	151083.2	151083	151061.3	150904.4	150684.5	149812.1	148307.11	PCM28	148116.1	5300	3.5
16	BWh	Medina	146810	144403.9	144404	141268.75	141560.1	142162.6	143021.4	143577.4	144403.9	144403.9	144403.7	144390.8	144325.3	144242.3	143494.8	142008.38	PCM28	141268.8	5542	3.8
17	BWh	Makkah	169722	167052.2	167052	163400.62	163922.7	164576.7	165487.5	166141.6	167052.2	167052.2	167052	167050.9	167045.8	166934.3	165989.9	163694.06	PCM28	163400.6	6321	3.7
18	BWh	Biskra	147729	145236.5	145237	142271.23	142635.4	143115.6	143752.2	144253.8	145236.5	145236.5	145236.3	145217.8	145074.3	144618	144040.8	142772.84	PCM28	142271.2	5458	3.7
19	BWk	Atyrau	91984	91017.03	91017	89663.95	89989.39	90133.4	90383.33	90566.49	91017.03	91017.03	91017.03	91011.03	90926.88	90734.37	90192.77	89656.18	PCM27	89656.18	2328	2.5
20	BWk	Turkestan	121376	119564.7	119565	117403.79	117697.5	117988.8	118434.4	118792.4	119564.7	119564.7	119564.6	119549.6	119446.2	119236.4	118730.8	117879.81	PCM28	117403.8	3973	3.3
21	BWk	Kazalinsk	79768	79011.59	79012	78267.45	78268.11	78300.18	78505.63	78652.56	79011.59	79011.59	79011.6	79006.43	78979.77	78912.33	78708.07	78261.36	PCM27	78261.36	1507	1.9
22	Cfa	Wuhan	161723	159136.8	159137	154483.43	155523.6	156487.2	157491.6	158051.3	159136.8	159136.8	159136.5	159107.1	158887.1	158151.2	157233.6	154924.53	PCM28	154483.4	7240	4.5
23	Cfa	Paris	59939	59722.76	59723	59222.22	59312.36	59331.7	59455.38	59524.41	59722.76	59722.76	59723.03	59674.57	59574.77	59454.47	59275.01	59210.07	PCM27	59210.07	729	1.2
24	Cfa	Srinagar	59998	59744.77	59745	59146.26	59245.86	59307.16	59481.17	59557.8	59744.77	59744.78	59745.11	59740.16	59715.96	59558.51	59340.09	59091.18	PCM27	59091.18	907	1.5
25	Cfb	Stockholm	48485	48547.45	48547	48324.04	48328.49	48324.51	48392.7	48424.94	48547.45	48547.51	48548.08	48563.73	48561.12	48585.22	48569.99	48474.16	PCM28	48324.04	161	0.3
26	Cfb	London	53866	53800.34	53800	53431.02	53477.05	53490.99	53596.37	53649.9	53800.34	53800.34	53800.6	53803.02	53771.26	53698.45	53570.63	53493.87	PCM28	53431.02	435	0.8
27	Cfb	Bogota	54820	54793.54	54794	54298.55	54382.87	54466.23	54582.21	54626.19	54793.54	54793.54	54793.72	54790.15	54801.33	54707.48	54516.4	54311.47	PCM28	54298.55	521	1.0
28	Csa	Gaziantep	115691	114030.4	114030	111757.91	112093	112485.7	112954.9	113333	114030.4	114030.4	114030.3	114022.1	113946.3	113717.3	113283.9	112315.68	PCM28	111757.9	3933	3.4
29	Csa	Kermanshah	113869	112111.3	112111	109851.4	110190.4	110500.9	110985.2	111390.1	112111.3	112111.3	112111.2	112101.8	112022.4	111740.5	111311.1	110333.16	PCM28	109851.4	4018	3.5
30	Csa	Lisboa	87581	86750.14	86750	85562.38	85798.97	85941.46	86195.22	86369.35	86750.14	86750.14	86750.03	86742.6	86671.28	86439.34	85985.17	85464.21	PCM27	85464.21	2117	2.4
31	Cwa	Kathmandu	69133	68707.1	68707	67920.86	68055.79	68182.92	68391.41	68479.78	68707.1	68707.1	68707.04	68701.1	68636.58	68520.99	68192.82	67919.37	PCM27	67919.37	1214	1.8
32	Cwa	Kunming	78094	77575.33	77575	76657.69	76848.98	76994.18	77215.35	77336.77	77575.33	77575.33	77575.29	77569.51	77511.04	77418.63	77046.88	76539.35	PCM27	76539.35	1555	2.0
33	Cwa	Nanning	165711	163370.3	163370	159191.03	160358.9	161182.5	162087.8	162619.7	163370.3	163370.3	163370	163368.6	163361.4	163221.3	162003.4	159489.52	PCM28	159191	6520	3.9
34	Dfa	Moscow	54913	54818.04	54818	54659.9	54582.22	54541.23	54620.9	54665.31	54818.04	54818.19	54818.66	54824.76	54869.01	55004.79	55116.5	54967.42	PCM30	54541.23	372	0.7
35	Dfa	Ottawa	87681	86910.81	86911	85824.79	86018.21	86144.16	86376.24	86530.96	86910.81	86910.82	86911.05	86908.47	86889.74	86827.01	86525.45	86043.48	PCM28	85824.79	1857	2.1
36	Dfa	St-Petersburg	44755	44883.74	44884	44870.43	44783.5	44733.62	44773.22	44792.12	44883.74	44884.24	44884.83	44895.45	44983.03	45190.05	45303.15	45162.46	PCM30	44733.62	21	0.0
37	Dfb	Helsinki	52153	52148.97	52149	51895.59	51910.62	51910.71	51976.44	52020.22	52148.97	52148.97	52148.99	52154.28	52116.53	52103.69	52104.71	52025.11	PCM28	51895.59	257	0.5
38	Dfb	Arhangelsk	35829	36094.81	36095	36066.52	36030.42	36007.29	36024.22	36037.25	36094.82	36094.96	36096.39	36109.54	36066.34	36113.17	36212.9	36180.71	PCM30	36007.29	-178	-0.5
39	Dfb	Umea	45089	45246.18	45246	45148.22	45110.08	45085.75	45128.25	45153.1	45246.18	45246.18	45246.29	45253.57	45315.45	45439.5	45502.41	45357.6	PCM30	45085.75	3	0.0

Appendix-B: Simulations results for comparing NV (B2-S_{NV}) with controlled case (B1-S_{Ref}).

	B2-SNV				
S.NO	Climate zone	City	CED[kWh]	CES (Compari to B1-Sref)	ECR
1	Am	Yangon	80777.88	44057.03	35.292235
2	Am	Douala	78015.94	40135.32	33.969439
3	Am	Hong-Kong	87558.31	41300.98	32.051224
4	Aw	Bangalore	62005.69	32036.06	34.065785
5	Aw	Addis-Ababa	39709.12	20932.35	34.51821
6	Aw	Miguel Hidalgo	65398.59	27132.09	29.322264
7	Af	Kuala Lumpur	89462.24	38777.87	30.238488
8	Af	Singapore	88069.99	41661.64	32.11371
9	Af	Georgetown	79778.09	38049.53	32.292539
10	BSk	Kokshetay	65266.45	18967.81	22.517928
11	BSk	Pavlodar	75551.75	19672.99	20.659537
12	BSk	Aktobe	59998.81	17921.5	22.99978
13	Bsh	Lahore	138651.07	34903.18	20.110818
14	Bsh	Monterrey	97558.3	33301.03	25.44796
15	Bsh	Jodhpur	115011.3	38405.12	25.033253
16	BWh	Medina	131383.67	15426.71	10.507915
17	BWh	Makkah	139022.11	30699.45	18.088126
18	BWh	Biskra	130286.93	17442.29	11.806933
19	BWk	Atyrau	71177.33	20806.59	22.619812
20	BWk	Turkestan	104446.87	16929.51	13.947944
21	BWk	Kazalinsk	62984.82	16783.19	21.040001
22	Cfa	Wuhan	124014.4	37708.62	23.316792
23	Cfa	Paris	41435.52	18503.33	30.870345
24	Cfa	Srinagar	43015.28	16983.15	28.305991
25	Cfb	Stockholm	32594.36	15890.58	32.774259
26	Cfb	London	35340.16	18525.71	34.392297
27	Cfb	Bogota	35128.17	19691.59	35.920606
28	Csa	Gaziantep	95226.23	20464.6	17.689042
29	Csa	Kermanshah	97238	16631.01	14.605387
30	Csa	Lisboa	63367.32	24214.05	27.647489
31	Cwa	Kathmandu	45656.45	23476.49	33.958472
32	Cwa	Kunming	50135.84	27958.52	35.800946
33	Cwa	Nanning	123433.19	42278.09	25.513103
34	Dfa	Moscow	41844.19	13068.54	23.798744
35	Dfa	Ottawa	63717.47	23963.85	27.330622
36	Dfa	St-Petersburg	31641.6	13113.02	29.299813
37	Dfb	Helsinki	35456.35	16696.41	32.014432
38	Dfb	Arhangelsk	24923.91	10905.12	30.436548
39	Dfb	Umea	33229.43	11859.61	26.302645

Appendix-C: Simulation results for only NV and PCM in combination with NV.

			B2-SNV			B2-SNV+PCM																	
S.NO	Climate zone	City	CED[kWh]	CES (Compari to B1-Sref)	ECR	PCM18	PCM19	PCM28	PCM29	PCM30	PCM31	PCM32	PCM20	PCM21	PCM22	PCM23	PCM24	PCM25	PCM26	PCM27	Opt PCM	CED(kWh)	CES (kWh)	ECR
1	Am	Yangon	80777.88	44057.03	35.292235	80195.33	80195.82	80120.64	80025.69	80025.07	80048.64	80086.49	80195.83	80195.83	80195.79	80195.59	80195.53	80195.52	80125.21	**80024.45**	PCM27	80024.45	753.43	1
2	Am	Douala	78015.94	40135.32	33.969439	77488.08	77488.43	77334.53	**77279.02**	77337.52	77367.06	77402	77488.43	77488.43	77488.39	77488.19	77488.13	77487.67	77430.76	77279.63	PCM29	77279.02	736.92	0.9
3	Am	Hong-Kong	87558.31	41300.98	32.051224	87059.02	87059.51	**86322.51**	I	86762.98	86920.29	86981.42	87059.51	87059.52	87059.47	87059.2	87059.06	87058.83	87052.34	86698.46	PCM28	86322.51	1235.8	1.4
4	Aw	Bangalore	62005.69	32036.06	34.065785	61320.87	61320.97	60715.4	60724.94	60884.7	61038.02	61113.4	61320.97	61320.97	61320.93	61319.69	61294.68	61158.69	60844.79	**60713.33**	PCM27	60713.33	1292.36	2.1
5	Aw	Addis-Ababa	39709.12	20932.35	34.51821	38874.3	38874.25	**38137.16**	38271.95	38481.89	38610.39	38714.53	38872.33	38859.63	38806.89	38677.18	38458.7	38294.57	38243.15	38139.7	PCM28	38137.16	1571.96	4.0
6	Aw	Miguel Hidalgo	65398.59	27132.09	29.322264	64319.7	64319.81	62982.73	63112.88	63351.29	63733.18	63937.86	64319.81	64319.81	64319.7	64314.58	64263.25	64071.45	63599.24	**62927**	PCM27	62927	2471.59	3.8
7	Af	Kuala Lumpur	89462.24	38777.87	30.238488	88762.61	88763.02	88677.26	88718.09	88626.92	**88613.58**	88652.63	88763.02	88763.02	88762.98	88762.8	88762.75	88762.69	88755	88702.18	PCM31	88613.58	848.66	0.9
8	Af	Singapore	88069.99	41661.64	32.11371	87496.1	87496.52	**87108.44**	87214.2	87233.46	87330.09	87410.77	87496.52	87496.52	87496.49	87496.31	87496.25	87496.18	87490.13	87313.1	PCM28	87108.44	961.55	1.1
9	Af	Georgetown	79778.09	38049.53	32.292539	79160.5	79160.81	**78556.14**	78715.55	78799.88	78948.54	79025.87	79160.81	79160.81	79160.78	79160.58	79160.48	79157.16	79032.9	78789.41	PCM28	78556.14	1221.95	1.5
10	BSk	Kokshetay	65266.45	18967.81	22.517928	64580.97	64580.75	**63402.21**	63781.43	64181.19	64339.07	64422.56	64578.54	64569.83	64547.98	64439.11	64299.95	64031.52	63756.43	63512.65	PCM28	63402.21	1864.24	2.9
11	BSk	Pavlodar	75551.75	19672.99	20.659537	74788.46	74788.65	73873.1	**73869.22**	74154.02	74407.47	74548.51	74788.56	74787.27	74780.56	74761.36	74723.02	74668.89	74487.23	74163.35	PCM29	73869.22	1682.53	2.2
12	BSk	Aktobe	59998.81	17921.5	22.99978	59199.31	59195.65	**58400.58**	58564.01	58746.9	58901.92	59008.51	59185.75	59166.52	59132.99	59089.33	59043.86	58954.1	58731.21	58478.61	PCM28	58400.58	1598.23	2.7
13	Bsh	Lahore	138651.07	34903.18	20.110818	137511.5	137512.6	137057.7	136599.7	**136516.1**	136708.5	136915.2	137512.6	137512.6	137512.5	137512.4	137512.4	137507.4	137478.6	137381.9	PCM30	136516.07	2135	1.5
14	Bsh	Monterrey	97558.3	33301.03	25.44796	96611.4	96611.72	96346.63	96385.85	96298.58	**96263.29**	96387.96	96611.72	96611.73	96611.69	96611.51	96611.48	96610.94	96601.38	96564.35	PCM31	96263.29	1295.01	1.3
15	Bsh	Jodhpur	115011.3	38405.12	25.033253	114027	114027.6	113749.1	113765.5	113785.5	**113746.7**	113750.1	114027.6	114027.6	114027.5	114027.4	114027.3	114027.3	114021.7	113952.4	PCM31	113746.74	1264.56	1.1
16	BWh	Medina	131383.67	15426.71	10.507915	130743.7	130744.2	130339.1	129805.1	**129745.4**	130067.8	130458.3	130744.2	130744.2	130744.2	130744	130743.9	130743.9	130743.4	130699.8	PCM30	129745.4	1638.27	1.2
17	BWh	Makkah	139022.11	30699.45	18.088126	137703.3	137704	137416.4	136869	**136581.7**	136798.6	137064.8	137704	137704	137704	137703.8	137703.8	137703.7	137703.7	137700	PCM30	136581.68	2440.43	1.8
18	BWh	Biskra	130286.93	17442.29	11.806933	129659.2	129659.8	129481.2	129078.7	**129043.1**	129218.5	129398.5	129659.8	129659.8	129659.8	129659.6	129659.6	129659.6	129658.4	129631.5	PCM30	129043.12	1243.81	1.0
19	BWk	Atyrau	71177.33	20806.59	22.619812	70448.8	70447.62	69544.87	69772.74	69974.02	70152.19	70250.98	70443.42	70435.74	70424.41	70397.98	70281.34	70020.55	69740	**69478.73**	PCM27	69478.73	1698.6	2.4
20	BWk	Turkestan	104446.87	16929.51	13.947944	103582	103582.3	103201.6	**102948.5**	102978	103075.5	103230.7	103582.3	103582.3	103582.3	103582.1	103582	103579.1	103561.3	103482.2	PCM29	102948.5	1498.37	1.4
21	BWk	Kazalinsk	62984.82	16783.19	21.040001	62122.78	62121.49	**61337.66**	61409.6	61583.43	61748.29	61860.05	62115.77	62104.44	62083.06	62048.46	62015.63	61954.82	61779.65	61542.87	PCM28	61337.66	1647.16	2.6
22	Cfa	Wuhan	124014.4	37708.62	23.316792	123250.1	123253.6	122445	**121723.3**	121754.8	122233.2	122716	123253.6	123253.6	123253.6	123253.4	123252.2	123242.8	123212.4	123098.6	PCM29	121723.3	2291.1	1.8
23	Cfa	Paris	41435.52	18503.33	30.870345	40527.35	40521.59	39799.4	39938.5	40128.19	40281.13	40382.47	40500.72	40452.38	40356.58	40099.48	39875.34	39644.53	**39563.98**	39637.04	PCM26	39563.98	1871.54	4.5
24	Cfa	Srinagar	43015.28	16983.15	28.305991	42170.7	42170.61	41149.78	41335.2	41612.77	41830.29	41953.35	42168.84	42158.05	42115.78	42001.35	41719.68	41336.14	**40954.19**	40955.87	PCM26	40954.19	2061.09	4.8
25	Cfb	Stockholm	32594.36	15890.58	32.774259	31674.27	31663.26	31080.25	31229.2	31381.81	31494.49	31589.33	31624.04	31542.1	31417.44	31149.81	30922.03	**30799.46**	30824.6	30951.08	PCM25	30799.46	1794.9	5.5
26	Cfb	London	35340.16	18525.71	34.392297	34328.17	34323.76	33634.05	33798.09	33977.88	34097.9	34213.31	34307.34	34254.65	34129.95	33835.29	33485.7	**33215.51**	33269.74	33469.18	PCM25	33215.51	2124.65	6.0
27	Cfb	Bogota	35128.17	19691.59	35.920606	34204.44	34204.46	33507.02	33718.79	33881.33	33987.42	34099.22	34202.18	34163.1	34026.65	33739.4	33365.19	33195	**33186.07**	33321.57	PCM26	33186.07	1942.1	5.5
28	Csa	Gaziantep	95226.23	20464.6	17.689042	94109.06	94109.3	93063.46	**92736.6**	92992.92	93337.51	93647.58	94109.31	94109.31	94109.27	94109.08	94108.02	94094.41	94027.23	93748.16	PCM29	92736.6	2489.63	2.6
29	Csa	Kermanshah	97238	16631.01	14.605387	96072.43	96072.68	95227.26	**95009.13**	95148.95	95315.99	95600.83	96072.68	96072.68	96072.64	96072.46	96072.28	96065.5	96020.62	95838.22	PCM29	95009.13	2228.87	2.3
30	Csa	Lisboa	63367.32	24214.05	27.647489	62573.42	62573.52	61538.52	61730.42	61984.58	62217.41	62335.9	62573.52	62573.53	62572.62	62564.38	62467.34	62257.4	61808.88	**61456.94**	PCM27	61456.94	1910.38	3.0
31	Cwa	Kathmandu	45656.45	23476.49	33.958472	44905.69	44905.74	44032.99	44269.97	44514.41	44644.08	44729.02	44905.75	44905.49	44895.56	44822.77	44614.8	44232.67	**43885.56**	43912.89	PCM26	43885.56	1770.89	3.9
32	Cwa	Kunming	50135.84	27958.52	35.800946	49292.38	49292.44	48392.47	48611.55	48830.68	48993.36	49079.95	49292.02	49288.02	49270.1	49203.02	49060.23	48778.75	48319.97	**48118.18**	PCM27	48118.18	2017.66	4.0
33	Cwa	Nanning	123433.19	42278.09	25.513103	122401.1	122405.4	121578.7	**121194**	121370.3	121764.8	122048.2	122405.4	122405.4	122405.4	122405.3	122405.2	122403.2	122377.5	122264.7	PCM29	121193.97	2239.22	1.8
34	Dfa	Moscow	41844.19	13068.54	23.798744	41227.54	41224.19	**40784.47**	40792.63	40922.7	41042.48	41116.42	41213.45	41185.81	41130.01	41070.25	41071.96	41048.54	40974.79	40907.76	PCM28	40784.47	1059.72	2.5
35	Dfa	Ottawa	63717.47	23963.85	27.330622	62957.76	62951.75	**62081.14**	62189.85	62456.03	62662.52	62771.34	62938.68	62916.44	62888.1	62857.15	62808.09	62681.03	62373.51	62184.47	PCM28	62081.14	1636.33	2.6
36	Dfa	St-Petersburg	31641.6	13113.02	29.299813	30825.96	30805.41	**30469.86**	30496.35	30597.52	30688.74	30762.48	30761.05	30687.4	30589.07	30544.67	30538.75	30592.31	30617.05	30501.52	PCM28	30469.86	1171.74	3.7
37	Dfb	Helsinki	35456.35	16696.41	32.014432	34509.84	34508.53	33909.25	34041.84	34195.63	34313.49	34415.64	34495.89	34443.09	34314.98	34044.94	33793.94	**33711.63**	33733.5	33813.71	PCM25	33711.63	1744.72	4.9
38	Dfb	Arhangelsk	24923.91	10905.12	30.436548	23923.46	23903.08	23433.56	23562.86	23688.47	23794.73	23883	23833.01	23685.6	23443.68	23063.59	**22951.09**	23039.24	23207.36	23350.28	PCM24	22951.09	1972.82	7.9
39	Dfb	Umea	33229.43	11859.61	26.302645	32456.51	32454.75	31904.5	32031.59	32177.19	32285.21	32374.1	32441.2	32392.06	32267.99	32067.79	31929.29	31855.71	**31796.13**	31813.05	PCM26	31796.13	1433.3	4.3

Appendix-D: Simulation results for changeover ventilation and PCM combination.

	B3-SCV			B3-SCV+PCM																	
	Climate zone	City	CED [kWh]	PCM18	PCM19	PCM28	PCM29	PCM30	PCM31	PCM32	PCM20	PCM21	PCM22	PCM23	PCM24	PCM25	PCM26	PCM27	Opt PCM	CED (kWh)	CES(kWh)	ECR
1	Am	Yangon	83560.55	82502.49	82502.82	81984.92	81727.95	82129.94	82256.13	82380.84	82502.82	82502.82	82502.79	82502.62	82502.58	82474.29	82113.6	81554.24	PCM27	81554.24	2006.31	2.4
2	Am	Douala	80189.95	79494.3	79494.6	79542.69	79339.22	79439.24	79493.23	79419.93	79494.6	79494.6	79494.57	79494.42	79494.36	79609.49	79688.06	79425.43	PCM29	79339.22	850.73	1.1
3	Am	Hong-Kong	86195.82	85795.7	85796.03	85290.16	85454.92	85657.88	85815.56	85748.53	85796.03	85796.03	85795.98	85796.48	85798.72	85796.36	85820.31	85364.21	PCM28	85290.16	905.66	1.1
4	Aw	Bangalore	68685.23	68855.29	68855.51	69914.57	69589.59	69103.85	68971.69	68953.92	68855.51	68855.51	68855.48	68517	68913.81	69311.62	70006.53	69902.87	PCM23	68517	168.23	0.2
5	Aw	Addis-Ababa	20681.46	19912.41	19912.46	19395.34	19590.08	19670.99	19800.9	19902.57	19922.34	19910.05	19771.37	19106.35	18221.16	17781.8	18030.35	18549.68	PCM25	17781.8	2899.66	14.0
6	Aw	Miguel Hidalgo	67900.26	68230.36	68230.62	69466.03	69649.19	69235.74	68909.68	68755.04	68230.62	68230.62	68230.23	67608	68235.98	68558.66	69465.34	69334.6	PCM23	67608	292.26	0.4
7	Af	Kuala Lumpur	89773.29	88869.25	88869.62	88618.64	88649.63	88695.15	88759.84	88735.2	88869.62	88869.62	88869.59	88869.45	88869.4	88863.84	88650.42	88605	PCM27	88605	1168.29	1.3
8	Af	Singapore	88373.43	87517.34	87517.69	87357.14	87377.07	87337.01	87406.54	87390.56	87517.69	87517.69	87517.66	87517.51	87517.45	87518.29	87290.81	87386.85	PCM26	87290.81	1082.62	1.2
9	Af	Georgetown	83494.03	82655.82	82656.13	82486.4	82418.3	82481.39	82433.76	82526.6	82656.13	82656.13	82656.12	82656.05	82656.01	82742.09	82677.82	82515.33	PCM29	82418.3	1075.73	1.3
10	BSk	Kokshetay	60538.84	60088.13	60088.2	59133.73	59872.47	60102.2	60094.8	60115.53	60087.67	60075.2	60003.22	59690.62	59145.33	58705.66	58461.72	58578.88	PCM26	58461.72	2077.12	3.4
11	BSk	Pavlodar	71851.96	71204.53	71204.8	70652.91	70978.92	71114.47	71164.05	71161.95	71204.81	71203.86	71180.32	71117.04	70906.75	70517.5	70205.16	70263.63	PCM26	70205.16	1646.8	2.3
12	BSk	Aktobe	52602.48	52210.86	52211.03	51572.25	51964.32	52150.81	52133.63	52205.47	52210.96	52211.13	52203.31	52019.96	51573.44	51098.02	51019.04	51132.72	PCM26	51019.04	1583.44	3.0
13	Bsh	Lahore	123413.46	121863.7	121864.5	121156.8	121185.9	121344.3	121723.3	121877.6	121864.5	121864.5	121864.4	121864.3	121868.4	121885.1	121855.3	121579.6	PCM28	121156.78	2256.68	1.8
14	Bsh	Monterrey	98537.38	97230.5	97230.88	96651.39	96826.25	97350.21	97183.24	97104.82	97230.89	97230.89	97230.89	97230.25	97230.21	97225.58	97055.8	97020.5	PCM28	96651.39	1885.99	1.9
15	Bsh	Jodhpur	109595.76	108032.9	108033.5	107430.3	107477.7	107623.1	107828.8	107898.3	108033.5	108033.5	108033.5	108033.4	108033.4	108058.4	107959	107606.1	PCM28	107430.25	2165.51	2.0
16	BWh	Medina	119518.17	117698.7	117699.2	116618.2	116411.6	116509.6	116924.2	117257.8	117699.3	117699.3	117699.3	117699.2	117699.2	117706.8	117675.9	117295.4	PCM29	116411.61	3106.56	2.6
17	BWh	Makkah	126084.21	124085.9	124086.6	123496.1	123312.3	123925.5	123964.3	123811.8	124086.6	124086.6	124086.6	124086.5	124086.4	124086.4	124069.6	123746.5	PCM29	123312.28	2771.93	2.2
18	BWh	Biskra	118805.13	117124.6	117125.2	116493.8	116325.6	116322.9	116500.7	116748.7	117125.2	117125.2	117125.1	117125	117125	117126.3	117101.6	116884.5	PCM30	116322.9	2482.23	2.1
19	BWk	Atyrau	71816.84	71261.66	71261.63	70733.08	70981.79	70967.57	71164.65	71233.17	71261.17	71246.49	71145.68	70893.79	70609.65	70612.99	70402.68	70284.48	PCM27	70284.48	1532.36	2.1
20	BWk	Turkestan	103108.79	101871	101871.4	101382.7	101281	101264.3	101394	101589.3	101871.4	101871.4	101871.4	101871.2	101871.3	101872.2	101874.6	101713.6	PCM30	101264.26	1844.53	1.8
21	BWk	Kazalinsk	58298.25	57883.81	57884.17	57445.71	57727.39	57687.24	57770.2	57858.85	57883.59	57870.47	57809.61	57630.69	57341.89	56986.24	56896.3	57124.02	PCM26	56896.3	1401.95	2.4
22	Cfa	Wuhan	108919.21	107630.3	107631	107129	107075.4	107405.3	107673	107555.7	107631	107631	107631	107630.7	107630.6	107664.4	107676.8	107469.2	PCM29	107075.38	1843.83	1.7
23	Cfa	Paris	23495.68	23323.77	23323.87	23098.38	23549.97	23452.27	23314.07	23364.23	23323.86	23319.68	23293.04	22933.73	22069.55	21523.65	21459.79	22011.74	PCM26	21459.79	2035.89	8.7
24	Cfa	Srinagar	30078.43	29506.25	29507.01	29152.9	29613.31	29538.01	29625.61	29693.74	29505.74	29475.72	29292.03	28722.83	27958.5	27548.87	27735.81	28280.08	PCM25	27548.87	2529.56	8.4
25	Cfb	Stockholm	4640.27	4478.14	4478.14	3887.48	4304.56	4420.13	4426.13	4496.32	4477.82	4472.55	4315.95	4150.88	3106.92	2490.09	2699.29	3298.24	PCM25	2490.09	2150.18	46.3
26	Cfb	London	6514.19	6157.4	6157.4	5447.99	5843.77	5957.36	6051.2	6126.37	6157.11	6149.84	6017.45	5355.79	4436.12	4106.66	4281.6	4824.03	PCM25	4106.66	2407.53	37.0
27	Cfb	Bogota	1556.01	1112.92	1112.92	805.86	941.53	978.32	1013.98	1091.75	1113.01	1106.29	1030.04	828.27	455.52	354.42	507.43	733.01	PCM25	354.42	1201.59	77.2
28	Csa	Gaziantep	96125.83	95094.87	95095.24	94371.27	94377.81	94528.24	94625.78	94779.14	95095.24	95095.24	95095.22	95095.08	95097.44	95101.46	94937.93	94629.76	PCM28	94371.27	1754.56	1.8
29	Csa	Kermanshah	98815.12	97528.93	97529.32	96812.93	96714.76	96656.57	96947.34	97191.49	97529.32	97529.32	97529.29	97529.19	97529.77	97534.36	97416.85	96982.75	PCM30	96656.57	2158.55	2.2
30	Csa	Lisboa	62507.03	62165.67	62165.87	62514.87	62525.51	62153.23	62165.56	62219.17	62165.87	62165.42	62137.01	61955.96	61631.97	61496.6	61709.53	62147.58	PCM25	61496.6	1010.43	1.6
31	Cwa	Kathmandu	41251.3	41194.91	41195.03	41329.63	41423.54	41113.69	41298.1	41302.36	41195.02	41193.64	41144.24	40904.64	40917.4	40843.03	40745.26	41032.56	PCM26	40745.26	506.04	1.2
32	Cwa	Kunming	43440.06	43023.89	43024.02	42978.74	43493.44	43405.21	43285.12	43265.65	43023.81	43018.12	42961.07	42515.59	41982.22	41635.48	41662.95	42009.25	PCM25	41635.48	1804.58	4.2
33	Cwa	Nanning	109168.21	107914.7	107915.3	107554.3	107535.4	107638.2	107894.6	107947.5	107915.3	107915.3	107915.3	107915.2	107914	107974.3	108040.5	107798.8	PCM29	107535.41	1632.8	1.5
34	Dfa	Moscow	26348.52	26335.9	26336.45	27054.57	26957.11	26663.16	26683.58	26604.81	26335.42	26322.72	26257.14	26059.68	25479.08	25148.5	25355.2	26309.79	PCM25	25148.5	1200.02	4.6
35	Dfa	Ottawa	57726.26	57638.54	57638.8	58097.2	58277.24	57839.29	57788.88	57800.32	57638.46	57621.48	57477.6	57276.73	56869.17	56492.8	56438.52	57146.21	PCM26	56438.52	1287.74	2.2
36	Dfa	St-Petersburg	6019.72	5952.28	5952.08	5542.9	5843.79	5919.54	5925.5	5999.98	5951.84	5937.48	5766.52	5155.99	4013.44	3751.05	4159.54	4807.65	PCM25	3751.05	2268.67	37.7
37	Dfb	Helsinki	7574.21	7583.83	7583.85	7389.23	7597.74	7637.86	7569.5	7608.86	7583.85	7583.68	7559.11	7378.74	6855.89	6485.68	6467.07	6847.7	PCM26	6467.07	1107.14	14.6
38	Dfb	Arhangelsk	6000	15555	15555	15555	15555	15555	15555	15555	15555	15555	15555	15555	5100	15555	15555	15555	PCM24	5100	900	15.0
39	Dfb	Umea	4050	3500	3500	3500	3500	3500	3500	3500	3500	3500	3500	3500	3314	3313	3500	3500	PCM25	3313	737	18.2